ministerie van verkeer en waterstaat

koninklijk nederlands meteorologisch instituut

stratocumulus modeling

P.G. Duynkerke

scientific reports WR-nr. 88-2

wetenschappelijke rapporten WR-nr. 88-2

de bilt, 1988

KNMI

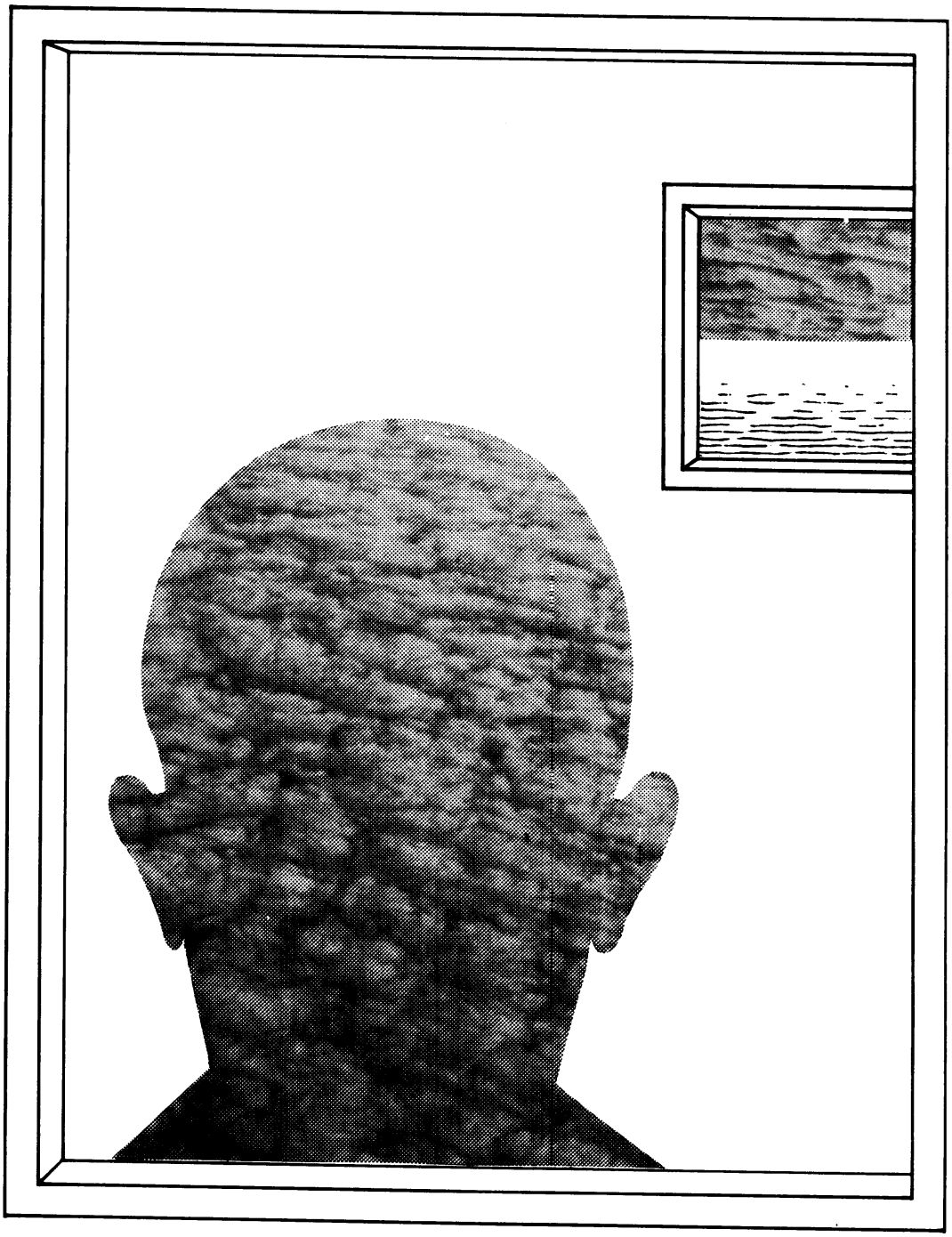

CONTENTS

page

VOORWOORD

Dit proefschrift is de afsluiting van een vierjarig promotie-onderzoek over de processen die het gedrag van stratocumulus bepalen. Gedurende deze tijd was ik in dienst van de VU te Amsterdam, faculteit der aardwetenschappen, vakgroep meteorologie. Voor de uitvoering van het werk was ik gedetacheerd op het KNMI in De Bilt waar het werk plaats vond onder begeleiding van Ad Driedonks. Mede dankzij de hulp en steun van anderen is het een leerzame en vruchtbare periode geweest; enkelen wil ik hier graag noemen.

Allereerst was de begeleiding door mijn co-promotor, Ad Driedonks, van groot belang. Ik ben je in het bijzonder dankbaar voor het uitstippelen van de grote lijn van dit onderzoek. Je stimulans om de wetenschappelijke resultaten vroegtijdig op te schrijven en je kritische redactionele opmerkingen en adviezen hebben veel bijgedragen aan de kwaliteit van dit proefschrift.

Mijn promotor, Henk Tennekes, ben ik erkentelijk voor de opmerkingen en adviezen tijdens de afronding van dit proefschrift. Henk en Ad wil ik tevens bedanken voor de mogelijkheid die ze me hebben gegeven om tijdens hun colleges aan de VU en RUU iets over mijn promotie-onderzoek aan de studenten te vertellen.

Frans Nieuwstadt, voor de tijd die je als referent aan dit proefschrift hebt besteed en voor je niet aflatende wetenschappelijke interesse die mij enorm heeft gestimuleerd. Het laatste heeft bovendien geresulteerd in een gezamenlijk geschreven artikel.

Kamergenoot Stephen Tjemkes wil ik bedanken voor de vele en soms heftige discussies over van alles en nog wat, maar in het bijzonder over straling. Over dit onderwerp heb ik veel van je geleerd en dit heeft geresulteerd in enkele gemeenschappelijke publicaties.

De collega's van de afdeling wetenschappelijk onderzoek ben ik erkentelijk voor de discussies, suggesties en de plezierige samenwerking. Met name bedank ik Anton Beljaars en Bert Holtslag.

William Cotton, professor aan de Colorado State University in Fort Collins, bij wie ik in 1985 twee maanden te gast was. De discussies die ik in die tijd met Graeme Stephens en Jean-Jacques Morcrette over straling heb gehad, zijn van groot belang geweest voor de voortgang van dit onderzoek.

Verder ben ik het KNMI erkentelijk voor de faciliteiten die het mij geboden heeft en de mogelijkheid om dit proefschrift af te ronden.

De uiteindelijke vormgeving van dit proefschrift is het resultaat van de vakbekwaamheid van de secretaresses van de afdeling, met name Marleen Kaltofen, de studio en de drukkerij.

SAMENVATTING

De bedoeling van dit proefschrift is de invloed van de verschillende fysische processen in een atmosferische grenslaag met een wolkendek van stratocumulus op de turbulente menging te onderzoeken. We zullen ons beperken tot stratocumulus boven zee.

De grenslaag is de onderste laag van de atmosfeer waarin turbulente menging plaats vindt. In onbewolkte omstandigheden varieert de dikte van de grenslaag van ongeveer 1000 m overdag tot ongeveer 100 m 's nachts, dit als gevolg van de verschillen in de netto straling aan het aardoppervlak. Overdag verwarmt de zonnestraling het aardoppervlak. Doordat dit warmer wordt dan de lucht ontstaan er convectieve (opstijgende) bewegingen. Hierdoor neemt de turbulentie toe en kan de grenslaag groeien. In de nacht daarentegen koelt het aardoppervlak tengevolge van infrarode straling af en wordt de temperatuur van het aardoppervlak lager dan die van de lucht. Een dergelijke temperatuuropbouw is stabiel. De door de wind opgewekte turbulente menging wordt door de stabiele opbouw van de lucht onderdrukt en de grenslaag blijft dun.

Vaak komt er in de grenslaag bewolking voor. Gemiddeld over de hele wereld is stratocumulus de meest voorkomende soort lage bewolking. Stratocumulus is een aaneengesloten wolkendek dat zich in het bovenste gedeelte van de grenslaag bevindt, met een karakteristieke wolkentop van 1000 m en een dikte van 500 m. Een wolkendek van stratocumulus heeft, zowel aan het aardoppervlak als aan de top van de atmosfeer, een grote invloed op de netto zonnestraling, terwijl de netto infrarode straling nauwelijks beïnvloed wordt. Ongeveer 75% van de zonnestraling wordt door stratocumulus bewolking terug gereflecteerd de ruimte in, 10% wordt in de wolk in warmte omgezet en de overige 15% wordt aan het aardoppervlak geabsorbeerd. Doordat stratocumulus de meeste inkomende zonnestraling reflecteert, is er aan de top van de atmosfeer netto minder stralingsenergie beschikbaar dan in het onbewolkte geval. Een toename in de hoeveelheid stratocumulus over de hele aarde zal dus leiden tot een afkoeling van de atmosfeer. Een toename van enkele procenten in de mondiale bedekkingsgraad van stratocumulus zou het broeikaseffect volledig kunnen compenseren.

Naast de mogelijke invloed op het wereldklimaat heeft stratocumulus ook consequenties voor het lokale weer. Stratocumulus ontstaat meestal boven zee, in onze omgeving meestal de Noordzee. Onder invloed van de wind kan de bewol-

king over land drijven. Hierdoor neemt de zonnestraling aan het aardoppervlak drastisch af waardoor het overdag koud en somber blijft. De kennis van het ontstaan, de ontwikkeling en het oplossen van stratocumulus is beperkt. Dat maakt het moeilijk een goede verwachting te maken van zonneschijn en (maximum) temperatuur.

Het al of niet aanwezig zijn van stratocumulus in het bovenste deel van de grenslaag heeft een grote invloed op de turbulentie in de grenslaag.Voor een beter begrip van het ontstaan, de ontwikkeling en het oplossen van stratocumulus is het nodig om de turbulente uitwisseling van impuls, warmte en vocht door de grenslaag te begrijpen. In een grenslaag zonder bewolking wordt de uitwisseling voornamelijk bepaald door wrijving en convectie aan het aardoppervlak en door wrijving aan de top van de grenslaag. In een grenslaag met een wolkendek van stratocumulus wordt de turbulente uitwisseling mede bepaald door straling en de faseovergang van waterdamp naar vloeibaar water. Zowel de straling als de faseovergang kan een lokale opwarming of afkoeling in de grenslaag geven. Hierdoor kan de temperatuuropbouw van de lucht onstabiel worden waardoor er turbulente menging optreedt. Het is uiteindelijk de interactie tussen de bovengenoemde fysische processen die de turbulente uitwisseling in de grenslaag bepaalt. Voor de onbewolkte grenslaag, waarin de turbulentie veroorzaakt wordt door wrijving en convectie aan het aardoppervlak, zijn er eenvoudige modellen ontwikkeld die de ontwikkeling van de grenslaag redelijk beschrijven. Echter, zowel de veelheid aan fysische processen als hun mogelijk ingewikkelde interactie maken het moeilijk een eenvoudig model te maken voor de grenslaag met een wolkendek van stratocumulus.

Meestal is een wolkendek van stratocumulus zeer uitgestrekt. In dat geval zijn de wind, temperatuur en vochtigheid redelijk horizontaal homogeen, zodat we alleen de afhankelijkheid van de hoogte hoeven te bezien. In de vergelijkingen voor de gemiddelde windsnelheid, temperatuur en vochtigheid komen onbekende fluxen tengevolge van turbulentie en straling voor. De modellen die in de literatuur gebruikt worden om een stratocumulusdek te beschrijven kunnen ingedeeld worden naar de complexiteit die voor modellering van de turbulente fluxen gebruikt wordt; van menglaagmodel tot modellen voor grote wervels.

In een menglaagmodel worden gelijkvormigheidsprofielen voor windsnelheid, temperatuur en vochtigheid in de grenslaag aangenomen en een discontinuïteit in de waarden van de variabelen aan de top van de grenslaag. Met deze veronderstellingen worden de voorspelvergelijkingen voor de grenslaag sterk

vereenvoudigd. Om de vergelijkingen echter op te kunnen lossen moeten de onbekende turbulente fluxen aan de top van de grenslaag uitgedrukt worden in bekende grootheden. Voor de onbewolkte grenslaag is deze relatie redelijk bekend, maar in een grenslaag met een stratocumulusdek is er nog geen bevredigende oplossing voor dit probleem gevonden. Bovendien blijkt uit waarnemingen dat niet altijd voldaan is aan de veronderstelling dat de profielen van windsnelheid, temperatuur en vochtigheid gelijkvormig zijn.

In een model voor grote wervels worden de grotere wervels expliciet opgelost en moet alleen het effect van de kleinere wervels op de turbulente menging geparameteriseerd worden. Dit is een veel eenvoudiger probleem omdat de kleinere wervels een veel eenvoudigere dynamica hebben. Deze modellen zijn drie-dimensionaal en hebben een hoge resolutie (ongeveer 50 meter) waardoor ze zeer veel rekentijd vergen.

In dit proefschrift is een één-dimensionaal model ontwikkeld waarin het effect van alle turbulente wervels geparameteriseerd wordt. De turbulente fluxen worden gemodelleerd als het produkt van een uitwisselingscoëfficiënt en het verloop van de desbetreffende grootheid met de hoogte. De uitwisselingscoëficiënt wordt weer berekend met vergelijkingen voor de turbulente bewegingsenergie en de visceuse dissipatie (omzetting van turbulente bewegingsenergie in warmte door de viscositeit). Voor zowel de zonnestraling als de infrarode straling is een model ontwikkeld waarin de effecten van waterdruppels, waterdamp, kooldioxide, ozon en moleculaire verstrooiïng op de stralingsflux zijn verwerkt. De complexiteit van het model is zodanig dat de rekentijd beperkt blijft maar dat het effect van alle belangrijke fysische processen redelijk beschreven kan worden.

Hoofdstuk 2 geeft een overzicht van waarnemingen en modelstudies uit de literatuur. Daarop volgt een bespreking van de belangrijkste problemen die nog opgelost moeten worden. De belangrijkste fysische transportprocessen en hun invloed op de turbulente structuur en ontwikkeling van een stratocumulusdek worden in detail besproken.

In hoofdstuk 3 wordt het model beschreven en de invloed van de verschillende fysische processen op de turbulente menging in een grenslaag met een wolkendek van stratocumulus worden onderzocht. Bovendien worden modelresultaten vergeleken met gedetailleerde waarnemingen, gedaan in een stratocumulusdek. In appendix I is het model geverifieerd voor de onbewolkte neutrale en stabiele grenslaag. Omdat dit onderwerp buiten het direkte bestek van dit

proefschrift valt is het toegevoegd als een appendix. In hoofdstuk 4 zijn de modelresultaten vergeleken met waarnemingen in een wolkendek waarin de wrijving aan de wolkentop domineerde. Uit deze hoofdstukken blijkt dat verschillende combinaties van fysische processen kunnen leiden tot een totaal verschillende turbulente structuur van de atmosferische grenslaag.

In hoofdstuk 5 wordt de dagelijkse gang van een stratocumulusdek bestudeerd; onder invloed van de zonnestraling varieert de turbulente structuur van de grenslaag als functie van het tijdstip van de dag. De dagelijkse gang in verschillende seizoenen wordt bekeken en resultaten voor een dagelijkse gang gedurende de winter en zomer worden besproken. In de winter is de dagelijkse gang klein omdat de opwarming door de zonnestraling klein is ten opzichte van de afkoeling door de infrarode straling, terwijl in de zomer de dagelijkse gang in de wolkendikte groot is; dun overdag en dik 's nachts. Uit een gevoeligheidsstudie van het model voor begin- en randvoorwaarden blijkt dat de modelresultaten hiervoor niet erg gevoelig zijn. Dit geeft goede vooruitzichten voor de voorspelling van grenslaagbewolking in atmosfeermodellen.

Uit de modelresultaten en waarnemingen blijkt dat in een grenslaag met een dek van stratocumulus de turbulentie meestal wordt veroorzaakt door de afkoeling tengevolge van de infrarode straling aan de top van de wolk. De afkoeling maakt de grenslaag onstabiel en veroorzaakt turbulente menging, van de top van het wolkendek tot aan het aardoppervlak. Overdag kan, afhankelijk van de zonshoogte, ook de opwarming van het wolkendek tengevolge van zonnestraling belangrijk zijn. Omdat de opwarming ten gevolge van de zonnestraling over een diepere laag plaats vindt dan de afkoeling ten gevolge van de infrarode straling, is de opwarming een gedeeltelijke compensatie voor de afkoeling aan de top van de wolk. Als de totale opwarming van de wolk door de zonnestraling ongeveer gelijk of groter is dan de totale afkoeling door infrarode straling kan de lucht binnen het wolkendek onstabiel worden. Er vindt dan alleen menging plaats in het wolkendek, want de laag juist onder het wolkendek blijft stabiel.

Naast de straling kan ook de wrijving aan de top van de grenslaag een belangrijke invloed op de turbulente menging hebben. De wrijving aan de top van de grenslaag zal het inmengen van warme lucht van boven de grenslaag bevorderen. In de meeste gevallen zal deze warme lucht de afkoeling door infrarode straling maar gedeeltelijk compenseren. Echter, in sommige gevallen is de wrijving zo groot dat de warme lucht de afkoeling door infrarode stra-

ling aan de wolkentop volledig teniet doet. Dan is er geen convectie en is de grenslaag neutraal. In dat geval zijn de convectieve patronen, die zo typerend zijn voor stratocumulus verdwenen. Bovendien heeft de turbulentie dan een veel fijnschaliger structuur hetgeen het wolkendek egaal grijs maakt. In dat geval noemt men het wolkendek stratus in plaats van stratocumulus.

We hebben alleen stratocumulus boven zee onderzocht. In de toekomst is het nodig verder onderzoek te doen naar de invloed van het land op de turbulente structuur van de grenslaag met een wolkendek van stratocumulus. Dit zal een veel ingewikkelder interactie tussen bewolking en turbulentie te zien geven, omdat de netto straling aan het aardoppervlak dan mede de turbulentie in de grenslaag bepaalt. Een gat in het stratocumulusdek kan er dan voor zorgen dat het gehele wolkendek oplost.

1. INTRODUCTION

1. Problem and approach

In this study we consider the stratocumulus-topped atmospheric boundary layer (ABL) over the sea. The cloud decks that we consider are part of the atmospheric boundary layer and have typical cloud-top heights of about 1000 m. The air in the atmospheric boundary layer is turbulent from cloud top down to the earth's surface. The development of the cloud depends strongly on the momentum, heat and moisture input from the surface and on the turbulent transport throughout the whole atmospheric boundary layer. Moreover, the cloud deck itself plays an active role in determining the turbulent structure of the ABL through its radiational properties and phase changes. It is the interplay between all these processes that determines the turbulent transport, and as a result the development of the stratocumulus deck.

In this thesis we discuss a model that incorporates the most important physical processes present in a stratocumulus-topped ABL. The model is one-dimensional. It employs ensemble-averaged equations for the horizontal velocity (u and v), the wet equivalent potential temperature (θ_q) and the total water content (q_w). The vertical velocity has to be prescribed. The turbulent fluxes are modeled with the gradient approach in which the exchange coefficient is calculated from the turbulent kinetic energy (E) and the viscous dissipation (ε), the so-called E-ε model. In the entropy equation we have heating or cooling due to the radiative flux divergence. We have a model for both longwave and shortwave radiation. For the longwave radiation we use the emissivity or the "grey-body" approximation to calculate the longwave radiative flux. The effect of water vapor, carbon dioxyde and liquid water on the emissivity is taken into account. The shortwave radiative fluxes are calculated with a two-stream approximation. The shortwave model includes Rayleigh scattering, absorption by atmospheric gases (water vapour, ozone and CO_2) and absorption and scattering by cloud droplets.

The model has been used to study the influence of the different physical processes on the turbulent structure of the stratocumulus-topped ABL. Moreover the model results have been compared against detailed observations made in stratocumulus decks around the United Kingdom and off the coast of California. Finally a sensitivity test of the model for initial and boundary conditions is presented.

2. Relevance

Globally stratocumulus and stratus have the greatest average coverage of any low cloud type (Chapter 5). For instance, around the North Sea the average frequency of occurrence is about 65% with a cloud amount of 70% when present. As a result the average cloud amount, which is the product of the two former quantities, is about 45%.

Stratocumulus decks have a considerable influence on the energy balance at the top of the atmosphere and at the surface. The high albedo (~0.7) of clouds compared with the earth's surface (~0.1) gives a strong reduction of the net incoming shortwave radiation at the top of the atmosphere and at the earth's surface. The net outgoing terrestrial radiation on the other hand, both at the earth's surface and at the top of the atmosphere, is only slightly reduced. As a result an increase in low-level cloud cover will lead to a global cooling of the atmosphere. The strong impact of stratocumulus clouds on the surface energy balance makes that they are important for the interaction between the oceanic and the atmospheric circulation.

From the perspective of weather forecasting stratocumulus clouds are important because of their high frequency of occurrence, transient behaviour, and their impacts on aviation, agriculture and recreation. The lack of understanding of the formation, maintenance and dissipation of stratocumulus clouds makes it difficult to make reliable predictions, particularly in coastal regions. Therefore it is necessary to obtain a better notion of the physical processes which control the dynamics of the stratocumulus-topped ABL.

3. Outline of the thesis

The chapters 2-5 and appendix I have been individually published or submitted as journal articles. As a result some redundancy in the subject matter of these chapters is unavoidable.

Chapter 2 is a review paper on the stratocumulus-topped ABL. It discusses the conditions under which the formation and maintenance of stratocumulus cloud decks are favorable and its importance in both climate studies and weather forecasting. The chapter discusses the physical processes which determine the structure of the stratocumulus-topped ABL. Moreover, a review is given of the observational and model studies in the literature. Finally some general conclusions are given in chapter 2.

A comparison of the model results against observational data has been given in the chapters 3 and 4 and appendix I. In appendix I we have tested the turbulence model for the cloud-free neutral and stable ABL. This model verification is partially out of the subject of this thesis and has therefore been added as an appendix. In the chapters 3 and 4 we have used the model to study various combinations of physical processes in a stratocumulus-topped ABL and their combined effect on the turbulent structure of the ABL. Moreover, the model results are compared with detailed observational data made in the stratocumulus-topped ABL under totally different conditions.

In chapter 5 we have used the model to study the diurnal variation of a marine stratocumulus layer, which is forced by the shortwave radiative heating. The diurnal variation during different seasons is investigated and results for a typical mid-latitude winter and summer situation are presented. Finally in this chapter a sensitivity study of the model for initial and boundary conditions is presented.

The reader who is not familiar with the subject of this thesis or not interested in the details of the model and its result is advised to read chapter 2. This chapter gives an overview of the physical processes, model studies and observational studies. The reader who is a little more familiar with the subject or more interested in the details of the model and its results should read the chapters 2, 3, 4 and 5.

2. CURRENT PROBLEMS IN THE STRATOCUMULUS-TOPPED ATMOSPHERIC BOUNDARY LAYER+

Abstract

Extended sheets of stratocumulus (Sc) in the upper part of the atmospheric boundary layer (ABL) often occur under favourable meteorological conditions. These cloud decks are important both in climate studies and in weather forecasting. We review the current knowledge of the turbulent structure of the ABL capped by a cloud deck, in the light of recent observations and model studies. The most important physical processes determining this structure are the longwave radiative cooling at cloud top, the shortwave radiative warming by absorption in the cloud, the surface buoyancy flux, and wind shear across the top of the ABL. As a result the turbulence can cause entrainment against the buoyancy jump at cloud top. In cases where only longwave radiative fluxes and surface buoyancy fluxes are important, the turbulent structure is relatively well understood. When shortwave radiative fluxes and/or wind shear are also important, the resulting turbulent structure may change considerably. A decoupling of the cloud from the sub-cloud layer or of the top of the cloud from the rest of the ABL is then regularly observed. In no case are the details of the entrainment at cloud top understood well enough to derive a relatively simple formulation that is consistent with observations. Cloud-top entrainment instability may lead to the break-up of a cloud deck (but also to cloud deepening). The role of mesoscale circulations in determining fractional cloudiness is not yet well understood.

+ Submitted to Boundary-Layer Meteorology with A.G.M. Driedonks as co-author.

1. Introduction

The literature on the stratocumulus topped atmospheric boundary layer (ABL) has been growing at a rapid pace in the last few years. The purpose of this paper is to summarize these developments, both in modeling and observations, and to point out the key issues that remain to be solved. We will discuss the most important physical processes that influence the dynamics of these Sc-decks, and investigate to what extent the modeling of these processes is supported by observations.

The low-level cloud decks that we consider here (with cloud tops typically $\lesssim$ 1000 m) are part of the atmospheric boundary layer. The air is turbulent from cloud-top down to near the earth's surface and the behavior of the cloud depends strongly on the heat and moisture input from the surface and on the turbulent transport throughout the whole boundary layer. The cloud-deck itself plays an active role in determining the turbulent structure of the ABL through its radiative properties and phase changes, as we will discuss later.

Stratocumulus decks occur frequently over large areas of the world, especially over sea. In some areas their occurrence has a quasi-permanent character, in others they are of a more transient nature. The formation and maintenance of these extensive cloud decks are associated with the presence of a combination of favourable conditions:

a) Unconditionally stable stratification over a deep layer in the air aloft that confines convection from the surface and cloud formation to a relatively shallow boundary layer under a strong inversion, such that deep convection is suppressed. This type of stratification will often be present in areas with large-scale subsidence, which is typically found in subtropical high pressure systems and also in mid-latitude high pressure ridges between frontal systems behind cold fronts. We also may expect stable stratification over a deep layer in cold-air outflows from high-latitude continents.

b) Moisture supply from the surface and vertical mixing throughout the ABL. This is crucial to form and maintain the cloud deck against factors that tend to dissipate it. The entrainment of dry air at cloud top, large-scale subsidence, heating of the ABL through a surface heat flux or through radiative absorption, are all effects that tend to dry-out the ABL. Enough moisture supply from the surface to the cloud may compensate for this and maintain the Sc-deck. Therefore Sc-decks are usually found over sea.

Over parts of the oceans these conditions occur quasi-permanently and extensive Sc-decks form a persistent feature of the climate there. Schubert et al. (1979) mention four of these principal areas that are associated with the subsidence regions to the east of the subtropical high pressure systems: the eastern North Pacific off the coast of California and Mexico, the eastern South Pacific off the coast of Peru and Chile, the eastern North Atlantic off the coast of northwestern Africa, and the eastern South Atlantic off the coast of southwestern Africa. Herman and Goody (1976) report extensive stratus cloud layers over the Arctic Basin in the summer. Schubert et al. (1979) also report on extensive Sc-decks near the coast of north-eastern Africa in the summer.

Other areas where favourable synoptic conditions frequently occur and Sc-decks are often observed are near the southern coast of Australia (Platt, 1976), at mid-latitudes over the northern Atlantic and over the North Sea (Slingo et al., 1982; Roach et al, 1982; Nicholls, 1984), and in a variety of regions when cold continental air flows out over warmer water (e.g. over the Kuroshio current (Lenshow and Agee, 1976), over the Great Lakes (Lenshow, 1973), or over the Gulf Stream). Despite an increasing number of observational studies on the properties of Sc-decks there is still a great lack of observational material (Randall et al., 1984) (Platt (1981) summarizes the state of the art in 1981, since then other studies have been published: Brost et al., 1982a,b; Caughey et al., 1982,1984; Slingo et al., 1982a,b; Bonnel et al., 1983; Nicholls, 1984; Albrecht et al., 1985; Rodgers and Telford, 1986; Nicholls and Leighton, 1986). The frequency of occurrence and the horizontal scales of the cloud decks, the cloud top radiative properties, the turbulent transports within the clouds and the entrainment at cloud top are not yet sufficiently documented. It is anticipated that in the context of the International Satellite Cloud Climatology Project (ISCCP) this type of data will be improved (WMO, 1982; FIRE Research Plan, 1983). Randall et al. (1984) summarize the major research problems on the subtropical marine stratus and stratocumulus clouds, whereas reports on current research were given at the ISC/CAS Workshop on Modelling of the Cloud-topped Boundary Layer (WMO, 1985).

The importance of Sc-decks for weather and climate on all scales can hardly be over-emphasized. Extended quasi-persistent cloud layers strongly influence the earth's radiative energy budget and have a climatic impact at least on the regional scale. The high albedo of Sc-decks (typically ~ 0.6-0.8) compared with the underlying earth's surface (typically ~ 0.05 for water, ~ 0.2 for land) leads to a large reduction of the total absorption of

shortwave radiation in a vertical column compared to cloudfree areas. Also, the flux of solar radiation reaching the surface is considerably less in the Sc-case (about 30% of the incoming flux) than in the case without clouds (where it is ~ 70%). Both at the top of the atmosphere and at the surface, the changes in the longwave radiative fluxes due to the presence of low-level clouds do not compensate in any significant way for the changes in shortwave fluxes. Thus an increase in low-level cloudiness will lead to a net radiative cooling of the global atmosphere. Any realistic climate model has to reproduce the extensive Sc-decks in order to be able to assess their influence on the radiative budgets and consequently on climatic changes.

In addition to these quasi-persistent influences on the earth's climate, low-level clouds also strongly influence the local weather on synoptic and sub-synoptic space and time scales, due to their predominant effect on the heat and moisture exchanges in the ABL and on the radiation budget at the surface. It is a well-known key problem for short-range weather forecasting, especially in coastal areas, to predict the formation, maintenance, and dissipation of low-level cloud decks coming in from the sea.

2. Physical processes controling a Sc-deck

We will consider a solid deck of clouds in the upper part of the ABL, with irregularities in cloud top and cloud base that have a vertical extension much smaller than the cloud thickness. The cloudy ABL is usually in turbulent motion and features a large range of eddy scales. As in all turbulent flows we are not particularly interested in the detailed structure of all the eddies but rather in their average effect. We will assume that the structure of the cloud-topped ABL is quasi-horizontally homogeneous (in the statistical sense), i.e. that an ensemble-mean value can be obtained by a horizontal average over a large enough area. This implies that such an area is simultaneously large compared with the irregularities in the ABL and Sc-deck and small compared with the large-scale inhomogeneous variations in the external conditions controling the Sc-deck. Thus we may e.g. identify an area-averaged vertical velocity field $\overline{w}$ on a scale that is clearly separated from the vertical velocity field in the smaller scales of motion. This concept of averaging is widely used in turbulent flows, but leads to particular difficulties in the case of a cloud layer because the radiation field depends on the thermodynamic

variables of state in a strongly nonlinear way. Thus the average radiation field in general cannot be obtained from the average thermodynamic field except in conditions where the variances are small. We will discuss this further in the next section.

The presence of a cloud leads to considerable complications compared to a dry ABL because of the important role played by radiative fluxes and phase changes. In a dry ABL the turbulent structure, the mean variables and their evolution in time are controled by the large-scale external conditions and by the momentum, heat, and moisture exchanges at the earth's surface. Besides the longwave radiative cooling in the nocturnal surface inversion (André and Mahrt, 1982), the radiative fluxes play a minor role in the cloud free ABL, except indirectly through the surface energy balance. In a cloudy ABL the surface fluxes are also important, but radiative fluxes produce local sources of heating or cooling within the interior of the ABL and therefore can greatly influence its turbulent structure and dynamics. In Figure 1 a schematic picture is given of the various processes that have to be taken into account for a typical ABL capped by a cloud layer that is optically thick for longwave radiation. We will discuss these processes in more detail.

The vertical profiles of the radiative fluxes lead to heating or cooling of the ABL. For a cloud over sea, Slingo et al. (1982b) and Nicholls (1984) measured a net longwave radiative flux at the top of the ABL of about 50 W/m^2, which for an ABL of 1000 m thick corresponds to an averaged cooling rate of about 3.5 K/day, or if confined to a cloud layer of 500 m thick, of about 7 K/day. The net shortwave heating, which of course is a strong function of the time of the day, almost compensated the longwave cooling averaged over the whole ABL in these measurements. However, as can be seen in Figure 1 the vertical distribution of the heating or cooling rates is far from homogeneous. This inhomogeneous heating or cooling may give rise to localized, distinct sources of turbulent kinetic energy (TKE) within the ABL, depending on whether the net effect is stabilizing or destabilizing.

Longwave radiation

The net longwave radiative flux divergence is concentrated in a shallow layer near cloud top. Measurements (Brost et al., 1982a,b; Slingo et al., 1982a,b; Nicholls, 1984) indicate that this layer is approximately 50 m deep, thus producing strong local cooling (Figure 1) (if there are no upper level clouds present). Additionally there is a weak longwave warming at cloud base.

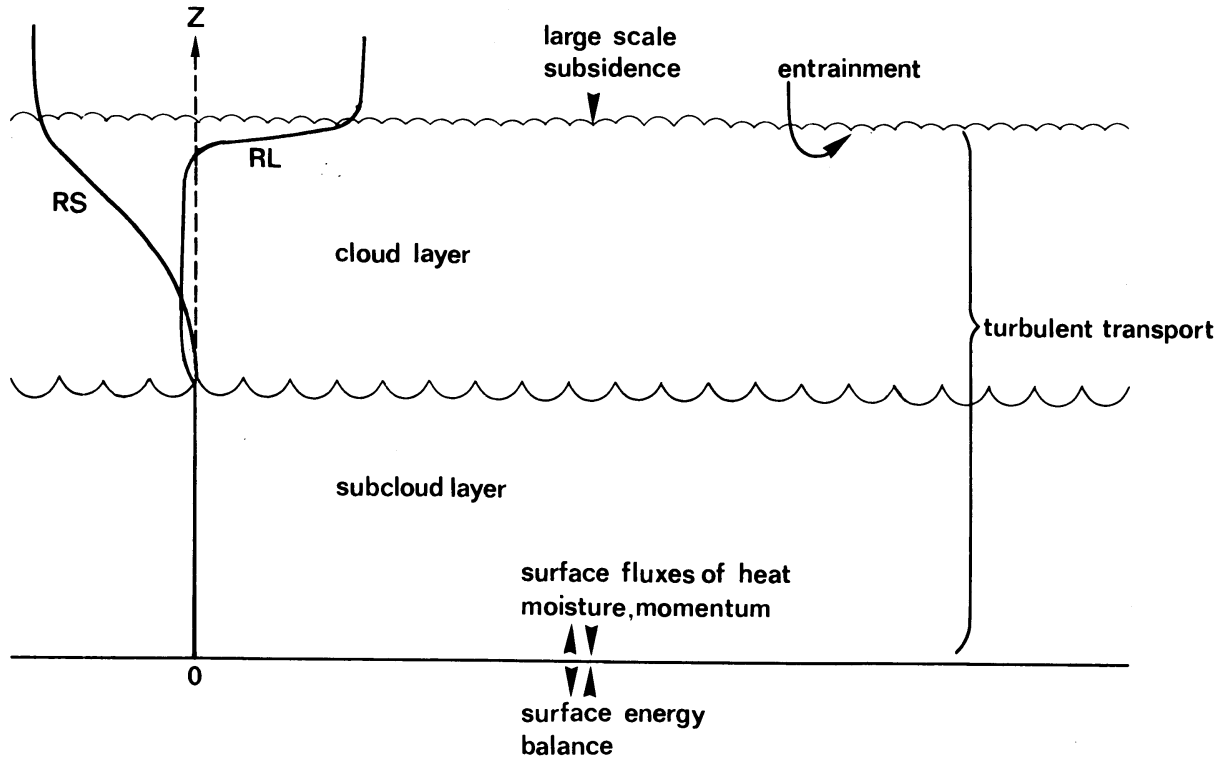

Figure 1. Schematic picture of the various interacting processes in a cloudy ABL: vertical profiles of net shortwave (RS) and net longwave (RL) radiation (minus their surface values), large-scale subsidence, surface fluxes, turbulent transport within the ABL, entrainment at the top.

One of the most common concepts of the effect of the cloud top cooling is that it destabilizes the whole ABL and generates convectively driven turbulence and an upward buoyancy flux throughout most of the ABL, much for the same reason that heating from the surface generates convective turbulence. Thus, even in the absence of any surface buoyancy flux, cloud top radiative cooling may generate enough turbulence to convectively mix the ABL.

Deardorff (1980b) in his three-dimensional large-eddy simulation of the cloud-topped ABL, simulated in one of his case studies a "dry cloud" that was radiatively cooled in the top 50 m while the surface buoyancy flux was about zero. The cooling at the top generated a positive buoyancy flux throughout most of the ABL with a maximum below cloud top and decreasing linearly to about zero at the surface. The dominant eddy size was indeed of the order of

the height of the ABL. The turbulence generated caused entrainment of stable air at the top of the ABL, with consequently a negative buoyancy flux there.

Condensation

In the case of a real cloud, in which phase changes occur, latent heat released by condensation forms an additional source for buoyant production of turbulence within the cloud and thus for entrainment at cloud top. Deardorff (1980b) discussed numerical simulations for such a case (in combination with cloud-top longwave cooling and an upward surface buoyancy flux). He found a tendency for the turbulent eddies not to extend over the whole ABL (cloud + subcloud layer) but to have dimensions related to the depth of the cloud or the subcloud layer. Caughey et al. (1982) made turbulence measurements in a layer of nocturnal Sc over England which were confined to the cloud layer. They found an increase in the integral length scale of the turbulence from cloud top to cloud base, toward a value about equal to the height of the whole ABL, thus not confirming the tendency found by Deardorff for an integral scale related to the depth of the cloud layer. They had no measurements in the subcloud layer, which contained a stably stratified, ~ 100 m deep layer adjacent to the surface, where apparently the convective turbulence generated by the cloud-top cooling did not contribute to the vertical transports. Yet it seems plausible, both from Deardorff's calculations and from the measurements of Caughey et al., that the main effect of the net longwave cooling, occurring in the upper ~ 50 m of the cloud, is to generate an upward buoyancy flux across the ABL which in turn drives the entrainment at the cloud-top. However, this picture may be considerably distorted when other turbulence production mechanisms are present or when cloud microphysics come into play.

Shortwave radiation

During the daytime, solar radiation will influence the cloud, both by its differential absorption and by its contribution to the surface energy balance. The vertical profile of the net shortwave radiative flux is markedly different from its longwave counterpart (Figure 1). Shortwave heating extends much deeper into the cloud than longwave cooling. Slingo et al. (1982b) argued that the combined effect of shortwave warming and longwave cooling may lead to a destabilization of the cloud layer itself, and to a decoupling of the cloud layer from the subcloud layer. In the presence of this decoupling, the entrained air at cloud top would only be used to warm and dry the cloud layer

instead of the cloud and the subcloud layer as is the case when both are mixed together. Further, the cloud would be cut off from the moisture input from the surface. Thus, this decoupling would lead to a much more rapid development and thinning of the cloud layer, resulting in breaking up of the solid cloud deck or at least to a marked daily cycle in its thickness. Both Slingo et al. (1982b) and Nicholls (1984) claim that this decoupling of the cloud and subcloud layers due to shortwave radiative effects plays an important role in Sc-dynamics. However, their measurements do not show a clear inversion at cloud base. Further support from measurements of the detailed turbulence structure, especially the length scales, in both layers is required.

Wind shear

Turbulence in the ABL may also be generated by wind shear. Wind shear in the vicinity of the top of the cloud layer can be quite strong, in particular in baroclinic circumstances or when the ABL is shallow (Brost et al., 1982a, b; Nicholls and Leighton, 1986 (case 564)). Even in the case of a dry convective ABL the role played by this wind shear in determining the entrainment is quite unclear (Deardorff, 1983; Driedonks and Tennekes, 1984). Measurements by Brost et al. (1982a, b) indicated that in their case the wind shear at cloud top generated turbulence locally, promoting entrainment of warmer air from above the inversion. This entrainment approximately balanced the cloud top radiative cooling. Thus in their study the cloud top radiative cooling did not generate convective turbulence throughout the ABL, in contrast to the usual concepts in the case without wind shear.

Cloud microphysics

Another complication might arise from the cloud microphysics. Cloud top radiative cooling might very well lead to condensation near cloud top, thus compensating the radiative cooling by local release of latent heat. The local increase in liquid water content may produce drizzle. Although this mechanism has not been conclusively verified, Brost et al. (1982a, b), Nicholls (1984), and Nicholls and Leighton (1986) found that the vertical flux of water by gravitational droplet settling was a significant fraction of the total.

Surface fluxes

An important role in the overall budget of the ABL is played by the surface fluxes of heat and moisture and by the entrainment of mass at the top

of the ABL. The surface fluxes depend strongly on the type of surface and its energy balance, and can vary in magnitude as well as in sign. Caughey et al. (1982) report a case of nocturnal Sc over land with a stable surface layer, Nicholls (1984) studied an Sc-deck over sea with upward surface fluxes.

Entrainment

The entrainment of mass at the cloud-top brings warmer and drier air down into the ABL, at the expense of turbulent kinetic energy. The amount of entrainment has to be parameterized in terms of the production of turbulence in the ABL by buoyancy forces and wind shear, and requires insight into the structure of the turbulence and its length and velocity scales as in the case of a dry ABL. This parameterization of the entrainment is still questionable in the cloud-topped ABL due to the complicated sources of turbulence that are related with radiation and condensation.

Entrainment instability

An additional complication in the cloud-topped ABL is related to evaporative cooling of the warm and dry air that is entrained. An entrained parcel of dry air will be cooled by evaporation of cloud droplets into it, thus promoting entrainment by effectively reducing the amount of potential energy that has to be overcome. This evaporative cooling can, under some circumstances, lead to an instability process in which the parcel is cooled so much that it becomes negatively buoyant and sinks through the cloud. This cloud top entrainment instability (Randall, 1980b; Deardorff, 1980a; Hanson, 1982, 1984, 1987; Mahrt and Paumier 1982; Randall, 1984b; Nicholls and Turton, 1986) leads to large entrainment rates and is thought to be one of the mechanisms at play in breaking up a solid cloud deck.

From observations (Mahrt and Paumier, 1982; Nicholls and Turton, 1986), however, it is found that even if the instability criterion of Randall (1980b) and Deardorff (1980a) is met the cloud is often not entraining more rapidly than usual. Nicholls and Turton (1986) have argued that it is necessary to include the fact that mixing takes place between various fractions of inversion air and cloudy air (Mahrt and Paumier, 1982). This in contrast to the assumption of Randall (1980b) and Deardorff (1980a) that the mixed parcel remains just saturated, and thus take into account only one mixing ratio. By evaluating the stability criterion as a function of the mixing ratio Nicholls and Turton (1986) showed that even if the instability criterion of Randall

(1980b) and Deardorff (1980a) is met, it may be that only over a very small range of mixing ratios are negatively buoyant mixtures produced. Assuming that all values of the mixing ratio are equally important, Nicholls and Turton (1986) defined a new stability parameter. This new stability parameter implicitly includes all the factors influencing evaporative cooling and is therefore a better measure of the stability of an inversion to mixing processes. It seems that this promising concept has to be tested further against measurements. Although entrainment of dry air from aloft could help to dissipate the cloud, Randall (1984b) demonstrated that under many realistic conditions the effect of entrainment is that the cloud top tends to rise more quickly than the cloud base, so that the cloud depth tends to increase with time. Randall (1984b) called this process "cloud deepening through entrainment" (CDE).

Mesoscale entrainment instability

Another instability, that has the structure and horizontal scale of mesoscale cellular convection (Rothermel and Agee, 1980; Fiedler, 1984), is called mesoscale entrainment instability (MEI). Fiedler (1984) showed that a mixed-layer model allowed for an instability in which mesoscale fluctuations in buoyancy and humidity are amplified in phase. His linear stability analysis of these disturbances revealed that the growth rate of this instability peaks at aspect ratios of about 30:1. The smaller scales are damped by horizontal diffusion and the larger scales by the dynamic response of the stable layer above the ABL. MEI may be one of the mechanisms in breaking up a stratocumulus deck; moreover, its relation with mesoscale cellular convection should be investigated.

Subsidence

The mean vertical subsidence velocity is of importance in determining whether the cloud deck will dissipate or not. In order to maintain the cloud deck against the subsidence, a large amount of warm and dry air has to be entrained at cloud top, which consequently requires a compensating supply of moisture from the surface. Caughey et al. (1982), in their study of nocturnal Sc over land, concluded that in their case subsidence was the main reason for drying out the ABL and dissipating the clouds.

In summary, the dynamics of a Sc-deck will be determined by the external conditions (subsidence, dynamic and thermodynamic conditions of the air aloft,

net radiative fluxes at cloud top, surface conditions) and by the internal structure and dynamics (sources of turbulence, structure of the turbulence, redistribution of heat and moisture in the ABL, the amount of entrainment that can be sustained by the turbulence in the ABL against the opposing conditions at the top).

3. Modeling of the ABL capped by a cloud deck

A description of the actual evolution of an ABL, capped by a cloud deck, thus requires knowledge of both these external conditions as well as the internal structure and dynamics. The flow in the ABL is turbulent and cannot be described in its intricate details. We are usually only interested in its statistically averaged properties. However, before being able to solve the equations for these statistically averaged properties we have to model part of the flow. This modeling requires a definition of the averaging process and a model for the unresolved part of the scales of eddies in the flow. Essentially two different types of averaging procedures are employed for turbulent flows: ensemble-averaging and volume-averaging. In ensemble-averaged models the averaged statistics do not show any chaotic turbulent behavior; the latter has been fully averaged. Thus the averaged statistics vary smoothly in time and space with typical scales of variation corresponding to the integral scales of the turbulence based on the geometry of the flow. In these models the combined effect of all the turbulent eddies has to be parameterized. Thus the closure of the higher-order terms in the equations requires a parameterization of the overall effect of all scales of turbulent eddies. This makes the parameterization in these models quite sensitive to the particular flow configuration and a lot of turbulence engineering is required. In volume-averaged models, or large-eddy simulations the variables are averaged over a volume that is small with respect to the large eddies in the ABL and large compared with the smallest eddies. Thus the structure of the large eddies is calculated explicitly (on the resolvable scales) and only the effect of the small eddies has to be parameterized. Since the averaging volume is presumably chosen to be in the inertial subrange of the turbulence, this parameterization might be relatively simple and not sensitive to the flow configuration. From large-eddy simulations, ensemble averages are usually obtained by taking horizontal space averages as well as averages in time. The amount of computer time required for

large-eddy simulations is as yet prohibitive for extensive experiments.

In the modeling of the cloudy ABL, only two studies have been done with a large-eddy simulation model (Deardorff, 1980b; Moeng, 1986). Other models employ ensemble-averaging. Most of the effort in the latter models has been spent on mixed-layer type of models, originated by Lilly (1968) and subsequently elaborated by a large number of authors (Betts, 1973; Deardorff, 1976a, 1980a, 1980b, 1981; Kraus and Schaller, 1978; Fravalo et al., 1981; Kahn and Businger, 1979; Randall, 1980a, 1980b; Schubert et al., 1979; Stage and Businger, 1981a, 1981b). Multi-level models with a number of layers in the ABL and employing higher-order closure schemes for the turbulence have been used e.g. by Oliver et al. (1978), Moeng and Arakawa (1980), Chen and Cotton (1983b), Bougeault (1985) and Duynkerke and Driedonks (1987).

Two aspects are of particular importance in all these models: the radiative fluxes and the turbulent transports as well as their interaction.

The radiative fluxes

The problem of the radiative flux distribution is related to the conditions at the top of the cloud layer where strong gradients in temperature and liquid water occur. In reality the local or instantaneous interface between the cloud top and the air above is very sharp and has a thickness of the order of a meter. Caughey et al. (1982) report from measurements a transition from turbulence to no turbulence within a distance of 4 m. However, this locally sharp interface exhibits irregularities in space and time in the form of domes and cusps with a vertical extension of typically some tens of meters, depending on the intensity of the turbulence in the ABL and on the stability above the cloud.

In numerical models, with only a limited vertical resolution, the local, instantaneous interface at cloud top cannot be resolved in any detail, but it is smeared out over the vertical grid distance, thus leading to large truncation errors. This sharp edge of the boundary layer is also present in the dry convective ABL and in other entraining turbulent flows. However, in the case of a cloud deck, a poor vertical resolution has a greater impact because the longwave radiative cooling, which is an important mechanism for the generation of turbulence in the ABL, occurs mainly over a small depth below cloud top. In fact, no dynamical model has as yet able to calculate the longwave radiative flux distribution near cloud top explicitly in detail, but it must be parameterized. In Deardorff's (1980b) large-eddy simulation the vertical

resolution (as well as the horizontal) was 50 meters and the longwave radiational cooling was rather arbitrarily prescribed to occur locally over the uppermost grid value with a given minimum liquid water content. Moeng (1986) used an emissivity model for the longwave radiation, which included the effect of water vapour and cloud droplets. The vertical resolution was 25 m up to the model top of 1 km. The radiation parameterization was applied at each vertical column for each time step. In principle, in a large-eddy model the grid size could be reduced to better resolve the cloud-top processes; however, this has not yet been done due to considerable computational difficulties.

In ensemble-averaged models, such as mixed-layer models, the averaging process itself introduces an additional problem for the calculation of the longwave radiative flux distribution and its effects on the turbulence. Although the local interface between the cloud top and the air above in a real-world ABL is very sharp, after ensemble-averaging (or horizontal averaging) the vertical profiles of temperature, liquid water, and other quantities will exhibit at the ABL-top a transition layer or entrainment zone with a vertical extension of some tens of meters (see Figure 2).

Within the entrainment zone the ensemble-averaged cloud fraction will gradually decrease from 100% below the cusps to 0% above the domes. Since this entrainment zone is not always small compared to the distance over which radiative cooling occurs, it becomes problematic in ensemble-averaged models to locate this cooling region and to model its effects, since an important fraction of it is associated with the entrainment zone. This issue has been the subject of extensive discussion in many papers (Lilly, 1968; Schubert, 1976; Kraus and Schaller, 1978; Deardorff, 1976a; Schubert et al., 1979; Kahn and Businger, 1979; Deardorff, 1980b; Randall, 1980a; Lilly and Schubert, 1980; Deardorff, 1981; Schaller and Kraus, 1981a, 1981b; Stage and Businger, 1981a, 1981b; Chen and Cotton, 1983a, b; Nieuwstadt and Businger, 1984). Deardorff (1976a, 1981) argued that in a realistic ensemble-averaged model part of the longwave cloud-top cooling should be located within the entrainment zone and that this part of the cooling serves to cool the entrainment zone directly without generating any turbulence. On the other hand, that part of the radiative cooling that occurs below the entrainment zone will produce turbulence through convection in the ABL much in the same way as does heating from below, thus promoting entrainment indirectly. Deardorff (1981) thus studied the radiative cooling distribution and its dependence on the depth of the entrainment zone and the radiative extinction length and concluded that

there is strong sensitivity of the ABL-dynamics to these factors. Kahn and Businger (1979), on the other hand, argued that longwave cloud-top cooling is never used to cool the entrainment zone directly but rather that this cooling is invariably associated with cloudy air and all of it should generate turbulence. They attributed Deardorff's argument to the use of averaged profiles and considered it to be artificial. They suggested that it is more realistic even in the averaged profiles to consider a very thin interfacial layer and to locate all in-cloud radiative cooling below it.

Schaller and Kraus (1981a, 1981b) and Fravalo et al. (1981) used a detailed model for calculating the radiative fluxes. This requires a clear positioning of the thermodynamic and of the cloud parameters. They considered the same structure of the averaged vertical profiles as in Figure 2, but did not let the cloud extend above h_o. Thus they did not associate Δh with an entrainment zone where turbulent and non-turbulent air coexist, but they

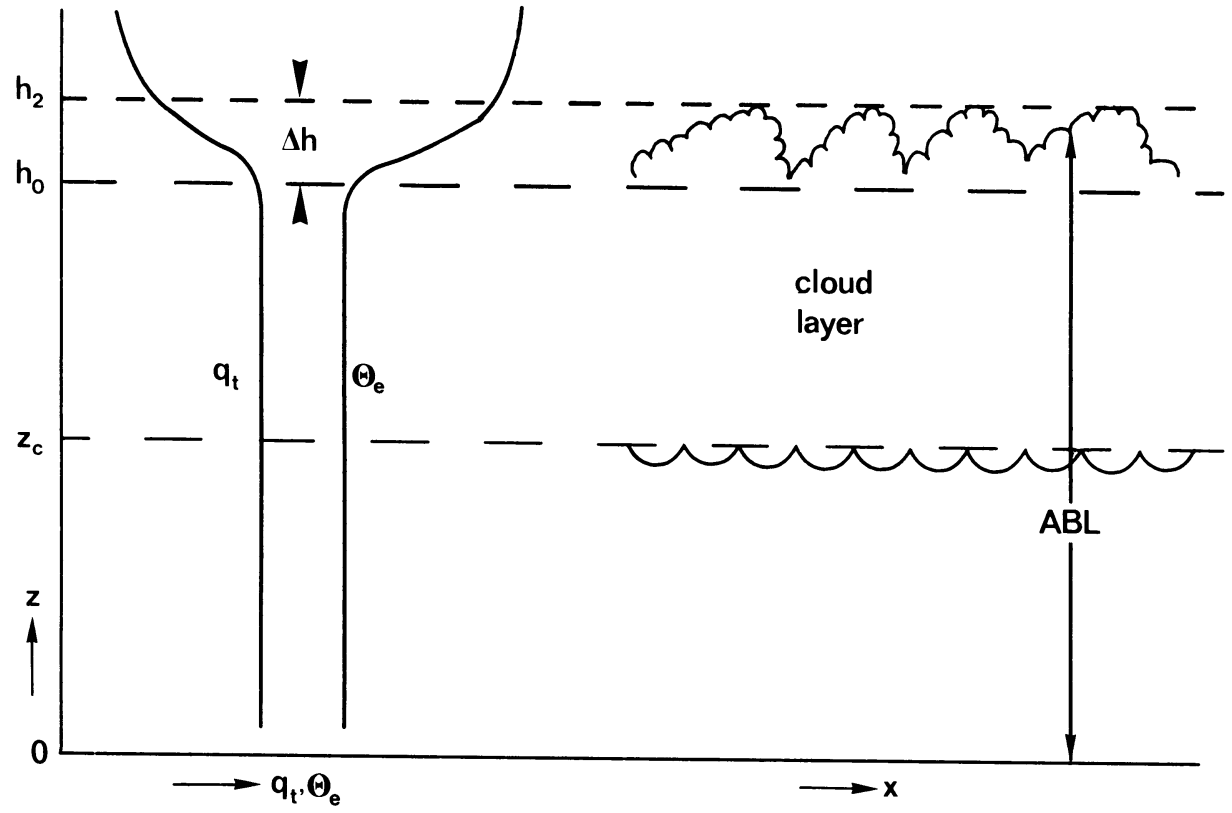

Figure 2. General structure of mean vertical profiles of equivalent potential temperature Θ_e, and total water content q_T, in a cloud-topped ABL. Cloud base is at z_c. The entrainment zone with fractional coudiness is labelled Δh. (After Deardorff, 1981).

considered Δh to be the depth of the above-cloud clear air inversion, with no clouds and turbulence in it. With this assumption the radiative flux profiles can be calculated, both in the cloud layer and within the clear air in the inversion. However, since these authors obviously did not associate Δh with entrainment, but rather with clear-air radiative fluxes, it is difficult to justify that their use of the overall differences in thermodynamic quantities over Δh to govern the entrainment. Nieuwstadt and Businger (1984) therefore proposed to split these overall differences into a part that is associated with entrainment (occurring over a very thin layer) and another part associated with clear-air radiation above the cloud. In fact, all these authors take the entrainment zone to be infinitesimally thin. In his large-eddy simulation Deardorff (1980b) also could not solve the problem, mainly because his radiation parameterization was very rudimentary. Moeng (1986) used a vertical grid distance of 25 m, which is of the same order as the e-folding depth (about 20 m) of the longwave radiative cooling. Chen and Cotton (1983b) used a multi-level ensemble-averaged model with vertical grid distance of 100 m. In order to account for an entrainment zone they used a partial condensation scheme within a grid volume. Their conclusions are dependent on this scheme.

It must be concluded that one of the remaining problems in understanding the detailed behavior of a Sc-deck is the proper distribution of the longwave radiative fluxes. Especially in the case where the vertical cloud top excursions are of comparable (or larger) distance than the radiative extinction length, this problem has not been solved.

Turbulent transport

The modeling of the turbulent transports is another major problem. Most of the effort has been spent on mixed-layer models in which both the subcloud and the cloud layer are well mixed up to a capping inversion right above cloud top. In idealized mixed-layer models the depth of the capping inverion is reduced to a discontinuity. It should be emphasized that a crucial assumption in mixed-layer models is that the turbulence is strong enough to actually mix the entrained air over the entire mixed-layer depth. Other assumptions are that the turbulence is in local equilibrium with the external conditions, i.e. that the time scale for the turbulence is small compared to the time scale for the change of the external conditions and that the entrainment itself does not influence the shape of the profiles. All these assumptions are necessary to

justify that the shape of the vertical profiles can be prescribed as in mixed-layer models and that this shape does not depend on time and can be written in self-similar form. Once well-mixed profiles are assumed, the crucial problem is to determine the entrainment rate. In mixed-layer models the entrainment rate has to be formulated in terms of bulk turbulence generating mechanisms within the mixed-layer and the opposing influences at the top of the ABL. Since the rate of change of TKE due to entrainment is only a small fraction of the total production of TKE in the mixed layer (most of it is lost to viscous dissipation), this parameterization is not easy and quite controversial and, especially in the cloud-topped ABL, poorly guided by observations. For a clear convective ABL without clouds, the entrainment formulation has been solved to a satisfactory extent for most practical applications in the atmosphere (e.g. Driedonks and Tennekes, 1984), although there are still some problems when significant wind shear near the ABL-top is present (Deardorff, 1983). In the case of the cloud-topped ABL no satisfactory solution whatsoever has been reached, even in the case when only buoyancy effects are relevant and without wind shear. The main reasons for this lie in the much more complicated turbulence production mechanisms in a cloud-topped ABL compared to a clear ABL and in the very scarce number of measurements of the structure of the cloud-topped ABL. Thus the entrainment relations rely on assumptions rather than on experimental guidance. Randall (1984a) summarized current ideas. To illustrate the general lines of thought we consider a dry cloud (without phase changes but with radiative effects) with no surface fluxes but yet well mixed as a result of buoyancy generated by radiative cooling at the top. This radiative cooling is taken to be localized in a very shallow layer δz_r below cloud top and the radiative flux profiles are taken to be linear. The vertical profiles of potential temperature, net longwave radiative flux, and total heat flux are shown in Figure 3. The governing equations for this mixed layer are ($\overline{w} = 0$):

$$\frac{\partial \theta_m}{\partial t} = \frac{-(\overline{\theta w}_h + \Delta R)}{h} \tag{1}$$

$$\frac{\partial \Delta\theta}{\partial t} = \gamma \frac{\partial h}{\partial t} - \frac{\partial \theta_m}{\partial t} \tag{2}$$

$$-\overline{\theta w}_h = \Delta\Theta \frac{\partial h}{\partial t} \, . \tag{3}$$

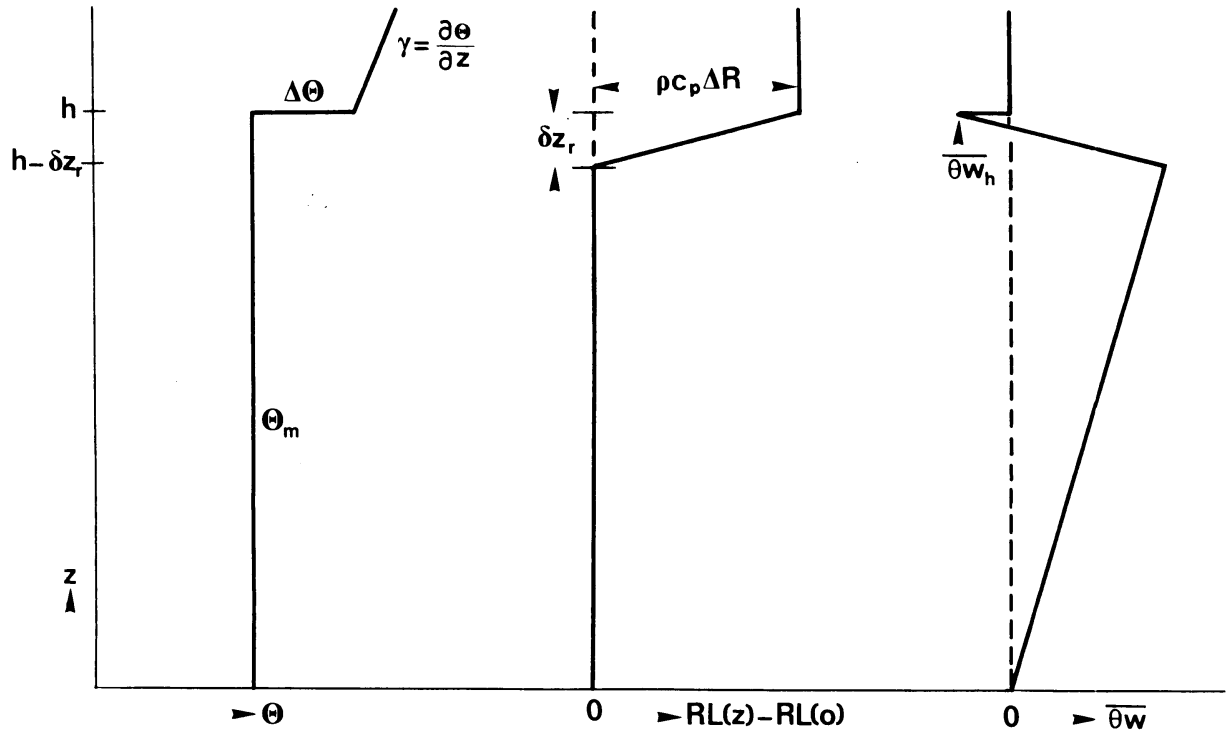

Figure 3. Vertical profiles of potential temperature Θ, net longwave radiative flux RL, and total heat flux $\overline{\theta w}$, for the case of a well-mixed ABL capped by a "dry cloud". No surface fluxes. Radiative cooling depth δz_R.

These equations have to be supplemented by an entrainment relation in order to be solved. For this purpose the vertically integrated TKE budget is used; which, with only the most important terms retained, this reads approximately:

$$\frac{g}{T} \int_0^h \overline{\theta w}\, dz = \int_0^h \varepsilon\, dz, \qquad (4)$$

with ε the viscous TKE dissipation. In symbolic notation (4) is written as:

$$B = D\ . \qquad (5)$$

A parameterization of the entrainment rate usually requires two further assumptions: a) the total buoyancy flux integral B can be split into a part P that produces TKE and a part N that destroys or consumes TKE (due to negative buoyancy forces); b) the dissipation D is a constant fraction (1-A) of P. Thus it is assumed that

$$D = (1 - A)P, \tag{6}$$

where A is a constant. Then, with $B = P - N$, (5) reduces to

$$AP = N. \tag{7}$$

Given the constant A (from experiments?!), closure is then achieved when P and N are defined.

This partitioning of B into P and N is a controversial issue with important consequences for the model results. Deardorff (1976a), Kraus and Schaller (1978), Randall (1980a), Fravalo et al. (1981) assumed that P is defined as the integral of the buoyancy flux $\overline{\theta w}$ over the region where it is positive, and N over the region where it is negative. Then, with the configuration of Figure 3, this leads to the entrainment relation (to first order in $\delta z_r/h$):

$$\frac{(\overline{\theta w}_h/\Delta R)^2}{(\overline{\theta w}_h/\Delta R) + 1} \frac{\delta z_r}{h} = A_D \tag{8}$$

In (8) A_D has a value of ~ 0.04, in analogy to the dry convective mixed layer. This expression has the following two properties:

a) In the limit for $\delta z_r/h \to 0$ this leads to: $\overline{\theta w}_h = -\Delta R$, independent of A_D. Thus in this formulation the cloud-top radiative cooling is generating direct entrainment (see earlier) by effectively cooling the air in the inversion above the cloud. This corresponds to the original formulation by Lilly (1968). It does not seem physically realistic, however, because the cloud-top cooling does not generate any turbulence in the ABL in this formulation.

b) The entrainment is rather sensitive to the depth over which radiative cooling takes place (δz_r), which is at least an inconvenient property.

Both properties of this formulation are not very attractive. Stage and Businger (1981a, 1981b) assumed quite a different partitioning of B into P and N. They supposed the <u>total</u> buoyancy flux to be the result of independently acting processes, each process being either productive (and thus contributing to P) or consumptive (and thus contributing to N). In the context of our simple example their reasoning leads to Figure 4, and thus to the entrainment relation:

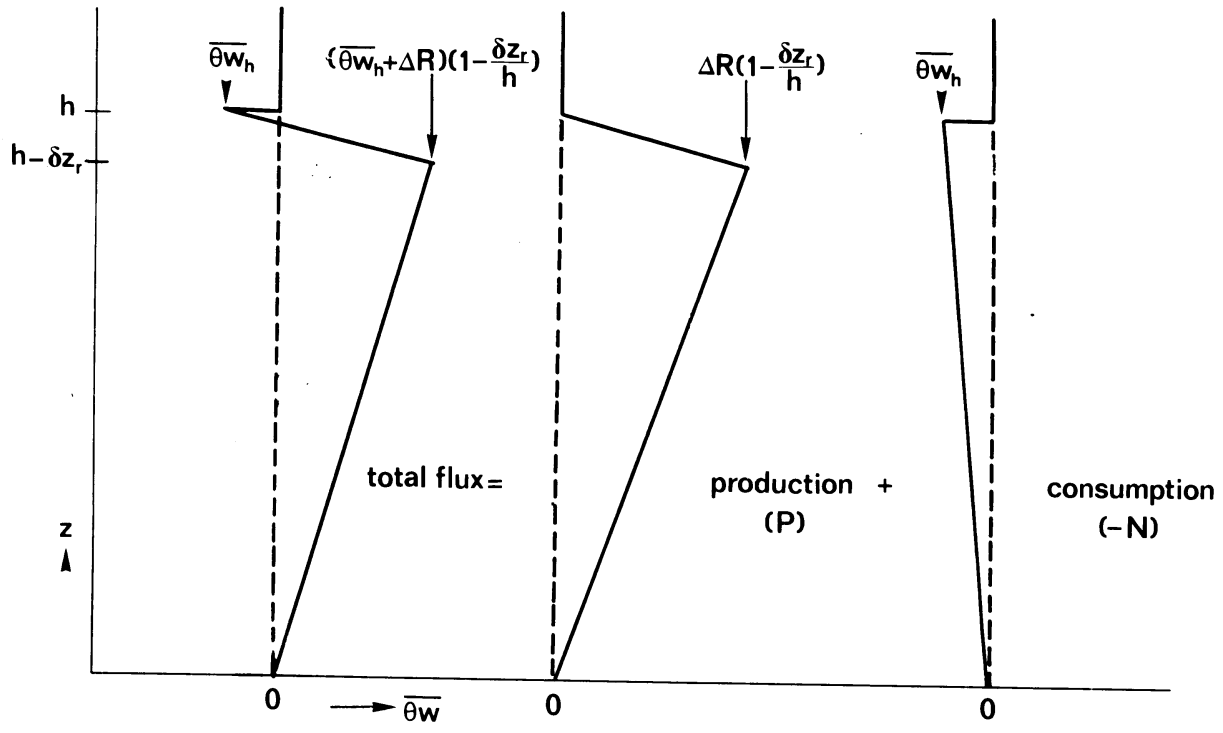

Figure 4. Partitioning of the total heat flux of Figure 3 into production (P) and consumption (-N), according to Stage and Businger (1981).

$$\frac{\overline{\theta w}_h/\Delta R}{1 - \frac{\delta z_r}{h}} = A_{SB} \ , \qquad (9)$$

where now A_{SB} has the value ~ 0.2, still in analogy with the dry convective mixed layer ($A_{SB}^2 = A_D$). This formulation and the former lead to equivalent results when applied to a dry convective mixed layer, forced only by a surface heat flux and without radiative effects. However, in the present case, (9) has quite different properties from (8):

a) In the limit for $\delta z_r/h \to 0$, eq. (9) leads to $-\overline{\theta w}_h = A_{SB}\ \Delta R$.
This formulation has as a physical interpretation that the cloud-top cooling generates an upward buoyancy flux in the ABL which in turn causes entrainment at the top (indirect entrainment).

b) This formulation leads to an entrainment relation that is not sensitive to the value of δz_r.

Randall (1984a) argued that the low sensitivity of the entrainment rate

to the depth of the layer where radiative cooling occurs (δz_R) in the formulation of Stage and Businger (9) is due to the fact that they interpreted the distribution of ΔR over the depth δz_R as a reduction of the total production P, and not as a reduction of the total consumption N (see Figure 4). He stated that the latter could equally well be the case (which would re-introduce the strong dependency of the entrainment on δz_R) because radiative cooling of warm entrained air parcels reduces their opposing buoyancy and thus decreases the consumption N or, equivalently, the amount of work to be done by the turbulence. The validity of Randall's argument depends on the question of whether the time scale for radiative cooling of warm air parcels is of the same order as the time scale of the turbulence. Coantic and Simonin (1984) did a study on the direct radiative modifications of a turbulent fluctuating temperature field. They concluded that, for usual conditions, the characteristic time scale for radiative dissipation of temperature fluctuations is much longer than the time scale for inertial turbulent transfer. Thus it seems likely that Randall's argument is invalid and addresses only a very small effect. Before radiation can appreciably cool entrained air parcels, they are already mixed by the turbulence. For this reason also, radiative-turbulence interactions do not play a significant role in the budgets for the heat flux and temperature variance. Radiative cooling does not influence the heat flux directly, but only indirectly by its action on the mean temperature gradient. Thus radiative cooling may be prohibited from generating much convective turbulence only when entrainment is forced by a local mechanism at the cloud top, e.g. wind shear, and the turbulent intensity in the bulk of the mixed layer is weak (no surface heat flux), as in Brost et al. (1982a, b). In that case the radiation would be used to locally cool the top of the ABL which would heat up due to entrainment. However, no entrainment relation has been formulated that includes these effects, not even for the dry convective ABL (Deardorff, 1983).

Deardorff (1980b) derived from his large-eddy simulation an entrainment relation based on the local vertical velocity variance at cloud top (σ_w). From his results it can be concluded that the ratio of σ_w/w_* (with w_* the generalized convective velocity scale defined by Deardorff (1980b)) at the inversion is enhanced if the buoyancy production takes place closer to the inversion (radiative cooling, phase changes). When this is the case relatively more TKE is converted to potential energy (entrainment) and thus less TKE is dissipated. This increased entrainment may be further enhanced by the evaporative cooling of entraining air. However it is not yet clear how to

specify this local vertical velocity variance at cloud top when only bulk properties are known.

In order to avoid the concept of a vertically well-mixed boundary layer which would not be appropriate for a description of the decoupling of the cloud layer from the sub-cloud layer as observed by Nicholls (1984), Turton and Nicholls (1986) developed a multiple mixed layer model. A constraint on the buoyancy flux profile was introduced which enables the well-mixed layer to separate into two independently driven layers. It was shown that the inclusion of decoupling leads to a stronger variation in cloud structure. This model can be a useful diagnostic tool because it has a number of features which are similar to those observed and provides a consistent framework within which the observations can be interpreted.

It must be concluded that there is as yet no general entrainment formulation for the cloud-topped ABL. It may be anticipated that the results obtained are applicable only to a limited range of cloudy ABL's.

Apart from mixed-layer models, in which the whole ABL is treated in a bulk formulation and the vertical profiles are assumed to have a self-similar form, multi-level ensemble-averaged models have been used to study the cloud-topped ABL (Moeng and Arakawa, 1980; Chen and Cotton, 1983b; Moeng and Randall, 1984; Bougeault, 1985; Duynkerke and Driedonks, 1987). In multi-level models, higher-order turbulence closure schemes (up to closure of the equations for the third-order moments) have been applied. Zeman (1981) and Wyngaard (1982) give reviews of these modeling techniques. Crucial problems are presented by the modeling of the effects of buoyancy in the closure of the pressure-velocity gradient terms, the triple correlation and transport terms and the mechanical and thermal dissipation rates. Moeng and Arakawa (1980) used a down-gradient diffusion assumption for the triple correlations, which is not correct in buoyancy driven turbulence. These terms often govern the dynamics in a convective ABL. Chen and Cotton (1983a) and Moeng and Randall (1984) used closure schemes for the pressure terms and the transport terms that are for the most part based on Zeman (1981). Zeman (1981) noticed some severe problems, especially for the pressure terms, in real boundary layers with large anisotropy or buoyancy effects.

In most higher-order closure models the turbulent time scale and length scale are essential parameters that have to be obtained through the viscous dissipation (time scale ~ energy/rate of viscous dissipation). However, modeling of the dissipation is a notoriously difficult task. Sometimes an

extra evolution equation is formulated for the dissipation with the unknown terms modeled by quantities that are accessible in the higher-order closure model (Zeman, 1975). Other authors instead use an evolution equation for the length scale (Mellor and Yamada, 1982). Most often, however, a dissipation or length scale equation is completely avoided and instead a diagnostic length scale is formulated (André et al., 1978; Chen and Cotton, 1983a). Such a diagnostic length scale formulation causes fewer problems but oversimplifies the turbulence, which is then constrained to have some anticipated state. Chen and Cotton (1983b) avoided this for the case of a stratocumulus-topped ABL and proposed a direct parameterization of the turbulent time scale (~ energy/ buoyancy production) which is equivalent to a rudimentary dissipation equation. Moeng and Randall (1984) noticed some spurious results in their model for the cloudy case. Bougeault (1985) presented results of a third-order turbulence closure model for a run of 7 days, which showed features very similar to those observed (Nicholls, 1984). Duynkerke and Driedonks (1987) showed results of a higher-order closure model that compare favourably with different types of experiments. Higher-order closure models seem to be able to describe a greater variety of phenomena in the cloud-topped ABL than the mixed-layer models since the assumption of well-mixedness is often too strong. Due to their flexibility higher-order closure models allow for the decoupling between the cloud layer and sub-cloud layer (Bougeault, 1985; Duynkerke and Driedonks, 1987), and they can simulate both shear and buoyancy production and its influence on the entrainment rate (Duynkerke and Driedonks, 1987). Additional information is available for diagnosis or prediction of fractional cloud coverage. However, there are still a number of theoretical and conceptual problems to be solved in higher-order closure models.

The use of large-eddy simulations (LES) as "controlled field experiments" on the computer (Deardorff, 1980b; Moeng, 1986) is a promising approach in this area, since problems with direct measurements can be quite severe over some stratus regimes, whereas the capability and accuracy of these LES is increasing. Recently Moeng (1986) presented results from a LES model for two different cases. From this study it can be concluded that the turbulent structure in the cloud-topped ABL differs significantly from one case to another, because of the many physical processes involved. A lack of understanding as to how these processes interact causes the uncertain usefulness of statistical models (e.g. mixed-layer models). Hence the LES can be used to study the closures in statistical models.

4. Observations of the stratocumulus-topped ABL

The development of theoretical models for stratocumulus behavior has a long and rich history. In particular the interaction between the mean fields in the cloudy ABL and the turbulence contains many unsolved problems and has given rise to a lot of assumptions. Unfortunately, the observations on which these assumptions should be based are very scarce, particularly observations in which both the mean conditions and detailed observations of the turbulence are documented.

Measurements of turbulent structure of a stratiform cloud have been taken by Coulman (1978), however without liquid water measurements. Recently, more complete sets of observations have been reported by Brost et al. (1982a, b) and Albrecht et al. (1985) on stratocumulus clouds off the California coast, by Roach et al. (1982), Caughey et al. (1982), and Slingo et al. (1982a) on nocturnal stratocumulus over the UK, by Nicholls (1984) on stratocumulus over the North Sea, Rodgers and Telford (1986) on stratocumulus off the California coast, and Nicholls and Leighton (1986) on six cases of stratocumulus around the UK. Other recent experimental results, mainly on the cloud and radiation parameters and not on the turbulence, have been reported by Slingo et al. (1982b), Bonnel et al. (1983), Hignett (1987) and Stephens and Platt (1987). Earlier experiments on mean conditions and radiation have been summarized by Platt (1981). We will discuss here mainly the recent observations including turbulence measurements, since they are most important in the light of the models discussed above.

The observational case studies all refer to a solid Sc-deck below an inversion. However, they differ greatly in the conditions that influence this Sc-deck.

In the case studies of Brost et al. the ABL was about 500-600 m thick with the cloud deck occupying about 300-400 m of it. The surface buoyancy flux was small at the sea surface. Shortwave radiation was not important because the measurements were taken around dawn. There were strong winds and a large shear near the top of the ABL.

In the case study of nocturnal stratocumulus over the UK the surface layer was slightly stable. The ABL was about 1100 m thick, with clouds in the upper 400 m. There were moderate winds without significant shear.

The third case (Nicholls, 1984) refers to Sc over the North Sea with a fairly unstable ABL. This ABL was about 800 m thick with clouds occupying the

upper 400 m. Moderate winds without significant shear were observed. In contrast to the other cases, this experiment was carried out around noon and therefore shortwave radiation was important. Furthermore there was also a significant amount of drizzle in and below the cloud.

In all case studies the vertical profiles showed an approximately isentropic ABL with constant equivalent potential temperature and total water content. At the top a stable density jump was found.

With regard to the vertical distribution of the mean moisture variables in the cloud, the conclusions drawn from the observations of Slingo et al. (1982a, b), and Nicholls (1984) are: a) the mean liquid water content distribution is very close to the adiabatic value, thus increasing linearly from cloud base to cloud top; b) the droplet concentration is nearly constant with height and the mean volume radius of the droplets increases linearly with height. According to Nicholls (1984), earlier measurements of liquid water content that gave values much smaller than the adiabatic ones, are not reliable due to instrumental inaccuracies, and are not in agreement with the measured radiative fluxes (Bonnnel et al., 1983). In stable Sc-decks the entrainment velocity is thus in general small compared to the velocity scale of the turbulence and entrained air loses its characteristics quickly.

Caughey et al. (1982) gave detailed results of the interfacial layer between the cloudy air and the non-turbulent air above. These results refer to the local or instantaneous interface, and not to a horizontal average. Their measurements showed that this instantaneous interface is characterized by very sharp jumps in temperature and a sudden change from turbulent to non-turbulent air. They measured a jump in temperature of 4K over a vertical distance of only 4 m. Above this interface the temperature increased more gradually. From their measurements they concluded that entrainment is a small-scale process that is caused by distortion of the interface by large eddies in the ABL that increase the local shear at their boundary, thus causing small-scale instabilities and consequently entrainment at the interface.

Slingo et al. (1982a) gave detailed longwave radiative flux measurements for the same case study as above (and some others). They show that for an individual vertical traverse (giving approximately an instantaneous profile) the net longwave radiative flux profile has the following characteristics: above the cloud the observed radiative flux profile shows a gradual increase in curvature as the cloud is approached, due to the increasing influence of the cool cloud top. As the cloud is entered the net upward flux rapidly

decreases until the cloud is optically thick after about 30-40 g/m^2 liquid water path. The distance over which this strong cooling takes place is ~ 50 m, but sensitive to the liquid water content profile. In the lower part of the cloud there is a slight longwave radiative warming.

In the nocturnal stratocumulus case study, cloud top excursions occurred with an amplitude of 20-50 m on a large space scale and the vertical profiles of temperature and radiation moved bodily with these excursions. Caughey et al. (1982) attributed this to mesoscale variatons of the ABL-height on scales of 10-50 km, thus with a very large aspect ratio (10-50) and apparently not caused by large turbulent eddies with an aspect ratio of order 1. In the case studies by Brost et al. (1982a) the amplitude of the vertical excursions of cloud top was approximately 50 m on horizontal scales with an aspect ratio of ~ 2-5. Nicholls (1984) also gave cloud-top excursions of ~ 40 m, however without indication of the horizontal scale. Slingo et al. (1982b) denoted excursions of cloud top of ~ 20 m and horizontal variations over distances of a few kilometers or less. Thus, although it is clear that the strong radiative cooling occurs entirely within the cloud locally, the depth over which this cooling occurs is comparable to the amplitude of the cloud top excursions.

The shortwave radiative flux profiles as measured by Slingo et al. (1982b) and Nicholls (1984) for stratocumulus decks over sea showed that the shortwave heating is distributed over a much deeper layer than the longwave radiative cooling. In both cases the radiative budget of the cloud layer as a whole was such that the shortwave heating and longwave cooling almost cancelled. However, their distribution within the cloud was quite different. As noted by Oliver et al. (1978) this has important consequences for the turbulence.

The turbulent structure and entrainment mechanisms in the three types of case studies differed considerably and give a good idea of how delicately several processes in the cloudy ABL may interact, even when at first glance the mean vertical profiles of e.g. temperature and moisture do not show dramatic differences.

In some of the case studies of Brost et al. (1982a,b) and one case of Nicholls and Leighton (1986), wind shear across the inversion dominated the structure of the whole ABL. The radiative cooling at cloud top, although present, did not generate convective turbulence, but instead cooled locally the warm air entrained from above. This entrainment was generated by local wind shear and not indirectly by radiative cooling, which was thus of little

influence on the turbulence in the ABL. The turbulence in the ABL showed characteristic features of a neutral boundary layer with small buoyant production of TKE throughout the bulk of the layer, and shear production at the top causing a negative buoyancy flux there. In the case of Brost et al. (1982a, b) the entrainment velocity was about 0.6-0.7 cm/s. They compared several existing entrainment hypotheses with the measurements. All of them gave poor agreement. A possible explanation for this is that in most entrainment hypotheses it is assumed that the dominant length scale of the turbulence is of the order of the ABL-height, whereas in these case studies it is probably more related to the thickness of the shear layer at the top. Brost et al. (1982b) also showed that the liquid water transport due to falling large drops (drizzle) was in their cases comparable to the turbulent flux of liquid water. They suggested that drizzle influences the stability of the ABL due to the heat release in the upper ABL where condensation on large drops occurs and cooling below the cloud where they evaporate. An interaction among drizzle, radiative cooling, and turbulence was also suggested by Brown and Roach (1978) from their model results.

In the nocturnal Sc case study over the UK, radiative cooling at cloud top was the dominating mechanism for the generation of turbulence in the ABL since wind shear was small and the surface heat flux negative. One thus might expect the characteristics of a convective layer upside down. Indeed, Caughey et al. (1982) reported a strong upward heat flux close to the cloud top, associated with inverted plumes of cooler air. The characteristic length scale, as derived from spectra of the vertical velocity, increased in the downward direction from a value of 150-200 m near cloud top to a value of ~ 800 m near cloud base (ABL-height was ~ 1100 m, cloud thickness ~ 400 m), which also indicates that the turbulent motions were of a convective nature. The variances of horizontal velocity (σ_u^2) and vertical velocity (σ_w^2) were almost constant with height in the cloud layer with a minor maximum for σ_w^2 in the middle. However, the expected dominance of σ_w^2 over σ_u^2 as in the daytime convective ABL was not present (here $\sigma_w^2 \sim \sigma_u^2$). No turbulence measurements were made in the sub-cloud layer, thus no definite conclusions could be drawn as to whether these layers were strongly coupled or not.

The entrainment velocity at the top of this nocturnal Sc was ~ 0.5 cm/s, the downward buoyancy flux at the top ~ $-25\ 10^{-3}$ K m/s, the net radiative flux jump near cloud top ~ 70 W/m^2, the depth of the radiatively cooled layer ~ 50 m, and the ABL-height ~ 1100 m. (These data are taken from Caughey et al.

(1982) and Slingo et al. (1982a).) Use of the data in mixed-layer entrainment formulations as given in section 3 gives quite different values for the entrainment constants than the usual values for a dry convective daytime ABL (we neglected the stable surface layer here). However, these estimates are very crude, especially because the vertical profiles of the buoyancy flux below cloud base are not known. Thus little can be said about the performance of entrainment hypotheses from these measurements.

The nocturnal Sc-deck dispersed after 2-4 hours. Roach et al. (1982) inferred from the measured heat budget of the ABL that this cloud dispersal could not be attributed to entrainment or other diabatic processes, but was most probably caused by locally large subsidence.

In the case study of Nicholls (1984) on a Sc-deck over the North Sea shortwave radiation played an important role, as did precipitation. Shortwave warming over a deep layer into the cloud, combined with longwave cooling concentrated at cloud top, tended to destabilize the cloud layer and to generate turbulence on the scale of the cloud depth. Additionally, precipitation that was evaporating in a (shallow) layer below cloud base cooled the air in the subcloud layer. Generally, the net effect of these porcesses is that a shallow stable layer develops near cloud base leading to a decoupling of the subcloud and cloud layers when the surface buoyancy flux is not strong enough to maintain the coupling. This seems to have occurred in the case of Nicholls (1984). The same tendency toward decoupling due to shortwave warming has been indicated by Slingo et al. (1982b). This picture is broadly confirmed by the turbulence measurements of Nicholls (1984). The measured vertical velocity variances showed a minimum near cloud base with two maxima both in the subcloud layer and in the cloud layer. Also, measurements of the vertical transport of TKE showed that there was no gain or loss due to this term near cloud base. Thus there was no TKE-transport between the layers.

Such a separation has an important effect on the dynamics and the behavior of the cloud. Mixed-layer models do not seem suitable under such conditions. Higher-order closure models (Bougeault, 1985; Duynkerke and Driedonks, 1987) on the other hand have been shown to be able to simulate this decoupling of the cloud layer from the sub-cloud layer.

5. Conclusions

A number of physical processes determine the turbulent structure of a cloud-topped ABL. Observations show that the resulting structure depends quite strongly on the interactions among these processes.

The longwave radiative cooling is concentrated in a shallow layer, of about 50 m deep, near cloud top. This cloud-top cooling tends to destabilize the whole ABL and to generate convectively driven turbulence. From observations (Nicholls and Leighton, 1986) this seems the most common mechanism for generating turbulence in the cloud-topped ABL. During day-time the solar radiation will heat up the cloud. Because shortwave heating extends much deeper into the cloud than longwave cooling, their combined effect may lead to destabilization of the cloud layer alone, and to decoupling of the cloud layer from the sub-cloud layer (Nicholls, 1984). The decoupling leads to a cut off of the moisture supply from the surface and thus to a much more rapid development and thinning of the cloud layer. Turbulence in the cloud-topped ABL may also be generated by windshear. Observational data (Brost et al., 1980 a, b; Nicholls and Leighton, 1986) show that the windshear at cloud top may promote the entrainment of warm air so effectively that it approximately balances the longwave radiative cooling. Instead of being convectively driven the ABL then has a near-neutral structure. Other production mechanisms of turbulence are surface fluxes and the release of latent heat by condensation. All the production mechanisms of turbulence in the ABL, discussed above, determine the entrainment of warmer and drier air from above the inversion. Due to the large number of processes and their complicated interaction the parameterization of the entrainment in mixed-layer models is still questionable.

The entrainment may be further complicated by evaporative cooling of warm and dry air that is entrained into the cloud layer. The evaporative cooling can under certain circumstances lead to an instability process in which the entrained air parcel is cooled so much that it becomes negatively buoyant and sinks through the cloud; this is called cloud top entrainment instability (Randall, 1980b; Deardorff, 1980a; Hanson, 1982, 1984, 1987; Randall, 1984b; Nicholls and Turton, 1986). Cloud top entrainment instability leads to large entrainment rates and may be one of the mechanisms in breaking up a solid stratocumulus deck. However, Randall (1984b) showed that, depending on the conditions above the cloud, the effect of entrainment may be that the cloud top rises more quickly than cloud base, so that the cloud depth

increases with time. Randall (1984b) called this process "cloud deepening through entrainment" (CDE).

For the dry ABL, with a positive surface heat flux, both observations and large-eddy simulations have revealed that its structure is governed by rather simple scaling laws. It has been shown that such a dry ABL is driven to a "convective state", once the stability parameter -h/L (where h is the ABL-height and L the (surface layer) Obukhov length) exceeds a value of 5-10. Above this value, the structure of the ABL becomes independent of -h/L, and thus independent of surface friction. In that case the variables in the bulk of the ABL show universal behavior if properly scaled with quantities that involve only the surface heat flux and the ABL-height; e.g. all velocities scale on the convective velocity scale w_* and all lengths scale on h. The dominance of these scales has made entrainment relations for the dry ABL successful.

One of the main reasons for the problems arising in the modeling of the cloud-topped ABL is the apparent absence of such simple scaling laws that characterize a large class of real-world cloudy boundary layers. In a cloudy ABL many more scaling quantities can be listed apart from the surface fluxes and ABL-height; e.g. the longwave radiative flux divergence, the thickness of the radiatively cooled layer, the shortwave radiative flux divergence, the thickness of the layer over which this occurs, the cloud microphysics, the thickness of the cloud and sub-cloud layer, the drizzle rate, wind shear at the top. From the reported sets of observations it is apparent that all these parameters may strongly interact in their influence on the dynamics of a Sc-topped ABL. As an example, wind shear at the ABL-top not only generates turbulence locally, but at the same time may completely rule out the possibility of generating convective turbulence by cloud-top radiative cooling.

Such a situation in which a large number of parameters dominate the dynamics of the problem is difficult to handle. The non-dimensionalized flow variables may depend on a multitude of characteristic parameters, e.g. a set of suitable Richardson-numbers. This makes the interpretation of experiments and the formulation of universal results from them quite complicated. In fact, the detailed experiments on different cloud-topped ABL's have elucidated this problem and shown that the turbulent structure of the cloudy ABL can differ drastically from one case to another, even when the mean profiles are rather similar in showing an isentropic vertical structure of the ABL.

The complicated turbulent structure of the cloud-topped ABL leads to considerable difficulties in modeling its behavior. In mixed-layer models, or other vertically-integrated models, the basic problem is the formulation of the entrainment rate at the top, which has to be parameterized in terms of the turbulence in the ABL. Since the detailed turbulent structure of the ABL is not resolvable in mixed-layer models, its state has to be pre-assumed or anticipated. It may be expected that this is only feasible in relatively uncomplicated situations.

Most effort on mixed-layer models for the cloudy ABL has been spent on the case in which only the surface buoyancy flux and the longwave radiative cooling at cloud top are important. In idealized mixed-layer models with a zero-order jump discontinuity at the top it is most logical to locate the cloud-top cooling within the mixed layer and not partly above it. Entrainment relations for this case as derived from a parameterized form of the TKE-budget are still controversial. The strong sensitivity of some of these models to the depth of the radiatively cooled layer does not seem very realistic and is a direct consequence of model assumptions. This sensitivity is less pronounced in the interpretation of Stage and Businger (1981a, b). This issue cannot be solved within the context of mixed-layer models. None of these entrainment parameterizations has been confirmed by field measurements. The large-eddy simulations of Deardorff (1980b) also do not support current parameterizations of entrainment. Instead, best results in his model are obtained for an entrainment relation that is based on the local turbulence intensity at cloud top. This is confirmed by field measurements. However, in mixed-layer models this local turbulence intensity is unknown and requires further assumptions.

In cases where, apart from a surface buoyancy flux and cloud-top cooling, wind shear at the top and shortwave radiative effects play a role, no satisfactory entrainment parameterization has been formulated. Of special importance is the tendency toward decoupling of the upper cloud layer from the lower part of the ABL, introducing new length scales.

Higher-order turbulence closure models are able to describe a greater variety of phenomena in the cloud-topped ABL than the mixed-layer models. For instance, sometimes the assumption of the ABL to be well-mixed is too strong and decoupling of the cloud layer from the sub-cloud layer may occur (Nicholls, 1984; Bougeault, 1985; Duynkerke and Driedonks, 1987). Moreover, higher-order closure models can simulate both shear and buoyancy and the influence on the entrainment rate (Duynkerke and Driedonks, 1987).

An important problem in higher-order turbulence closure is presented by the dissipation equation. In models used to date this dissipation is dealt with in a rudimentary way, in contrast to the amount of sophistication that is applied to the modeling of other unknown terms.

Under certain conditions (Deardorff, 1980a; Randall, 1980b; Hanson, 1984) cloud-top entrainment instability may occur, leading to a rapid increase of the entrainment rate. It is usually envisaged that this cloud-top entrainment instability is responsible for the break-up of a Sc-deck into scattered cumulus. However, in the measurements by Hanson (1984) and Brost (private communication) the theoretical conditions for this instability were fullfilled without its actual occurrence. The conditions that lead to the break-up of a Sc-deck are far from understood and mesoscale variability may play a central role in it (Rothermel and Agee, 1980; Roach et al., 1982; Fiedler, 1984).

References

Albrecht, B.A., R.S. Penc and W.H. Schubert, 1985: An observational study of cloud-topped mixed layers. J. Atmos. Sci., 42, 800-822.

André, J.C., G. De Moor, P. Lacarrère, G. Therry, and R. du Vachat, 1978: Modeling of the 24-hour evolution of the mean and turbulent structure of the planetary boundary layer. J. Atmos. Sci., 35, 1861-1883.

André, J.C. and L. Mahrt, 1982: The nocturnal surface inversion and influence of clear-air radiative cooling. J. Atmos. Sci., 39, 864-878.

Betts, A.K., 1973: Non-precipitating cumulus convection and its parameterization. Quart. J. Roy. Met. Soc., 99, 178-196.

Bonnell, B., Y. Fouquart, J.C. Vanhoutte, C. Fravalo, and R. Rosset, 1983: Radiative properties of some African and mid-latitude stratocumulus clouds. Contr. Atmos. Phys., 56, 409-439.

Bougeault, Ph., 1985: The diurnal cycle of the marine stratocumulus layer: A higher-order model study. J. Atmos. Sci., 42, 2826-2843.

Brost, R.A., D.H. Lenschow, and J.C. Wyngaard, 1982a: Marine stratocumulus layers. Part I: Mean conditions. J. Atmos. Sci., 39, 800-817.

Brost, R.A., J.C. Wyngaard, and D.H. Lenschow, 1982b: Marine stratocumulus layers. Part II: Turbulence budgets. J. Atmos. Sci., 39, 818-836.

Brown, R. and W.T. Roach, 1976: The physics of radiation fog: II-a numerical study. Quart. J. Roy. Met. Soc., 102, 335-354.

Caughey, S.J., B.A. Crease, and W.T. Roach, 1982: A field study of nocturnal stratocumulus. II. Turbulence structure and entrainment. Quart. J. Roy. Met. Soc., 108, 125-144.

Caughey, S.J., and M. Kitchen, 1984: Simultaneous measurements of the turbulent and microphysical structure of nocturnal stratocumulus cloud. Quart. J. Roy. Met. Soc., 110, 13-34.

Chen, C., and W.R. Cotton, 1983a: Numerical experiments with a one-dimensional higher turbulence model: simulation of the Wangara Day 33 case. Boundary-Layer Meteor., 25, 375-404.

Chen, C., and W.R. Cotton, 1983b: A one-dimensional simulation of the stratocumulus-capped mixed layer. Boundary-Layer Meteor., 25, 289-321.

Coulman, C.E., 1978: Convection in stratiform cloud. J. Rech. Atmos., 12, 21-33.

Deardorff, J.W., 1976a: On the entrainment rate of a stratocumulus-topped mixed layer. Quart. J. Roy. Met. Soc., 102, 563-528.

Deardorff, J.W., 1980a: Cloud top entrainment instability. J. Atmos. Sci., 37, 131-146.

Deardorff, J.W., 1980b: Stratocumulus-capped mixed layers derived from a three-dimensional model. Boundary-Layer Meteor., 18, 495-527.

Deardorff, J.W., 1981: On the distribution of mean radiative cooling at the top of a stratocumulus-capped mixed layer. Quart. J. Roy. Met. Soc., 107, 191-202.

Deardorff, J.W., 1983: A multi-limit mixed-layer entrainment formulation. J. Phys. Oceanogr., 13, 988-1002.

Driedonks, A.G.M., and H. Tennekes, 1984: Entrainment effects in the well-mixed atmospheric boundary layer. Boundary-Layer Meteor., 30, 75-105.

Duynkerke, P.G. and A.G.M. Driedonks, 1987: A model for the turbulent structure of the stratocumulus-topped atmospheric boundary layer, J. Atmos. Sci., 44, 43-64.

Fiedler, B.H., 1984: The mesoscale stability of entrainment into cloud-topped mixed layers. J. Atmos. Sci., 41, 92-101.

FIRE, the First ICCP Regional Experiment, 1983. Research Plan. Available from the National Climate Program Office, Room 108, 11400 Rockville Pike, Rockville MD 20852, USA.

Fravalo, C., Y. Fouquart, and R. Rosset, 1981: The sensitivity of a model of low stratiform clouds to radiation. J. Atmos. Sci., 38, 1049-1062.

Hanson, H.P., 1982: Note on mixed-layer entrainment closure. J. Atmos. Sci., 39, 470-473.

Hanson, H.P., 1984: Stratocumulus instability reconsidered: A search for physical mechanisms. Tellus, 36A, 355-368.

Hanson, H.P., 1984: On mixed-layer modeling of the stratocumulus-topped marine boundary layer. J. Atmos. Sci., 41, 1226-1234.

Hanson, H.P., 1987: Reinterpretation of cloud-topped mixed-layer entrainment closure. Tellus, 39A, 215-225.

Herman, G., and R. Goody, 1976: Formation and persistence of summertime Arctic Stratus clouds. J. Atmos. Sci., 33, 1537-1553.

Hignett, P., 1987: A study of the shortwave radiative properties of marine stratus: Aircraft measurements and model comparisons. Quart. J. Roy. Met. Soc., 113, 1011-1024.

Kahn, P.H., and J.A. Businger, 1979: The effect of radiative flux divergence on entrainment of a saturated convective boundary layer. Quart. J. Roy. Met. Soc., 105, 303-385.

Kraus, H., and E. Schaller, 1978: Steady-state characteristics of inversions capping a well-mixed planetary boundary layer. Boundary-Layer Meteor., 14, 83-104.

Lenschow, D.H., 1973: Two examples of planetary boundary layer modification over the great lakes. J. Atmos. Sci., 30, 568-581.

Lenschow, D.H., and E.M. Agee, 1976: Preliminary results from the air mass transformation experiment (AMTEX). Bull. Amer. Meteor. Soc., 57, 1346-1355.

Lilly, D.K., 1968: Models of cloud-topped mixed layers under a strong inversion. Quart. J. Roy. Meteor. Soc., 94, 292-309.

Lilly, D.K., and W.H. Schubert, 1980: The effects of radiative cooling in a cloud-topped mixed layer. J. Atmos. Sci., 37, 482-

Mahrt, L. and J. Paumier, 1982: Cloud-top entrainment instability observed in AMTEX. J. Atmos. Sci., 39, 622-634.

Mellor, G.L., and T. Yamada, 1982: Development of a turbulence closure model for geophysical fluid problems. Rev. of Geoph. and Space Phys., 20, 851-875.

Moeng, Chin-Hoh, and A. Arakawa, 1980: A numerical study of marine subtropical stratus cloud layer and its stability. J. Atmos. Sci., 37, 2661-2676.

Moeng, Chin-Hoh, and D.A. Randall, 1984: Problems in simulating the stratocumulus-topped boundary layer with a third-order closure model. J. Atmos. Sci., 41, 1588-1600.

Moeng, Chin-Hoh, 1986: Large-eddy simulation of a stratus-topped boundary layer. Part I: Structure and budgets. J. Atmos. Sci., 43, 2886-2900.

Nicholls, S., 1984: The dynamics of stratocumulus: aircraft observations and comparisons with a mixed-layer model. Quart. J. Roy. Met. Soc., 110, 783-820.

Nicholls, S., and J. Leighton, 1986: An observational study of the structure of stratiform cloud sheets: Part I. Structure. Quart. J. Roy. Met. Soc., 112, 431-460.

Nicholls, S. and J.D. Turton, 1986: An observational study of the structure of stratiform cloud sheets: Part II. Entrainment. Quart. J. Roy. Met. Soc., 112, 461-480.

Nieuwstadt, F.T.M., and J. Businger, 1984: A note on radiative cooling near the top of a cloudy mixed layer. Quart. J. Roy. Met. Soc., 110, 1073-1078.

Oliver, D.A., W.S. Lewellen, and G.G. Williamson, 1978: The interaction between turbulent and radiative transport in the development of fog and low-level stratus. J. Atmos. Sci., 35, 301-316.

Platt, C.M.R., 1976: Infrared absorption and liquid water content in stratocumulus clouds. Quart. J. Roy. Met. Soc., 102, 553-561.

Platt, C.M.R., 1981: Extended clouds and radiation. WMC/ICSU report, World Climate Programme, WCP-18. Obtainable from World Meteorological Organisation, C.P. 5, Geneva, Switzerland.

Randall, D.A., 1980a: Entrainment into a stratocumulus layer with distributed radiative cooling. J. Atmos. Sci., 37, 148-159.

Randall, D.A., 1980b: Conditional instability of the first kind upside-down. J. Atmos. Sci., 37, 125-130.

Randall, D.A., 1984a: Buoyant production and consumption of turbulent kinetic energy in cloud-topped mixed layers. J. Atmos. Sci., 41, 402-413.

Randall, D.A., 1984b: Stratocumulus cloud deepening through entrainment. Tellus, 36A, 446-457.

Randall, D.A., J.A. Coakley, Ir. C.W. Fairall, R.A. Kropfli, and D.H. Lenschow, 1984: Outlook for research on subtropical marine stratiform clouds. Bull. Amer. Meteor. Soc., 65, 1290-1301.

Roach, W.T., R. Brown, S.J. Caughey, T.A. Crease, and A. Slingo, 1982: A field study of nocturnal stratocumulus: I. Mean structure and budgets. Quart. J. Roy. Met. Soc., 108, 103-123.

Rodgers, D.P. and J.W. Telford, 1986: Metastable stratus tops. Quart. J. Roy. Met. Soc., 112, 481-500.

Rothermel, J. and E.M. Agee, 1980: Aircraft investigation of mesoscale cellular convection during AMTEX 75. J. Atmos. Sci., 37, 1027-1040.

Schaller, E., and H. Kraus, 1981a: The role of radiation in an inversion-capped planetary boundary layer. Part I: The need for a detailed consideration of radiative processes. Boundary-Layer Meteor., 20, 485-495.

Schaller, E., and H. Kraus, 1981b: The role of radiation in an inversion-capped planetary boundary layer. Part II: The internally interactive radiative-convective model. Boundary-Layer Meteor., 20, 497-513.

Schubert, W.H., 1976: Experiments with Lilly's cloud-topped mixed layer model. J. Atmos. Sci., 33, 436-446.

Schubert, W.H., J.S. Wakefield, E.J. Steiner, and S.K. Cox, 1979: Marine stratocumulus convection. Part I: Governing equations and horizontally homogeneous solutions. J. Atmos. Sci., 36, 1286-1307.

Slingo, A., R. Brown, and C.L. Wrench, 1982a: A field study of stratocumulus. III. High resolution radiative and microphysical observations. Quart. J. Roy. Met. Soc., 108, 145-165.

Slingo, A., S. Nicholls, and J. Schmetz, 1982b: Aircraft observations of marine stratocumulus during JASIN. Quart. J. Roy. Met. Soc., 108, 833-856.

Stage, S.A., and J.A. Businger, 1981a: A model for entrainment into a cloud-topped marine boundary layer. Part I: Model description and application to a cold-air outbreak episode. J. Atmos. Sci., 38, 2213-2229.

Stage, S.A., and J.A. Businger, 1981b: A model for entrainment into a cloud-topped marine boundary layer. Part II: Discussion of model behavior and comparison with other models. J. Atmos. Sci., 38, 2230-2242.

Stephens, G.L., and C.M.R. Platt, 1987: Aircraft observations of the radiative and microphysical properties of stratocumulus and cumulus cloud fields. J. Climate Appl. Meteor., 26, 1243-1269.

Turton, J.D. and S. Nicholls, 1986: A study of the diurnal variation of stratocumulus using a mixed layer model. Quart. J. Roy. Met Soc., 113, 969-1009.

WMO, 1982: The International Satellite Cloud Climatology Project (ISCCP). Preliminary implementation plan. WMO/ICSU World Climate Programme, report nr. WCP-35. Obtainable from World Meteorological Organisation, C.P. 5, Geneva, Switzerland.

WMO, 1985: Report of the JSC/CAS workshop on modelling of cloud-topped boundary layer. WMO World Climate Programme, report nr. WCP-106, WMO, Geneva, Switzerland.

Wyngaard, J.C., 1982: Boundary-Layer modeling. In: Atmospheric Turbulence and Air Pollution Modelling, Eds. F.T.M. Nieuwstadt and H. van Dop. Reidel Publ. Cy., Dordrecht, Holland, pp. 69-106.

Zeman, O., 1981: Progress in the modeling of planetary boundary layers. Ann. Rev. Fluid Mech., 13, 253-272.

Reprinted from JOURNAL OF THE ATMOSPHERIC SCIENCES, Vol. 44, No. 1, 1 January 1987
American Meteorological Society

3. A Model for the Turbulent Structure of the Stratocumulus-Topped Atmospheric Boundary Layer +

P. G. DUYNKERKE

Free University, Amsterdam

A. G. M. DRIEDONKS

Royal Netherlands Meteorological Institute, De Bilt, The Netherlands

(Manuscript received 7 February 1986, in final form 7 July 1986)

ABSTRACT

A multilevel ensemble-averaged model has been developed to study the cloud-topped atmospheric boundary layer (ABL). Turbulence closure is formulated by using an equation for the turbulent kinetic energy and either a diagnostic formulation of the integral length scale or a parameterized version of the dissipation equation. The latter two options are compared. The model is used to study various combinations of physical processes in a cloud-topped ABL and their combined effect on the turbulent structure. The physical processes considered are an upward buoyancy flux at the surface, longwave radiative cooling near cloud top, shortwave radiative heating in the cloud, and wind shear near cloud top. We discuss a case with only a surface buoyancy flux (no radiation) and a case with only longwave radiative fluxes (no surface fluxes). The usual concept that the latter is the upside-down version of the former is not confirmed by the model results. Furthermore, we apply the model to the datasets of Brost et al. and Nicholls. The pronounced differences in the observed turbulent structure of the ABL in these two cases (due to different combinations of physical processes) are well simulated by the model.

1. Introduction

As shown by satellite images, extended sheets of low-level stratocumulus (Sc) clouds, often exceeding 10^6 km^2, frequently occur over particular areas of the world, especially over the sea. The occurrence of these Sc-decks is associated with subtropical high-pressure systems, where they have a quasi-permanent character, or with high-pressure ridges between frontal systems at midlatitudes, where their character is more transient. Schubert et al. (1979) give an account of the typical areas of the world where the quasi-permanent Sc-decks occur and their associated climates.

Stratocumulus-decks have a considerable influence on climate as well as on local weather. First, these extensive low-level cloud sheets modify the energy balance at the top of the atmosphere and at the surface quite drastically. Their high albedo (~0.6–0.8) compared with the underlying earth's surface (~0.2 for land, ~0.05 for water) leads to a strong reduction of the net incoming shortwave radiative flux at the top of the atmosphere in comparison with the cloud-free case while at the same time the infrared loss to space is not altered significantly, due to the low altitude of the clouds. Thus an increase in low-level cloud cover will lead to global cooling of the atmosphere. Randall et al. (1984) gave a qualitative argument that an increase of a few percent in this cloud cover may offset the warming caused by a doubling of the CO_2-content of the atmosphere. In addition, the quasi-persistent Sc-decks over parts of the world seas have a strong impact on the energy balance of the sea water. Thus, in simulations of the climate with coupled ocean–atmosphere models, a correct position and frequency of occurrence of low-level cloud decks is required, a goal not yet achieved.

Apart from the climatic impact of Sc-decks, there is also a strong influence on local weather, especially in regions where the clouds are transient. It is well known, particularly in coastal regions, that poor predictions of the formation, maintenance and dissipation of Sc-decks may degrade the quality of forecasts of such weather elements as temperature and sunshine. As a typical example, Fig. 1a shows a satellite picture of a Sc-deck formed over the North Sea under the influence of a high pressure system west of Scotland. The cloud deck is advected with a northwest wind over The Netherlands and a north wind over Germany. In Fig. 1b its effect on the shortwave radiative flux is shown as measured at different locations in The Netherlands. It can be seen that the presence of such a cloud deck reduces the incoming radiative flux at the surface by considerably more than 50% in comparison to the cloud-free stations.

The type of Sc-deck we are discussing usually has tops below 1000 m and is part of the atmospheric boundary layer (ABL), which consists of a subcloud layer and a cloud layer. In this paper we will consider

© 1987 American Meteorological Society

+ Published in Journal of the Atmospheric Sciences, 1987, 44, 43-64, with A.G.M. Driedonks as co-author.

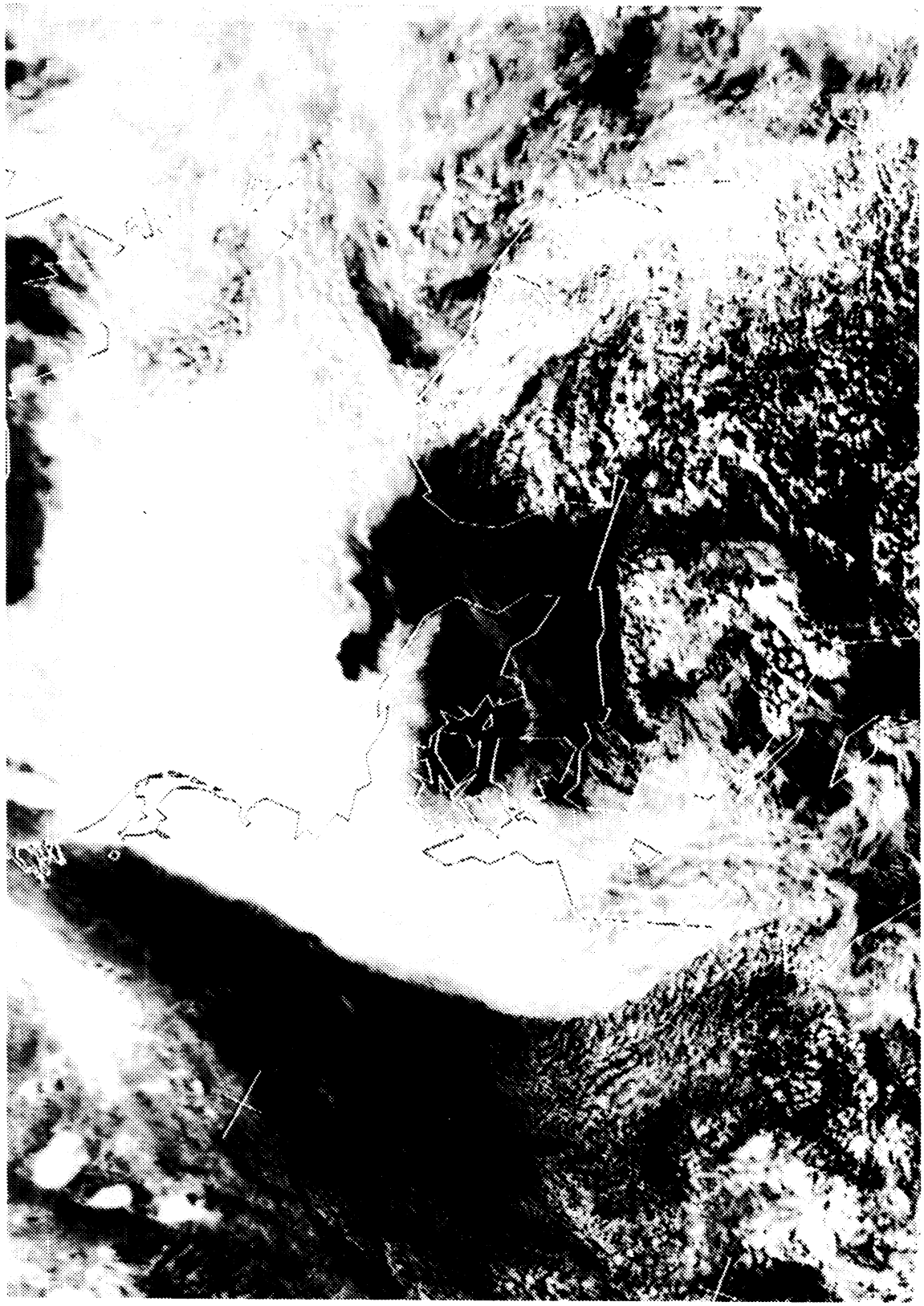

FIG. 1a. The NOAA satellite picture (visible) for 1312 UT 25 July 1984 showing a Sc-deck over the North Sea, which is advected over the Netherlands and Germany with a northwest wind.

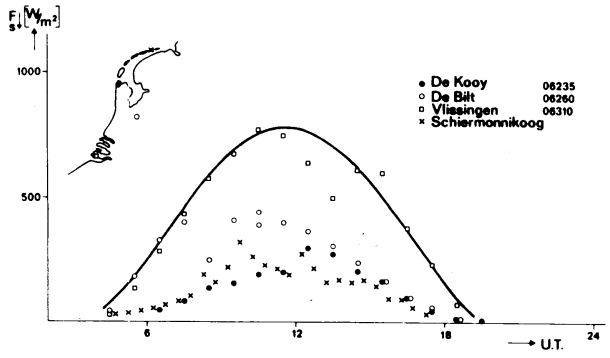

FIG. 1b. Downward shortwave flux measured on 25 July 1984 at four different ground stations in the Netherlands. See upper left for location of stations. The curve gives an average of the measured values for clear sky cases during that period.

a horizontally homogeneous cloud deck (in a statistical sense) and study its vertical structure. Driedonks (1986) discusses the most important physical processes in such an ABL. One of the crucial points in understanding the behavior of such a Sc-topped ABL is to know how the turbulent transports of heat, moisture and momentum are influenced by the presence of a cloud layer. In contrast to a cloud-free ABL, the cloud introduces several new possible sources of turbulent energy due to localized heating or cooling through radiative flux divergences and phase changes. It is the interplay between these processes that determines the turbulent transport in a cloud-topped ABL.

In a cloud-free ABL, turbulence dynamics is affected primarily by 1) wind shear at the surface, 2) wind shear at ABL top, and 3) buoyancy flux at the surface. In a cloud-topped ABL, the turbulence is also influenced by 1) longwave radiative cooling at cloud top, 2) shortwave radiative heating inside the cloud layer, and 3) phase changes. In the cloud-free ABL's dominated by the buoyancy flux and wind shear at the surface, relatively simple models have been developed that describe the evolution of the ABL quite successfully (Driedonks, 1982). For the cloud-topped ABL, however, both the large number of processes involved and their complicated interactions show that simple scaling laws will be difficult to find.

Improved understanding of the cloud-topped ABL has to be based on detailed observations. It is only recently that some good observational studies on the turbulent structure of a Sc-deck have been reported. Brost et al. (1982a,b) analyzed data collected off the coast of California. Roach et al. (1982), Caughey et al. (1982), and Slingo et al. (1982) analyzed a case of nocturnal stratocumulus over the United Kingdom. Nicholls (1984) described a case of stratocumulus over the North Sea. Hanson (1984), as well as Albrecht et al. (1985), studied clouds off the coast of California.

In this paper we will study the role of different turbulent production mechanisms in determining the transports in the ABL. For this, it is quite relevant that the observations by Brost et al. (1982a,b) and Nicholls (1984) showed that different combinations of physical processes may lead to a totally different turbulent structure of the ABL. In the observations of Nicholls (1984), the most important processes were longwave radiative cooling at cloud top and shortwave heating inside the cloud layer. The cooling at cloud top and heating inside the cloud led to an instability of the cloud depth itself and to decoupling of the cloud layer from the subcloud layer. A completely different turbulent structure of the cloud-topped ABL was observed by Brost et al. (1982a,b). During their observations, the most important physical processes were longwave radiative cooling at cloud top and wind shear at both the surface and at cloud top. The wind shear at cloud top was enhancing the entrainment of warm air so effectively that the entrained warm air fully balanced the cloud top radiative cooling. Thus the latter did not generate a strong upward buoyancy flux throughout the ABL, and the turbulent structure of the ABL was determined by the wind shear near the surface, creating a near neutral cloud-topped ABL.

In this paper we develop a model that incorporates the most important physical processes and study their influence on the turbulent structure of the cloud-topped ABL. We will compare the results with the recent sets of observations of Nicholls (1984) and Brost et al. (1982a,b) discussed previously.

Since the early study of Lilly (1968), increasingly sophisticated models for the cloud-topped ABL have been developed. Especially the mixed-layer type of model has been pursued quite far (Deardorff, 1976; Schubert, 1976; Schubert et al., 1979; Stage and Businger, 1981a,b; Schaller and Kraus, 1981a,b; Fravalo et al., 1981; Hanson, 1984). This type of model is simple and attractive and can accommodate results from more complicated models and from observations. However, in order to study the conditions under which the assumptions for mixed-layer models are justified, it is necessary to use more detailed studies. In addition, to date, no fully satisfactory entrainment formulation for the turbulent fluxes at cloud top has been devised for these models. In trying to solve some of these problems, studies have been conducted with large-eddy simulation models which, since the early work of Deardorff (1974), have also been applied to the cloud-topped ABL (Sommeria, 1976; Deardorff, 1980; Moeng and Wyngaard, 1985). Although interesting results have been obtained, these large eddy models require extensive computer resources and only in the future will be feasible for studying a number of different cases.

In the present study we take an intermediate point of view and develop a multilevel ensemble-averaged model for the cloud-topped ABL. In this type of model, with a number of layers in the ABL, the combined effect of all eddy sizes has to be parameterized, for which a hierarchy of turbulent closure hypotheses has

been developed (e.g., Mellor and Yamada, 1982). Several of these closure schemes have been applied to the cloudy case (Oliver et al., 1978; Moeng and Arakawa, 1980; Bougeault, 1981; Chen and Cotton, 1983; Moeng and Randall, 1984; Bougeault, 1985). The closure hypotheses are based mainly on observational data from the clear-sky ABL. Therefore, results of these models have to be evaluated carefully against experimental data obtained for the cloud-topped ABL.

We develop a multilayered model in which turbulence closure is formulated by using the equation for turbulent kinetic energy and either a diagnostic formulation for the integral length or a prognostic equation for the viscous dissipation. These latter two options are compared. This type of turbulence closure is simpler than third-order closures (e.g., Bougeault, 1985), but it contains the most important physics and may be suitable for use in operational numerical weather prediction.

The model is used to determine the combined effect of several physical processes in determining the turbulent structure of the ABL, in the light of recent observations as cited previously. We will focus on the case of a Sc-deck over sea, where the surface radiation budget does not control the surface fluxes. Furthermore, since we are mainly interested in the gross effects of physical processes, we did not apply a partial condensation scheme. Also, the radiative fluxes are parameterized in a rather simple way.

Section 2 gives a full description of the one-dimensional model. The results of the model are presented in section 3. Sections 3a and 3b give the results for two idealized cases. In the first, the sea surface temperature is higher than the air temperature, giving rise to convection at the surface; no radiative fluxes are taken into account. In the second, the cloud top is cooled by longwave radiation and the surface fluxes are set to zero. The radiative cooling gives rise to convection generated from cloud top. In sections 3c and 3d, the results are compared with observational data. The first deals with a stratocumulus deck on the North Sea, described by Nicholls (1984); the second concerns a stratocumulus deck off the California Coast (Brost et al., 1982a,b).

2. Model description

The model is used in a one-dimensional horizontally homogeneous version. The ensemble-averaged equations describing the dynamics of the stratocumulus-capped ABL are given in section 2a. We have prognostic equations for the horizontal velocities (u and v), the entropy and the total water content. The vertical velocity has to be prescribed. Due to the ensemble averaging, unknown turbulent fluxes appear in these equations. A turbulence model, which relates the unknown turbulent fluxes to known variables, is introduced in section 2b. In section 2c a new variable is introduced for the entropy, and its relation with pressure, temperature and total water content discussed. In the entropy equation the total radiative flux, causing radiative cooling or heating, is another unknown. A radiation model for both longwave and shortwave radiation is presented in section 2d. Section 2e deals with the surface boundary conditions used in the model. Finally, section 2f gives details on the numerical techniques used in the computer program.

a. Governing equations

In horizontally homogeneous conditions the ensemble-averaged equations describing the dynamics of the stratocumulus-capped ABL reduce to

$$\frac{\partial u}{\partial t} = f(v - v_g) - \frac{\partial \overline{u'w'}}{\partial z} - w\frac{\partial u}{\partial z}, \tag{1}$$

$$\frac{\partial v}{\partial t} = -f(u - u_g) - \frac{\partial \overline{v'w'}}{\partial z} - w\frac{\partial v}{\partial z}, \tag{2}$$

$$\frac{\partial \theta_q}{\partial t} = -\frac{\partial}{\partial z}\overline{w'\theta'_q} - \frac{\theta_{q0}}{\rho_0 c_{pd} T_0}\frac{\partial F}{\partial z} - w\frac{\partial \theta_q}{\partial z}, \tag{3}$$

$$\frac{\partial q_w}{\partial t} = -\frac{\partial}{\partial z}\overline{w'q'_w} - w\frac{\partial q_w}{\partial z}, \tag{4}$$

with (u, v, w) the ensemble-averaged wind velocities in the (x, y, z) directions, respectively, and primed quantities denoting turbulent fluctuations. Equation (3) is the entropy equation, expressing diabatic heating by radiation. For the entropy a new variable (θ_q) is introduced, known as the wet equivalent potential temperature (Pointin, 1984). The definition of θ_q will be further discussed in section 2c. The atmospheric radiative cooling or heating rate is represented by

$$-\frac{\theta_{q0}}{\rho_0 c_p T_0}\frac{\partial F}{\partial z},$$

with F the total radiative flux defined by $F = F\uparrow - F\downarrow$, where, $F\uparrow$ and $F\downarrow$ are the upward and downward flux, respectively. The variable q_w is the specific humidity for total water, $q_w = q_v + q_l$, with q_v water vapor and q_l liquid water. The equations are in Boussinesq form, where ρ_0, T_0, θ_{q0} denote the reference state, which is only a function of z, and correspond to the midlatitude standard atmosphere (Eskinazi, 1975). The pressure is calculated by integration of the hydrostatic equation downward from the model top.

b. Turbulence closure

In order to close Eqs. (1) to (4), the turbulent fluxes are expressed as

$$-\overline{u'w'} = K_m\frac{\partial u}{\partial z}, \tag{5a}$$

$$-\overline{v'w'} = K_m\frac{\partial v}{\partial z}, \tag{5b}$$

$$-\overline{w'\theta'_q} = K_h \frac{\partial \theta_q}{\partial z}, \tag{5c}$$

$$-\overline{w'q'_w} = K_h \frac{\partial q_w}{\partial z}, \tag{5d}$$

in which the index m refers to momentum and h to heat. The exchange coefficient for moisture is taken to be equal to that for heat.

The exchange coefficients are taken as (Mailhot and Benoit, 1982)

$$K_{m,h} = c_\mu^{1/4} l_{m,h} E^{1/2}, \tag{6}$$

where c_μ is a constant, $l_{m,h}$ a length scale and E the turbulent kinetic energy (TKE). The numerical values for c_μ and for all other constants used in the turbulence model are given in appendix A.

Usually, a *diagnostic* equation is formulated for the length scale (e.g., see André et al., 1978), relating it to the distance from the surface, to the vertical distribution of TKE, and to the stability of the air. In this type of formulation it is assumed that the turbulence has some anticipated state. Although this approach can be quite successful for certain types of ABL, we doubt its applicability to turbulent flows with important internal sources of turbulence as in the cloud-topped ABL. Therefore, we also formulated a *prognostic* equation for the dissipation rate of TKE, ϵ, which is analogous to a prognostic equation for the length scale l through the relation (Rodi, 1980)

$$l = c_\mu^{3/4} E^{3/2} / \epsilon. \tag{7}$$

The alternative to (6), now using the dissipation, is then of the form

$$K_{m,h} = c_\mu E^2 / \epsilon. \tag{8}$$

The diagnostic relation for l is discussed in subsection 2b1, the dissipation equation in subsection 2b2.

Both formulations (6) and (8) need an equation for the turbulent kinetic energy which in one-dimensional form is

$$\frac{\partial E}{\partial t} = \underbrace{-\overline{u'w'}\frac{\partial u}{\partial z} - \overline{v'w'}\frac{\partial v}{\partial z}}_{\text{S}} \underbrace{- g\frac{\overline{w'\rho'}}{\rho_0}}_{\text{B}} - w\frac{\partial E}{\partial z} \underbrace{- \frac{\partial}{\partial z}\left(\overline{w'E'} + \frac{\overline{p'w'}}{\rho_0}\right)}_{\text{T}} \underbrace{- \epsilon}_{\text{D}}. \tag{9}$$

Several of the terms on the right-hand side of (9) have to be parameterized. For the shear production terms (S) we can use (5a) and (5b). The buoyancy term (B) first has to be related to the entropy flux and the moisture flux by means of thermodynamic relations and the Clausius–Clapeyron equation. Because we shall use an "all or nothing" condensation scheme, we have to distinguish only two different cases: saturated and unsaturated air. A derivation is given in appendix C and the result can be expressed as

$$-\frac{\overline{w'\rho'}}{\rho_0} = C_{\theta_q}\frac{\overline{w'\theta'_q}}{\theta_{q0}} - C_{q_w}\overline{w'q'_w}, \tag{10}$$

in which C_{θ_q} and C_{q_w} are given in Table 1. We then further use (5c) and (5d).

The transport term (T) is modeled as (Rodi, 1980)

$$-\left(\overline{w'E'} + \frac{\overline{p'w'}}{\rho_0}\right) = \frac{K_m}{\sigma_E}\frac{\partial E}{\partial z}, \tag{11}$$

in which σ_E is the turbulent Prandtl number for E, taken as a constant (see appendix A).

When we use the dissipation equation as an additional prognostic equation, ϵ is no longer an unknown in (9), and therefore at this stage we do not have to model it. When we use a diagnostic length scale, however, to calculate the eddy viscosity [Eq. (6)], we have to model ϵ in (9). It is modeled in the usual way as

$$\epsilon = c_\mu^{3/4} E^{3/2} / l_m. \tag{12}$$

1) DIAGNOSTIC LENGTH SCALE

When we make use of a diagnostic length scale formulation, we can express the eddy viscosity as in Eq. (6). In general we can distinguish three different length scales: a length scale in the surface layer, proportional to the distance to the surface, z; a length scale (l_∞) in the bulk of the convective layer, proportional to the depth of the convective layer, h; and a third length scale (l_s) for the stable layer and depending upon the TKE and the Brunt-Väisälä frequency, N_m. The final mixing length for (6) is then taken as some suitable interpolation between these three length scales, usually taken in the form (André et al., 1978)

$$l_{m,h} = \min(l_b, l_s), \tag{13}$$

in which

$$l_s = c_s E^{1/2} / N_m, \tag{14}$$

with

$$N_m^2 = -\frac{g}{\rho_0}\left(\frac{\partial \rho}{\partial z} - \frac{\partial p}{c_m^2 \partial z}\right) = g\left(\frac{C_{\theta_q}}{\theta_{q0}}\frac{\partial \theta_q}{\partial z} - C_{q_w}\frac{\partial q_w}{\partial z}\right),$$

TABLE 1. The coefficients C_{θ_q} and C_{q_w} in Eq. (10) for saturated and unsaturated air.

Class	C_{θ_q}	C_{q_w}
Unsaturated	1	$\frac{l_v}{c_{pd}T} - \frac{1-\epsilon_r}{\epsilon_r}$
Saturated	$\frac{1+\frac{l_v q_{vsat}}{R_d T}}{1+\frac{q_{vsat}\epsilon_r l_v^2}{c_{pd}R_d T^2}}$	1

(see appendix C, Eq. 44), and l_b is the formulation of the length scale according to Blackadar (1962)

$$l_b = \frac{\kappa z}{(\kappa z/l_\infty) + \phi_{m,h}}, \tag{15}$$

in which $\phi_{m,h}$ are the stability functions for the non-dimensionalized vertical gradients of wind (m) and temperature (h) in the surface layer according to Businger et al. (1971) and

$$l_\infty = c_\infty \frac{\int_0^h E^{1/2} z dz}{\int_0^h E^{1/2} dz}. \tag{16}$$

In (14) and (16) both c_s and c_∞ are constants (see appendix A).

Both analytically and numerically it is not very convenient to have different mixing length formulations under different circumstances. It is much easier to have one single equation. Moreover, length scale prescriptions oversimplify the turbulence. For example, from experimental studies (Nicholls, 1984) it is clear that the cloud layer can be decoupled from the subcloud layer. Under those circumstances the length scale in the cloud layer is determined by physical processes inside the cloud, and the length scales described previously are obviously inadequate. One way to address this problem is to use a prognostic length scale equation. An example of such a prognostic equation is the dissipation equation which will be discussed in the subsection 2b2.

2) THE ϵ-EQUATION

Using the ϵ-equation, we can express the exchange coefficients as in (8). Therefore, calculating ϵ by means of a prognostic equation is analogous to calculating l_m by a prognostic equation. The use of the ϵ-equation goes back to the work of Harlow and Nakayama (1967) and Daly and Harlow (1970). We will use a dissipation equation analogous to the one employed by Wyngaard (1975), Wyngaard et al. (1974) and Lumley and Khajeh-Nouri (1974). An exact transport equation for ϵ can be derived from the Navier–Stokes equations. This equation contains complex correlations whose behavior is poorly known. Fairly drastic model assumptions must be introduced in order to make this equation tractable. Therefore, the exact ϵ-equation is not given here.

At high Reynolds number the rate of dissipation is equal to the molecular kinematic viscosity times the mean-square vorticity fluctuations ($\overline{\omega_i' \omega_i'}$). Tennekes and Lumley (1972) show that at sufficiently high Reynolds numbers, there is a balance between the generation of $\overline{\omega_i' \omega_i'}$ due to turbulent vortex stretching and the destruction of $\overline{\omega_i' \omega_i'}$ due to viscosity. The terms next in order are the rate of change, advection and turbulent transport of $\overline{\omega_i' \omega_i'}$. Other terms (many of which appear in the full equations) are of higher order and can be neglected. The transport, generation and destruction terms require model assumptions. The transport term is modeled with the gradient assumption. The generation and destruction cannot be modeled separately: it is the difference that has to be modeled. We used a formulation of the dissipation equation that is almost equivalent to the one used by Wyngaard (1975):

$$\frac{\partial \epsilon}{\partial t} = -w \frac{\partial \epsilon}{\partial z} + \frac{\partial}{\partial z} \frac{K_m}{\sigma_\epsilon} \frac{\partial \epsilon}{\partial z} + c_{1\epsilon} \frac{\epsilon}{E} \max(\mathrm{S}, \mathrm{B} + \mathrm{S}) - c_{2\epsilon} \frac{\epsilon^2}{E}, \tag{17}$$

in which σ_ϵ is the turbulent Prandtl number for ϵ and S and B are, respectively, the shear and buoyancy production in the TKE-equation (9). The second term on the right-hand side of (17) is the turbulent transport term. The third and fourth term together represent the modeled generation *and* destruction of ϵ. In the modeled equation (17) the third term can be named "production" of ϵ and the fourth term the "destruction" of ϵ, although they do not correspond to the generation and destruction terms in the original exact equation. The constants we used are given in appendix A.

c. *Thermodynamics*

In section 2a, a new variable was introduced for the entropy known as the wet equivalent potential temperature, θ_q. The variable θ_q is defined as the temperature which a saturated (or unsaturated) air parcel would have when it would be transformed isentropically to a reference pressure p_* (taken as the surface pressure) and all water condensed; i.e. $q_v = 0$ and $q_l = q_w$. The wet equivalent potential temperature was introduced by Paluch (1979). The expression for θ_q is

$$\theta_q = T \left(\frac{p_d}{p_*} \right)^{-R/c_p} \exp\left(\frac{L_1 q_v}{T c_p} \right), \tag{18}$$

where the index d denotes the dry air value and

$$R = R_d(1 - q_w),$$

$$c_p = c_{pd}\left[1 + q_w \left(\frac{c_{pl}}{c_{pd}} - 1 \right) \right],$$

$$L_1 = l_v - R_v T \ln(e/e_{\mathrm{sat}}).$$

(See appendix A for list of symbols.) Later θ_q was also used by Durran and Klemp (1982). A useful discussion of the accuracy of θ_q as a variable is given by Pointin (1984). He also compares it with other prognostic variables; e.g., the equivalent potential temperature or the liquid potential temperature.

Processes in the atmosphere are nearly isentropic. In order to keep the numerical errors small, it is advantageous to use the entropy or the wet equivalent potential temperature as a prognostic variable instead

of the temperature. However, the temperature has to be calculated diagnostically in order to be able to tell whether a parcel is saturated or unsaturated. To calculate the temperature from (18) we have to give the relation between the partial saturation vapor pressure and the temperature, $e_{sat} = e_{sat}(T)$. In appendix B two relations are discussed for e_{sat}(T): an empirical fit and a polynomial fit that is accurate over a sufficiently large temperature range. From appendix B, it follows that the latter has a significant computational advantage.

d. Radiation model

From experimental data it is clear that by far most of the radiative flux divergence takes place inside the cloud layer. Therefore, as a first approximation we neglect the radiative flux divergence outside the cloud. We prescribe the incoming shortwave and longwave radiative flux at the top of the model. At the surface we prescribe an albedo a and assume that the surface radiates as a blackbody. The upward and downward radiative fluxes are unchanged as long as we are outside the cloud.

1) LONGWAVE RADIATION

The longwave radiation model makes use of the effective emissivity. This concept has been discussed by Cox (1976). The radiative fluxes are then given by

$$F_L^{\downarrow}(z) = F_L^{\downarrow}(z_{ct})[1 - \epsilon^{\downarrow}(z)] + \epsilon^{\downarrow}(z)\sigma T^4(z), \quad (19a)$$

$$F_L^{\uparrow}(z) = F_L^{\uparrow}(z_{cb})[1 - \epsilon^{\uparrow}(z)] + \epsilon^{\uparrow}(z)\sigma T^4(z). \quad (19b)$$

In these formulas, T is the temperature at height z and $F^{\uparrow}(z_{cb})$ and $F^{\downarrow}(z_{ct})$ are the impinging fluxes at cloud base and cloud top, respectively. It is necessary to define two different effective emissivities since the spectral composition of the two beams incident on the cloud boundaries are quite different. Based on observations, Stephens (1978) parameterized $\epsilon^{\uparrow\downarrow}$ as follows

$$\epsilon^{\uparrow\downarrow} = 1 - \exp(-a_0^{\uparrow\downarrow} W), \quad (20)$$

in which W is the liquid water path length, given by

$$W = \left\| \int_{z_{ct}, z_{cb}}^{z} \rho_0 q_l dz \right\|.$$

The mass absorption coefficients for upward and downward emissivity are

$$a_0^{\uparrow} = 130\ \mathrm{m^2 kg^{-1}}$$

$$a_0^{\downarrow} = 158\ \mathrm{m^2 kg^{-1}}. \quad (21)$$

2) SHORTWAVE RADIATION

The shortwave radiation model is a parameterization described by Manton (1980). It is based on a two-layer model, a cloud layer and a subcloud layer, overlying a surface with albedo a. He gives the reflectance R, absorptance A, and transmittance T as a function of cloud height H, total water content W_t, and droplet concentration N. The expressions at zero zenith angle are

$$R_0 = \exp(-117/(HW_tN)^{1/4}), \quad (22a)$$

$$T_0 = 1 - \exp(-24.5/(HW_t^3N)^{1/4}), \quad (22b)$$

$$A_0 = 1 - R_0 - T_0, \quad (22c)$$

in which H is in m, W_t in kg m^{-2} and N is in m^{-3}. The reflectance, absorptance and transmittance also depend upon the solar zenith angle ϕ. A reasonable approximation is obtained from the following empirical formula (Manton, 1980):

$$R_1 = 1 - (1 - R_0)\cos^{1/4}\phi, \quad (23a)$$

$$T_1 = (1 - R_1)/(1 + A_0/T_0), \quad (23b)$$

$$A_1 = 1 - R_1 - T_1. \quad (23c)$$

When the albedo of the surface is greater than zero, the reflectance, absorptance and transmittance will also depend upon a. Neglecting gaseous absorption in the atmosphere beneath cloud and assuming that the reflectance and transmittance for upward radiation at cloud base are the same as those for downward radiation at cloud top, Manton (1980) finds that the effect of the surface albedo can be incorporated as

$$R = R_1 + aT_1^2/(1 - aR_1), \quad (24a)$$

$$T = (1 - a)T_1/(1 - aR_1), \quad (24b)$$

$$A = 1 - R - T. \quad (24c)$$

In the parameterization, A is the absorptance over the whole cloud layer. In the numerical model, we want to know the shortwave flux throughout the cloud layer. We have used the formula

$$F_S^{\downarrow}(z) - F_S^{\uparrow}(z) = AF_S^{\downarrow}(z_{ct})e^{-(20W/\cos\phi)} + TF_S^{\downarrow}(z_{ct}), \quad (25)$$

which is a fit on the heating-rate profiles presented by Manton (1980).

e. Boundary conditions

In this paper we deal with marine stratocumulus only and prescribe a constant sea surface temperature T_s. As lower boundary condition for the specific humidity, we take $q_{ws} = q_{vsat}(T_s)$, where q_{vsat} is the saturation value. The roughness height over the sea is prescribed as $z_0 = 2 \times 10^{-4}$ m.

To calculate the turbulent fluxes near the surface, we use Monin–Obukhov similarity theory to relate the fluxes to the vertical gradients in the surface layer:

$$\frac{\partial \|\vec{v}\|}{\partial z} = \frac{u_*}{\kappa z}\phi_m(z/L), \quad (26a)$$

$$\frac{\partial \theta_q}{\partial z} = \frac{\theta_{q^*}}{\kappa z}\phi_h(z/L), \quad (26b)$$

$$\frac{\partial q_w}{\partial z} = \frac{q_{w*}}{\kappa z}\phi_h(z/L), \tag{26c}$$

in which L is the Monin–Obukhov length,

$$L = \frac{u_*^3/\kappa}{(g/\rho_0)\,\overline{w'\rho'}_s}, \tag{27}$$

and the relation between the scaling variables and the surface fluxes is defined by

$$u_*^4 = (\overline{u'w'})_s^2 + (\overline{v'w'})_s^2, \quad \theta_{q*} = -(\overline{w'\theta_q'})_s/u_*,$$

$$q_{w*} = -(\overline{w'q_w'})_s/u_*,$$

where the index s denotes the surface-layer value of the fluxes. Furthermore, the similarity functions ϕ are taken the same for temperature and humidity. The functions ϕ_m and ϕ_h have to be determined from experiments. We took the functions given by Businger et al. (1971) from the Kansas experiment. Equations (26) are used in integrated form from the surface to a height z_1 (index 1 corresponds to lowest model level) in the surface layer to relate the differences $\vec{v}_1$, $\theta_{q1} - \theta_{qs}$ and $q_{w1} - q_{ws}$ to the turbulent surface layer variables u_*, θ_{q*} and q_{w*}.

The solution of the TKE-equation and the ϵ-equation requires specification of E and ϵ or their fluxes in the surface layer. We prescribed the values of E and ϵ at the first level above the surface following André et al. (1978):

$$E_1 = c_\mu^{-1/2}u_*^2 + 0.35w_*^2, \tag{28}$$

$$\epsilon_1 = \left\{u_*^3\left(\frac{\phi_m}{\kappa z} - \frac{1}{\kappa L}\right)\right\}_{z_1}, \tag{29}$$

in which

$$w_* = \left[-\left(\frac{g}{\rho_0}\overline{w'\rho'}\right)_s h\right]^{1/3},$$

where h is the boundary-layer height. The convective velocity scale w_* has been included to reflect the horizontal motions induced by the large eddies in unstable conditions. The surface boundary condition for ϵ is based on the fact that in the atmospheric surface layer viscous dissipation balances shear production and buoyancy (Lenschow et al., 1980).

At the top of the model the second derivative of the variables θ_q, q_w, u and v and the first derivative of E and ϵ were set equal to zero.

f. Numerical aspects

1) VERTICAL RESOLUTION

The most straightforward method of discretization is to take an equidistant grid in the vertical. However, vertical variation is large in the surface layer and near the top of the ABL. In order to simulate correctly these strong gradients, we have to increase our resolution in these two regions. Near the surface, a logarithmic coordinate transformation is adequate. Near the top of the ABL we use a hyperbolic tangent coordinate transformation to compress the grid there. As a result, our transformation can be written as

$$\zeta = \frac{z}{A} + \ln\left(\frac{z+B}{B}\right) + C\left[\tanh\left(\frac{z-H}{D}\right) + 1\right] \tag{30}$$

in which A, B, C, D and H are constants that determine the stretching of the grid. The grid is equidistant in ζ between z_1, close to the surface and the top of the model. The constant B is of the order of the roughness height z_0; H is taken as the expected inversion height, whereas D is a measure for the distance over which the tanh has effect. Some experimentation is required to find suitable values for the constants. Table 2 gives the correspondence between the transformed coordinate ζ and z, for a set of constants used.

2) NUMERICAL DISCRETIZATION

A standard explicit leapfrog scheme was used for the discretization in time. A central discretization in space was used, with the diffusion terms lagged in time. In order to remove any tendency toward decoupling the odd and even time steps, the time filter proposed by Robert (1966) is used in the model. The variables are spatially staggered on the grid, as given in Fig. 2. The model is set up to be two-dimensional. In the present one-dimensional version the horizontal staggering is not effective.

3. Model results and comparison with observations

The model developed is used to study various combinations of physical processes in a cloud-topped ABL and their combined effect on the turbulent structure. The most important factors influencing the turbulence are (Driedonks, 1986): 1) upward buoyancy flux at the surface, 2) longwave radiative cooling near cloud top,

TABLE 2. Correspondence between level number and height z. (See also Fig. 2 for level numbering.) Parameters used are A = 200, B = 0.01, C = 2.25, D = 150 and H = 600.

Level	z (m)	Level	z (m)
1	2.0	21	491.2
3	4.8	23	540.0
5	11.1	25	582.4
7	25.1	27	623.2
9	52.6	29	666.7
11	99.8	31	718.8
13	168.9	33	789.0
15	255.7	35	892.2
17	348.4	37	1025.0
19	429.3	39	1172.0
		41	1323.3

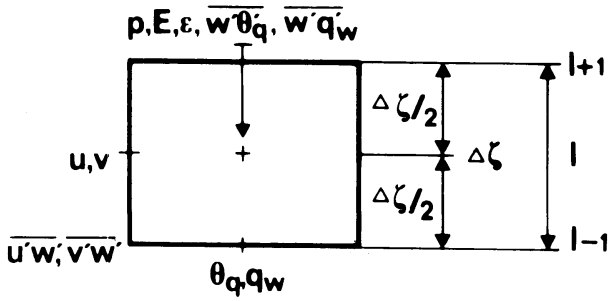

FIG. 2. Spatially staggered mesh with locations of variables and fluxes; l = the level (see also Table 2). The staggering in the horizontal is not effective in the present one-dimensional model.

3) in-cloud warming due to shortwave radiative absorption, and 4) wind shear near cloud top.

The first two of these processes are usually considered to have similar effects. The cooling at cloud top generates convective mixing because cool parcels of air sink, much in the same way as a warm lower surface generates convective mixing as warm thermals rise. In order to study this similarity we first consider two idealized cases. In the first case, we apply an upward surface buoyancy flux at the bottom of a cloud-topped ABL and turn off all radiative processes. This case is similar to a convective dry mixed layer, apart from the cloud layer in the upper half of the ABL, which leads to latent heat release and evaporative cooling. In the second case, we set the surface buoyancy flux to zero and turn on the longwave radiation.

In these two cases we use model versions both with a diagnostic length scale formulation and with a dissipation equation (equivalent to a prognostic length scale equation), as given in subsections 2b1 and 2b2, respectively. The results of these different turbulence closures are evaluated.

The third and fourth case studies are set up to compare the model results with actual observations. In these two cases, there are rather complicated vertical distributions of sources and sinks controlling the turbulence. Therefore, we used in these cases the model with a dissipation equation only, in order to allow the turbulence to evolve more freely than it would with a diagnostic length scale. The third case represents the observations by Nicholls (1984) in a Sc-deck over the North Sea. Crucial here is the combined effect of longwave cooling at cloud top, in-cloud heating by shortwave absorption, and a small upward surface buoyancy flux. A special feature that has to be studied is the possible decoupling of the cloud layer from the subcloud layer. This means that there is turbulent mixing inside both the cloud layer and subcloud layer but that the interaction between both layers is rather small. This decoupling is mainly due to the shortwave heating deep inside the cloud.

The fourth case represents the observations by Brost et al. (1982a,b) of a Sc-deck off the California Coast. The dominant physical processes in this case were longwave cooling and strong local wind shear, both at cloud top. Shortwave absorption and surface buoyancy flux were not important. Brost et al. claim that in their case the cloud-top cooling was compensated by entrainment of warmer air from above the inversion, instead of generating a positive buoyancy flux throughout the ABL. The entrainment is then supposedly caused by turbulence generated by the local wind shear at the ABL-top.

In all model calculations the large-scale vertical velocity has been set equal to zero and the model is run for a time long enough to ensure that the turbulence is in equilibrium with the imposed boundary conditions. This means, that the simulation time has to be longer than the characteristic time scale of the turbulence, but small enough to ensure that the mean characteristics (θ_q, q_w, q_l, h, etc.) have not changed too much. Therefore, the following results are no steady state solutions for the mean variables, which evolve slowly, but are solutions in which the turbulence is in local equilibrium with the external conditions.

a. Surface-based convection

This case concerns a (hypothetical) cloud-topped ABL, in which the turbulence is driven by convection from the surface, and radiational effects are turned off. The surface buoyancy flux is controlled by the surface temperature (T_s = 290 K) and the temperature and specific humidity in the overlying air (287.9 K and 8.5 g kg^{-1} respectively). A geostrophic wind of 6 m s^{-1} is prescribed in the ABL. The resulting buoyancy production term in the TKE budget is about 10^{-3} m^2 s^{-3} at the surface, equivalent to a surface virtual heat flux of 37 W m^{-2}. The ABL is 920 m high with a cloud between 450 and 920 m. The value of the stability parameter $-h/L$ is about 50. The initial profiles for θ_q and q_w are given in Fig. 3 and Table 3.

The model described in section 2 is run for 1 h of simulation time in two versions: the first uses a diagnostic length scale as described in subsection 2b1, while the other uses the dissipation equation as described in

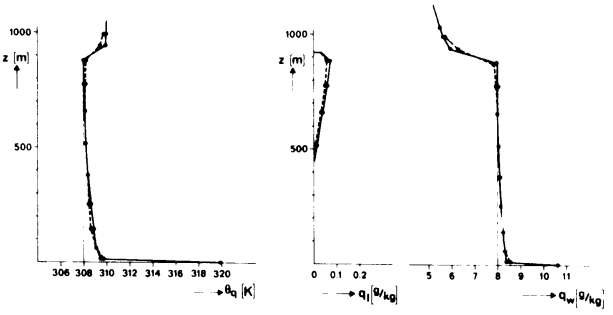

FIG. 3. Profiles of the mean variables θ_q, q_l and q_w. Solid line: initial profile; solid line with dots: l-run; dashed line with dots: ϵ-run.

TABLE 3. The initial profiles used in the different simulations. Given are the height-independent values of θ_q and q_w in the ABL, the jumps in θ_q and q_w at the inversion, the gradient in θ_q and q_w above the inversion, and the boundary layer height.

Section	θ_q (K)	q_w (g/kg)	$\Delta\theta_q$ (K)	Δq_w (g/kg)	$\frac{\partial\theta_q}{\partial z}$ (K/km)	$\frac{\partial q_w}{\partial z}$ [g/(kg km)]	h [m]
3*a* and 3*b*	308	8	2	−2	0	−3.6	900
3*c*	308	8.2	2	−2.2	0	−3.3	800
3*d*	304.2	7.4	8.8	−3.4	0	−1.0	600

subsection 2b2. We will denote these by the *l*-run and ϵ-run, respectively. The final profiles for θ_q, q_w and q_l are given in Fig. 3 and are almost the same for both runs. Figure 4 shows the vertical profile for turbulent kinetic energy (E). This vertical profile is typical for a convective boundary layer (Dearforff, 1974b). There are only small differences between the *l*-run and ϵ-run.

In Fig. 5 the results for the turbulent fluxes of the conservative quantities θ_q and q_w are given. The *l*-run and ϵ-run give roughly the same result in the lower half of the ABL. However, they differ considerably near cloud top. The entrainment, defined by the minimum in the fluxes at the inversion base, is about four times higher in the ϵ-run than in the *l*-run.

The cause of these differences can be made clearer through inspection of the turbulent kinetic energy budget, depicted in Fig. 6a, b. Inspection of the various terms near the top of the ABL shows that in both runs the transport term is about equally large. Shear production is negligible. Since the rate of change of TKE ($\partial E/\partial t$) is also very small, there is a balance between buoyancy B, transport T, and dissipation D. There is a large difference between the dissipation calculated in the *l*-run and in the ϵ-run. In the *l*-run, the dissipation is quite large and rather anomalous. The cause of this large dissipation is the small diagnostic length scale that is chosen in the stable layer at the top of the ABL (see subsection 2b1). The length scale in stable conditions is borrowed from turbulence in a stable nocturnal boundary layer over land where there is a balance between total turbulent production and dissipation, while the transport term is negligible (e.g., see Brost and Wyngaard, 1978). In the present application, where entrainment occurs at the top of the ABL, the situation is quite different because transport is important and the choice for the diagnostic length scale is highly questionable, leading to an anomalously large dissipation rate at the ABL-top. Thus the results obtained with the ϵ-run seem to be better than with the *l*-run.

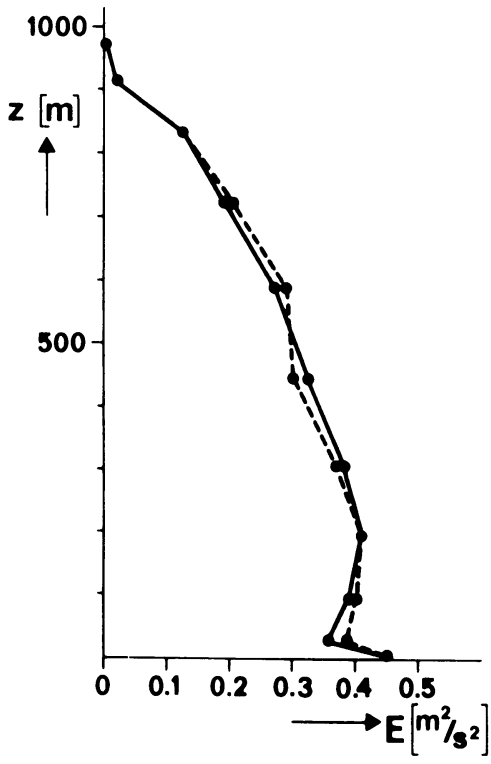

FIG. 4. Profile of TKE as predicted by the model. Solid line: *l*-run; dashed line: ϵ-run.

b. *Longwave radiative cooling*

In this experiment, we study a cloud-topped ABL in which the turbulence is driven only by longwave radiative cooling at cloud top. Thus, compared to the foregoing case, we set the surface buoyancy flux to zero and turn on the longwave radiative fluxes. Other conditions are the same. The profiles for θ_q and q_w after

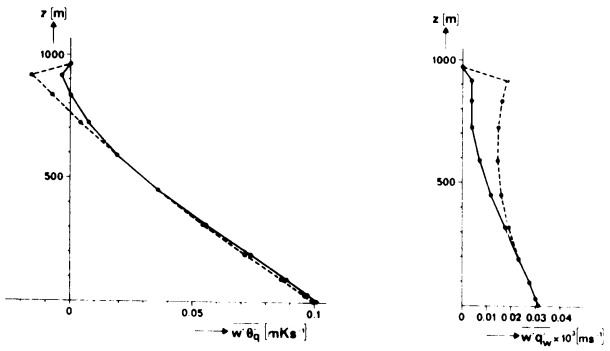

FIG. 5. Profiles of the fluxes $\overline{w'\theta'_q}$ and $\overline{w'q'_w}$. Solid line: *l*-run; dashed line: ϵ-run.

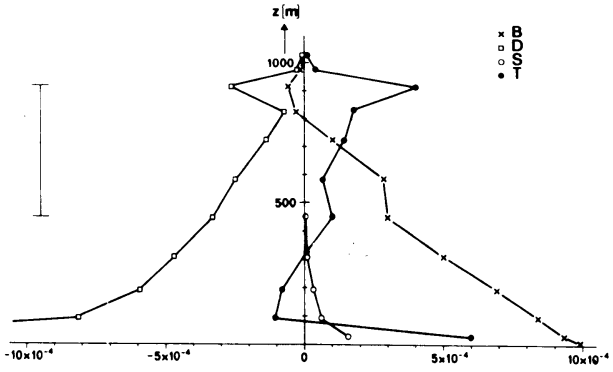

FIG. 6a. TKE-budget as calculated in the *l*-run with: B, buoyancy production; D, viscous dissipation; S, shear production; and T, turbulent transport. The extent of cloud layer is indicated by vertical bar.

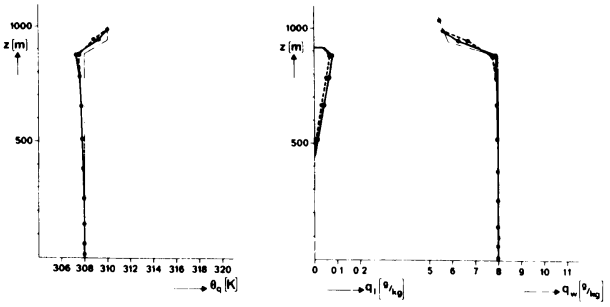

FIG. 7. As in Fig. 3.

1 h of simulation time are shown in Fig. 7, again both for the *l*-run and ϵ-run. The longwave radiative flux profile is shown in Fig. 8 and leads to a strong cooling rate at cloud top of about 3.7 K h^{-1} due to the radiative flux divergence of 90 W m^{-2} over only 70 m. There is also a weak radiative heating near cloud base. The calculations have also been carried out with this weak cloud base heating turned to zero, and the results did not show any significant difference. Thus, it appears to have no important consequences for the dynamics.

The profiles of the vertical fluxes of the conservative variables θ_q and q_w are given in Fig. 9; they show that the cloud top cooling generates upward turbulent fluxes but that these are mostly confined to the upper part of the ABL. The evolution of θ_q is controlled by the sum of $w'\theta_q'$ and $(\theta_{q_0}/T_0)(1/\rho_0 c_{pd})F$, [see Eq. (3)]. The sum of these fluxes from Figs. 8 and 9 results in a vertical profile with two distinct regions: an almost linear part with a rather strong gradient in the cloud layer and an almost constant total flux in the subcloud layer. Thus θ_q evolves in a different way in both regions and the mixing does not extend down to the surface. Another demonstration of the difference between this case and the foregoing one is given by the distribution of TKE in Fig. 10 (cf. Fig. 4). Here the TKE is almost exclusively confined to the upper half of the ABL with almost no energy in the subcloud layer, quite different from the upside-down version of Fig. 4.

The various terms in the TKE-budget are shown in Fig. 11a, b (for the *l*-run and ϵ-run, respectively). In general, there is a balance between buoyancy B, transport T, and dissipation D. The cloud top cooling generates an upward buoyancy flux throughout the upper half of the ABL. Below cloud base the fluxes are small. The maximum in the buoyancy flux, generated below cloud top in this case, has about the same magnitude as the upward buoyancy flux in section 3a. However, it doesn't extend all the way down to the surface as it extended all the way up to the ABL top in the foregoing case.

As in the first case, the dissipation rate at cloud top for the *l*-run is anomalously large. The negative buoyancy flux is about two times smaller than for the ϵ-run. As in the former case, here also the results of the ϵ-run seem more realistic than of the *l*-run. For further calculations, we therefore use only the ϵ-formulation.

The conclusion from the results of this section compared with the foregoing must be that there is consid-

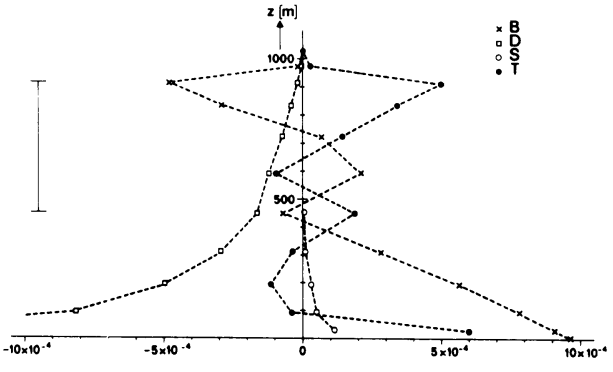

FIG. 6b. As in Fig. 6a but in the ϵ-run.

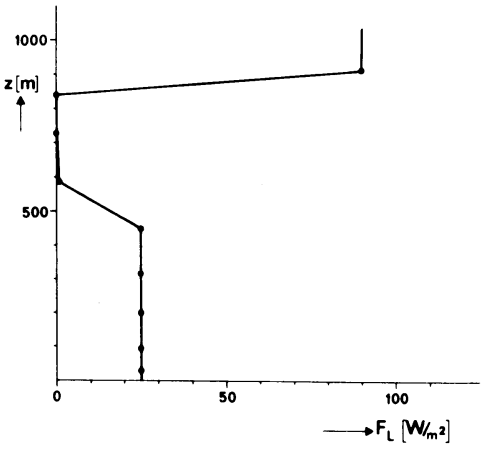

FIG. 8. The net longwave radiative flux as a function of height.

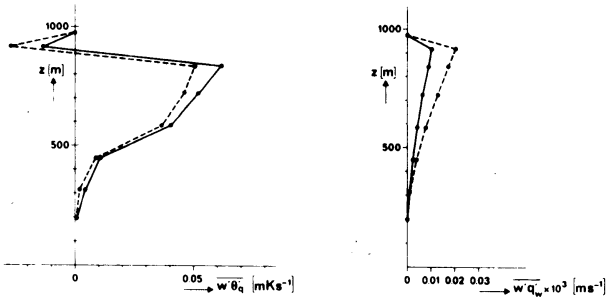

FIG. 9. The profiles of the fluxes $\overline{w'\theta_q'}$ and $\overline{w'q_w'}$. Solid line: *l*-run; dashed line: ϵ-run.

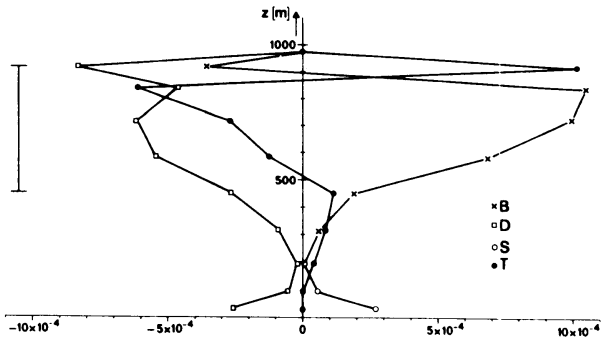

FIG. 11a. As in Fig. 6a. The TKE-budget for the *l*-run. The extent of the cloud layer is indicated by the vertical bar.

erable difference in structure of a cloud-topped ABL when heated from below or cooled from above even when the maximum buoyancy flux in both cases is about the same. Cloud top cooling is less effective in generating turbulent kinetic energy throughout the whole ABL than surface heating.

As a result, there will be a tendency to confine the mixing of entrained air to the cloud layer. Depending on the properties of the overlying air, the cloud layer can then stabilize with respect to the subcloud layer (leading to further decoupling) or destabilize (reestablishing the interaction again). The decoupling is favored when the cloud is heated by shortwave absorption. This effect is studied in the next case, a comparison with an observational study by Nicholls (1984).

c. *North Sea stratocumulus*

We now compare our model with detailed turbulence measurements taken by Nicholls (1984) from an aircraft in a stratocumulus deck over the North Sea.

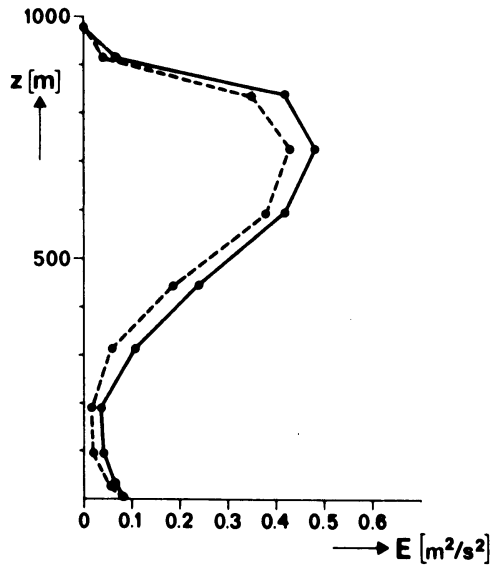

FIG. 10. The TKE-profile: Solid line: *l*-run; dashed line: ϵ-run.

His data consist of mean profiles, turbulent fluxes, radiative fluxes and cloud microphysics. They constitute a good dataset for comparison with model simulations. The most dominant physical processes in this Sc-deck are the longwave radiative cooling at cloud top, in-cloud warming due to shortwave radiative absorption, and a (rather small) surface buoyancy flux. Wind shear was not important. Nicholls (1984) noted a significant amount of drizzle (or, as he called it, gravitational water droplet settling). Although this may be an extra effect in the water budget and may cause additional evaporative cooling of the subcloud layer, we will not consider it in our model. Instead we will concentrate on the physical processes listed above.

Nicholls took his measurements around noon in the central part of an extensive sheet of stratocumulus covering a large part of the North Sea on 22 July 1982. The clouds were formed and maintained in the northerly flow caused by an almost stationary anticyclone west of Ireland. The wind speed was about 8.5 m s^{-1} from the north, with little vertical shear. The air was slightly cooler than the sea water, causing an upward virtual heat flux ($\rho c_{pd} \overline{w'\theta_v'}$) at the surface of about 14 W m^2. Cloud top and cloud base were, on the average, at 800 and 400 m, respectively. Throughout the ABL

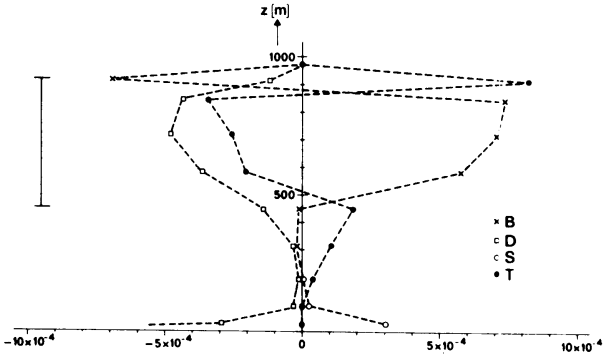

FIG. 11b. As in Fig. 6b. The extent of the cloud layer is indicated by the vertical bar.

the variations of θ_q and q_w were small up to cloud top where there were sharp jumps of 5 K in temperature and -2 g kg^{-1} in humidity.

The turbulence measurements in this case are quite interesting since they show that this combination of physical processes in the ABL may lead to decoupling of the cloud layer from the subcloud layer in a sense that the layers are both turbulent but that their interaction is small. This effect, already touched upon earlier, is envisaged to be favored by the combination of longwave radiative cooling concentrated in a very shallow layer near cloud top, and the shortwave radiative warming extending much deeper into the cloud. This combination may lead to instability on the scale of the cloud depth itself, introducing a corresponding length scale for the turbulence independent of the depth of the subcloud layer and to decoupling. The decoupling is enhanced by the entrainment of warm and dry air from above the inversion which is then mixed only over the cloud layer, establishing a stable layer near cloud base. The decoupling also will be favored when the surface buoyancy flux is small, since strong surface-based convection will establish mixing over the whole ABL again. Nicholls (1984) noted that these factors, combined with the cooling of the subcloud layer by evaporating drizzle favor the formation of a stable layer at cloud base.

The model simulation was started with the vertical profiles for θ_q and q_w given in Fig. 12 and Table 3. The sea surface temperature was set at 288 K and the air just above the sea surface was saturated at this temperature. The model run was started at 10 UT, continuing for 2 h simulation time. Unlike the preceding cases, we took only the dissipation equation as turbulence closure here (ϵ-run).

The vertical profiles of calculated net shortwave and longwave radiative fluxes are given in Fig. 13. The overall longwave radiative flux divergence over the cloud layer is -58 W m^{-2}, the overall shortwave absorption is 79 W m^{-2}. The former is 3 W m^{-2} less than the observed value of Nicholls (1984); the latter is only 6 W m^{-2} more than his calculations with a rather complicated model and it is 20 W m^{-2} more than his observations. The bulk effect of the radiation is thus an

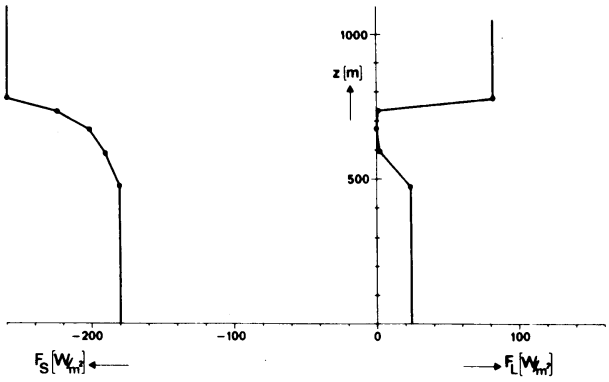

FIG. 13. As in Fig. 8 but including the net shortwave radiative flux.

absorption of 21 W m^{-2} over the cloud layer, corresponding to an average heating rate of about 0.15 K h^{-1}. For the turbulence, however, the vertical distribution of the heating and cooling rates within the cloud is more important than the overall effect. The longwave flux leads to strong localized cooling near cloud top and a small local heating near cloud base. In contrast to these, the heating rate caused by the shortwave radiative flux is distributed more smoothly over the whole cloud layer. The combined effect of both types of radiation will thus be the heating of layers deep into the cloud and the cooling of the cloud top.

The final profiles for θ_q, q_w and q_l are also shown in Fig. 12. The cloud layer is between 450 and 780 m. The profile of θ_q does not show much structure, except perhaps for a slight increase above cloud base. In the humidity profile of q_w, however, it is clear that the moisture input from the sea surface and the input of dry air from above are not well mixed over the whole ABL but are mostly confined to the subcloud layer and the cloud layer, respectively. The measurements of Nicholls (1984) showed roughly the same tendency in the profiles for θ_q and q_w.

The turbulent fluxes $\overline{w'\theta'_q}$ and $\overline{w'q'_w}$ are shown as a function of height in Fig. 14. Agreement between the

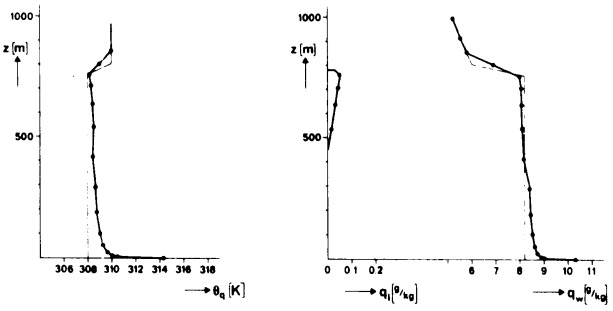

FIG. 12. As in Fig. 3 but solid line with dots: ϵ-run.

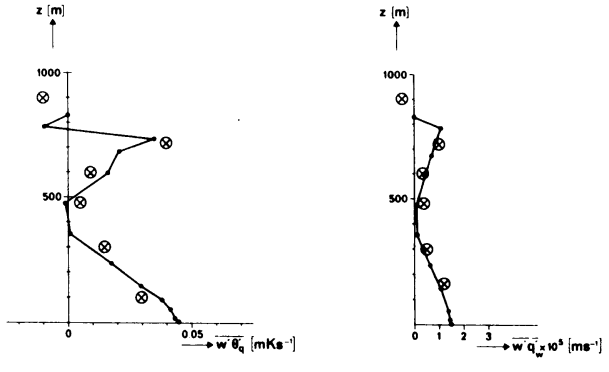

FIG. 14. The profiles of the fluxes $\overline{w'\theta'_q}$ and $\overline{w'q'_w}$ compared with the averaged results of Nicholls (1984) ((×)).

model calculations and the average values of the observations is remarkably good. The computed, as well as the observed vertical profile of $\overline{w'q'_w}$, is not linear from the surface up to cloud top, as would be the case in a well-mixed ABL, but has two distinct regions. The vertical gradient of $\overline{w'q'_w}$ is linear but negative in the subcloud layer, so q_w increases with time there, and linear but positive in the cloud layer, so there q_w decreases with time. The combined effect of both is an increase in height of the base of the Sc-deck and simultaneously a lowering of the lifting condensation level (LCL) in the subcloud layer. Thus there will be a tendency for cumulus clouds to be formed clearly below the base of the Sc-deck. Nicholls (1984) reported that cumulus rising into stratocumulus was frequently observed during his experiment. Extension of the simulation time of the model calculations with two more hours also showed the formation of secondary clouds below the upper cloud deck.

If the ABL would be well mixed, the profile of $w'\theta'_q + [\theta_{q0}/(\rho_0 c_{pd} T_0)]F$ would be linear with height. Combining Figs. 13 and 14, one can show that in this case this sum is not linear with height throughout the ABL, indicating again that the ABL is not well mixed. From the sea surface upwards this sum decreases linearly with height throughout the subcloud layer. Near cloud base the sum remains constant, and above cloud base it decreases again with height. Both in the subcloud layer and in the cloud layer, θ_q increases with time, whereas at their interface θ_q remains constant.

The formation of a stable layer near cloud base (as described here) can be made clearer through inspection of the turbulent kinetic energy budget. The various terms from the model calculations are shown in Fig. 15a. The negative buoyancy term near cloud base clearly indicates the formation of a stable layer. In the subcloud layer there is a production of TKE by shear and buoyancy balanced by viscous dissipation. Transport is relatively unimportant in this region. In the cloud layer TKE is produced by buoyancy balanced by viscous dissipation and turbulent transport. The transport term is negative in the cloud layer and positive at the inversion and near cloud base. Thus, part

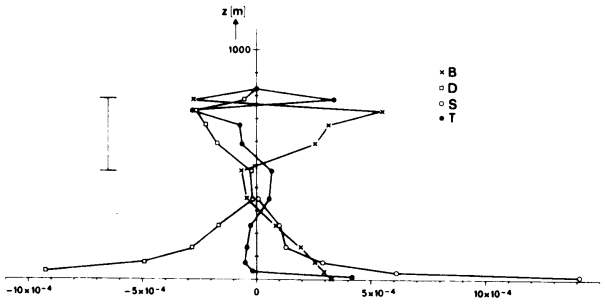

FIG. 15a. The computed TKE-budget, the extent of the cloud layer is indicated by the vertical bar.

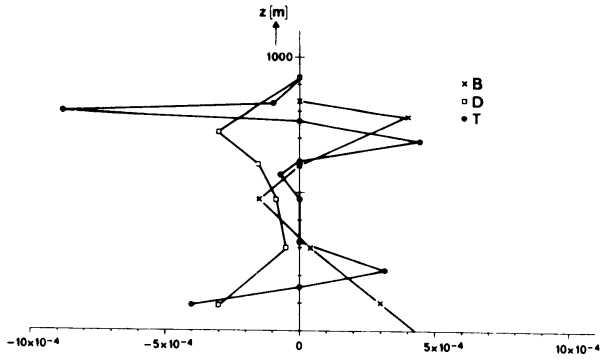

FIG. 15b. The TKE-budget measured by Nicholls (1984).

of the TKE produced in the cloud layer by buoyancy is transported upwards and downwards, intruding both into the stable layer above the inversion and the stable layer near cloud base. The buoyancy, dissipation and transport as measured by Nicholls (1984) are shown in Fig. 15b. Comparison of Fig. 15a, b shows that the computed profiles for buoyancy and dissipation are roughly the same as those measured by Nicholls (1984) except for the entrainment zone that is not resolved in the measurements. The transport terms, however, differ considerably. This is probably due to the fact that the measured transport in Fig. 15b contains only contributions from third-order velocity correlations. The residue in Fig. 15b is attributed by Nicholls (1984) to the transport by pressure–velocity correlations, included in Fig. 15a. Thus the terms T in Fig. 15a, b do not represent the same quantities.

The computed profile of TKE is shown in Fig. 16, together with the average values of TKE as measured by Nicholls. The vertical distributions of TKE are similar with a minimum in the vicinity of cloud base, although in the calculations this local minimum is more pronounced than in the measurements. Recently Bougeault (1985) made a simulation of the JASIN experiment with a third-order turbulence closure model. The turbulent kinetic energy profiles he found are quite similar to ours.

d. Case of Californian stratocumulus

In this case study we use our model to simulate observations described by Brost et al. (1982a,b) taken in a stratocumulus deck over the sea off the California Coast, a region where extended Sc-decks are fairly common during summer. We will focus our attention on the aircraft data taken on 17 June 1976, because of the particular combination of physical processes that determined the turbulence and that was quite different from the cases described in the foregoing sections. The measurements were taken during the night and early morning, so shortwave radiative fluxes were of no importance. Wind shear, however, was of great signifi-

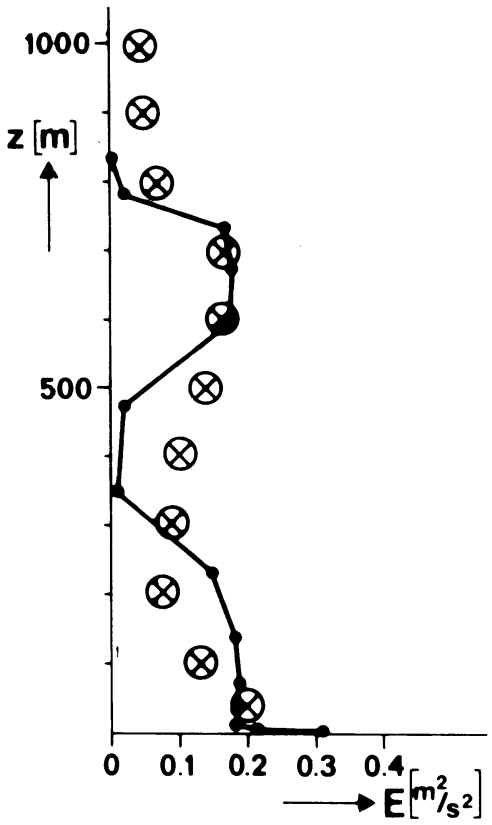

FIG. 16. The profile of TKE computed by the model compared with the averaged results of Nicholls (1984) ((×)).

cance. Wind speed was rather high with a strong jump localized near cloud top, generating turbulence there. Cloud top longwave radiative cooling was also important, but the surface buoyancy flux was very small. Brost et al. (1982a,b) also noted some drizzle in the cloud, which was not considered in our model calculations.

The measurements of Brost et al. (1982a,b) were taken on 17 June 1976 and centered around ~37.5°N and 126.5°W. There were strong winds in the ABL with little variation up to the ABL-height where strong jumps occurred. We consider the observations from flight legs labeled 17-2. The surface buoyancy flux was very small. The ABL-height was about 600 m with a solid cloud deck in the upper half. The vertical variation of θ_q and q_w was small up to the sharp inversion at cloud top. Brost et al. (1982a) denote rather small values of the liquid water content in the cloud layer, much smaller than the adiabatic values. However, for instrumental reasons, their mean values of q_l are probably not as reliable as their turbulence data (Brost et al., 1982a).

The turbulence measurements in this case revealed a vertical structure quite different from the cases discussed in the foregoing sections. Brost et al. (1982b)

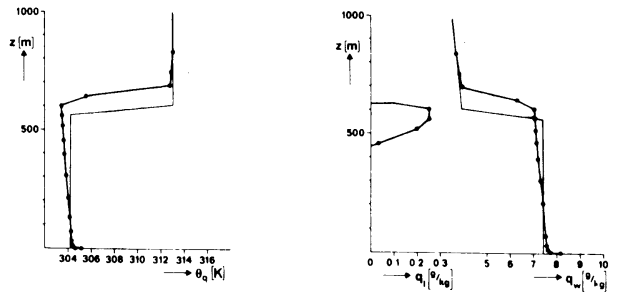

FIG. 17. As in Fig. 3 but solid line with dots: ϵ-run.

argue that in the present case the longwave cloud-top cooling did not generate a strong upward buoyancy flux throughout at least a large fraction of the ABL. Instead, the local strong wind shear generated a significant amount of turbulence near cloud top and the resulting entrainment of warm air from above compensated the longwave cooling of the cloud in a local sense. Thus the cloud-top processes were hardly felt farther down into the ABL, which therefore showed the typical structure of a neutral ABL with small buoyancy fluxes. In this way the present combination of

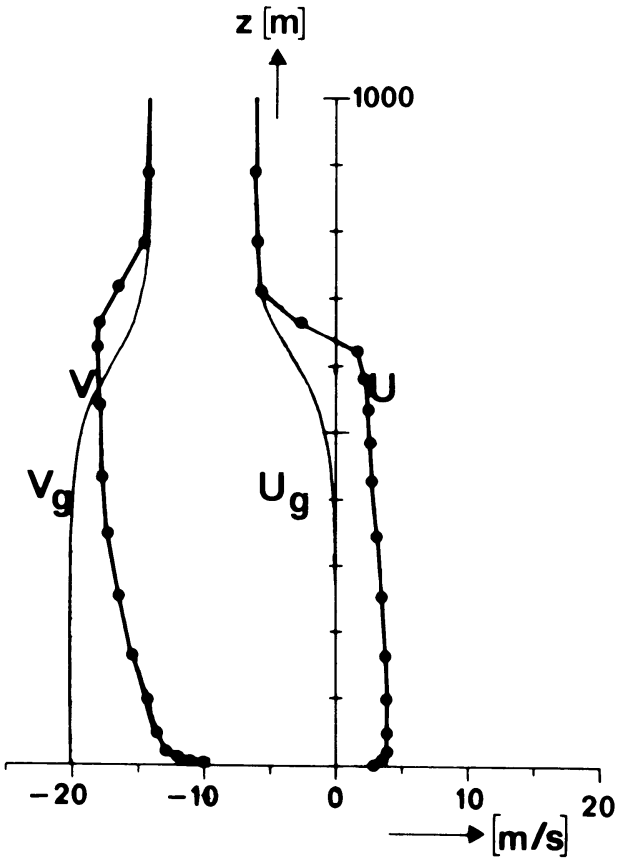

FIG. 18. The profiles of the prescribed geostrophic winds and the velocities calculated by the model.

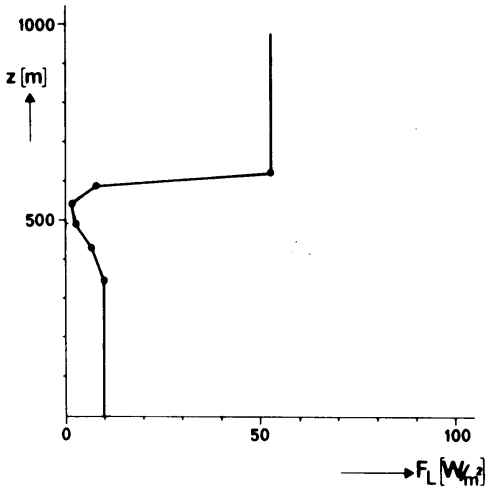

FIG. 19. As in Fig. 8.

physical processes generates a type of cloud-topped ABL that is quite different (from the point of view of the turbulent structure) from the foregoing cases.

The model simulation was set up in a way to see whether this type of turbulence structure could be simulated. We initialized θ_q and q_w with values close to those of Brost et al. (1982a) for his run 17-2 (Fig. 17) but with a somewhat lower initial cloud top. Sea surface temperature (T_s = 284.5 K) was such that surface buoyancy flux was very small. The run was done at a latitude of 37°N. The vertical profiles of the prescribed geostrophic wind components, taken from Brost et al. (1982a), are given in Fig. 18 and show a strong geostrophic wind shear near the ABL-top. As in the foregoing case, we took the dissipation equation of subsection 2b2 as turbulence closure (ϵ-run). The model was run for 4 h simulation time.

The vertical profile of the net longwave radiative flux (at the end of the simulation time) is shown in Fig. 19. There is a strong cooling rate close to cloud top and a weak warming near cloud base. We did also model experiments with this weak cloud-base warming turned off but this did not alter the dynamics in any significant way.

The resulting profiles of θ_q, q_w and q_l at the end of the simulation time are shown in Fig. 17. It is clear that a considerable amount of entrainment has occurred and that the ABL-height has increased. The final profiles of θ_q and q_w show a slight decrease over the ABL.

The wind profiles at the end of the simulation time are shown in Fig. 18. In the stable layer above the ABL, the wind equals its geostrophic value. Throughout the ABL, however, the wind strongly deviates from the geostrophic wind; above the surface layer it is nearly constant with height as high as cloud top where there is a sharp jump.

The most important and interesting aspect of the case of Brost et al. is the turbulent structure of the ABL. The computed profiles of the turbulent fluxes $\overline{w'\theta'_q}$ and $\overline{w'q'_w}$ are compared with the values measured by Brost et al. (1982a) in Fig. 20. Agreement between the computed and measured results is quite good. Throughout the ABL the computed and measured profiles of $\overline{w'\theta'_q}$ show only a slight variation, with somewhat higher values of the computed results. Near cloud top, both results give a large negative peak of $\overline{w'\theta'_q}$; note that the computed value almost equals the measured one. Like the profiles of $\overline{w'\theta'_q}$, again the computed and measured profiles of $\overline{w'q'_w}$ show only a slight vertical variation in the ABL. Near cloud top the computed profile of $\overline{w'q'_w}$ has a maximum which is, however, not so pronounced as the peak in the measured profile.

The TKE-budget at the end of the simulation time is shown in Fig. 21a and the TKE-budget measured by Brost et al. (1982b) is given in Fig. 21b. In both budgets the dominant terms in the ABL are the production of TKE by shear and the viscous dissipation. The buoyancy and transport terms are much smaller, although the computed values are somewhat higher than the measured ones. Also, the behavior of the two budgets near cloud top is similar. Both the measured and computed results indicate that TKE is produced by shear balanced by buoyancy and viscous dissipation, whereas the transport term is of little importance.

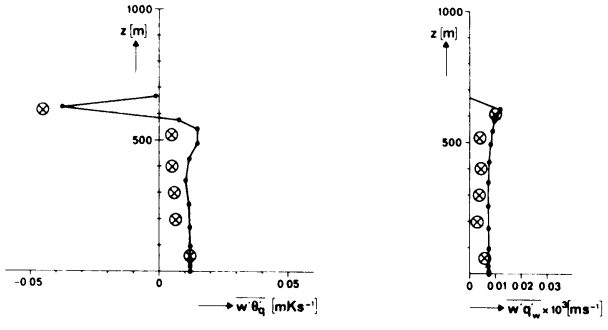

FIG. 20. As in Fig. 14 but with values measured by Brost et al. (1982b) ((×)).

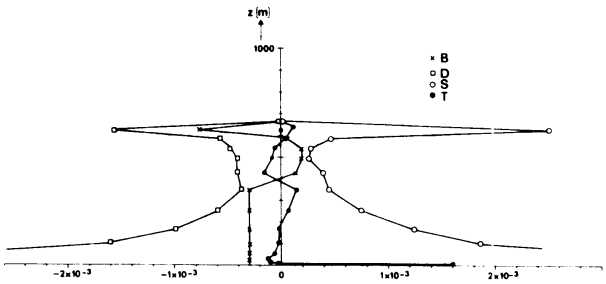

FIG. 21a. The TKE-budget computed by the model.

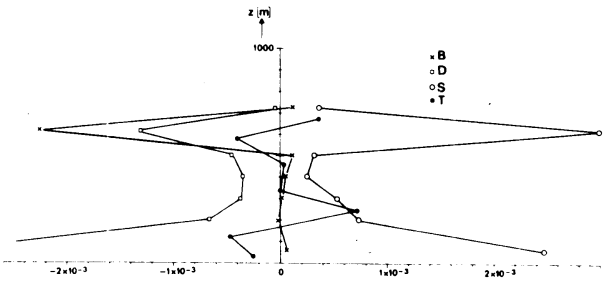

FIG. 21b. The TKE-budget (17-2) measured by Brost et al. (1982b).

The computed profile of the TKE is given in Fig. 22, together with the measured values of Brost et al. (1982a). In the ABL the measured TKE-profiles look much like those in a neutral laboratory boundary layer, except for the peak near cloud top. It is not clear whether this peak is a wavelike phenomenon or due to turbulence. In the ABL the computed results look very much the same, except for the maximum inside the cloud layer.

4. Discussion and conclusions

In this paper we have used a multilevel, ensemble-averaged model to study the cloud-topped ABL. Turbulence closure is formulated by using an equation for the turbulent kinetic energy and either a diagnostic formulation of the integral length scale or a parameterized version of the dissipation equation.

The model developed is used to study various combinations of physical processes in a cloud-topped ABL and their combined effect on the turbulent structure. The processes discussed in this paper are an upward buoyancy flux at the surface, longwave radiative cooling near cloud top, in-cloud warming due to shortwave radiative absorption, and wind shear near cloud top. We considered two idealized cases in which the only active physical process were an upward buoyancy flux at the surface and longwave radiative cooling at cloud top. Moreover, the model results are compared with comprehensive observational data on real world Sc-decks: the dataset presented by Nicholls (1984) on a Sc-deck over the North Sea and the dataset presented by Brost et al. (1982a,b) on a Sc-deck off the California Coast.

The turbulent closure uses either a diagnostic length scale or a parameterized version of the dissipation equation. From the results presented in section 3, we can conclude that the ϵ-equation gives more realistic results, because the diagnostic l-formulation gives an anomalously high dissipation near the inversion. Moreover, the ϵ-equation is preferred when the turbulent structure of ABL is not known in advance.

Longwave radiative cooling near cloud top is usually considered to generate a convectively turbulent ABL, much in the same way as when the ABL is heated from below. However, from a comparison of the two cases in sections 3a and 3b, we conclude that there is a considerable difference in structure of a cloud-topped ABL when it is only cooled at the top or when it is only heated from below. Cloud-top cooling is less effective in generating turbulent kinetic energy throughout the ABL than is surface heating.

In the observational study of Nicholls (1984) the combination of longwave radiative cooling at cloud top and shortwave radiative heating inside the cloud layer is important for the turbulent structure, favoring a decoupling of the cloud layer from the subcloud layer and the formation of a stable layer near cloud base. The model results presented in section 3c are very similar to the observations by Nicholls (1984). The resemblance between the computed and measured profiles of the fluxes $\overline{w'\theta'_q}$ and $\overline{w'q'_w}$ is remarkable, both indicating that two separate mixed layers are formed, the cloud layer and the subcloud layer. The distribution of turbulent kinetic energy has two maxima, one near the surface and one inside the cloud layer, both also present in the observations. From the results presented in section 3c, it is clear that with our model the turbulent structure of the Sc-deck as observed by Nicholls (1984) can be simulated quite well.

Brost et al. (1982a,b) argue that in their observations cloud-top longwave radiative cooling did not generate convection in the ABL, but the cooling at cloud top was directly balanced by entrainment of warm air from above the inversion. This entrainment was a result of the strong wind shear near cloud top. Further, owing to the small buoyancy flux at the surface, the turbulent structure of the ABL was near neutral. The model run

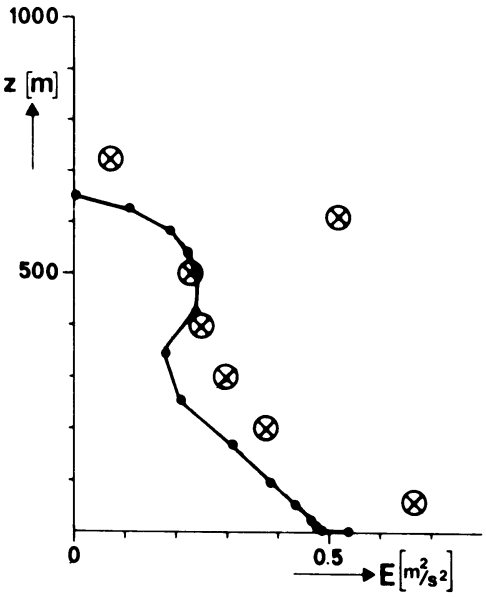

FIG. 22. The profile of TKE computed by the model (solid line), compared with the values measured by Brost et al. (1982b) (circled ×'s).

gives very similar results. At cloud top the viscous dissipation and the negative buoyancy flux are mainly balanced by shear production. This is in contrast to the usual case in which the negative buoyancy flux and viscous dissipation are balanced by turbulent transport. Both, the computed and measured profiles of the fluxes $\overline{w'\theta'_q}$ and $\overline{w'q'_w}$ show only very little variation throughout the ABL with a sharp negative peak of $\overline{w'\theta'_q}$ at cloud top.

In the past, much attention has been given to simple mixed-layer models for the description of a Sc-topped ABL. However, the observations and the present model results indicate that the mixed-layer assumption is probably an oversimplification for real world Sc-topped ABL's. Recently, Turton and Nicholls (1986) tried to describe the decoupling process with a model that considers the ABL to consist of two (separate) mixed layers. Then, however, a number of assumptions regarding the separation of the two layers and the entrainment are needed. Moreover, in their model the effect of wind shear is still neglected and difficult to incorporate.

Recently, Bougeault (1985) made a simulation of the turbulent structure of the cloud-topped ABL observed over the North Sea during JASIN. His model included a third-order turbulence closure, a partial condensation scheme, and a detailed radiation scheme. Although the model is much more complicated than ours, his results are quite similar. During the night he finds a turbulent structure of the ABL close to those presented in section 3b, whereas during daytime the turbulent structure is quite similar to those presented in section 3c.

Acknowledgments. The authors are indebted to H. R. A. Wessels for stimulating discussions and to H. Tennekes for useful comments on the first draft.

APPENDIX A

Symbols

A	absorptance of shortwave radiation
a	albedo
a_0	mass absorption coefficients
c, c_m	speed of sound for dry and moist air, respectively
c_p	specific heat of moist air at constant pressure
C_{θ_q}, C_{q_w}	coefficients in Eq. (44)
E	turbulent kinetic energy
e	water vapor pressure
F	total radiative flux
f	Coriolis parameter
g	acceleration due to gravity
H	depth of the cloud layer
h	boundary-layer height
$K_{m,h}$	exchange coefficients for momentum and heat
L	Monin–Obukhov length
$l_{m,h}$, l_b, l_s, l_∞	length scales (section 2b)
l_v	latent heat for vaporization of water
N	droplet concentration
N_m	Brunt–Väisälä frequency
p	pressure
p_*	reference pressure ($=1.013 \times 10^5$ Pa)
q_w, q_v, q_l	specific humidity for total water, water vapor and liquid water, respectively
q_{w*}	specific humidity scale, $q_{w*} = -(\overline{w'q'_w})_s/u_*$
R	reflectance of shortwave radiation in (22), (23) and (24); specific gas constant
Ri_g, Ri_f	gradient Richardson number and flux Richardson number, respectively
Ri_b	bulk gradient Richardson number
s	entropy
T	temperature; transmittance of shortwave radiation in Eqs. (22), (23), (24) and (25)
T_t	temperature at the triple point
t	time
u, v	horizontal wind components in x and y direction, respectively
u_g, v_g	geostrophic wind components in x and y direction, respectively
u_*	friction velocity
W	liquid water path length
W_t	total water content of the cloud
w	vertical velocity
w_*	convective velocity scale
z	vertical coordinate
z_0	surface roughness height
Δ	difference between the value above and below the inversion
ϵ	dissipation rate of turbulent kinetic energy
$\epsilon_r = R_d/R_v$	ratio of the gas constants for dry air and water vapor
$\epsilon^{\uparrow\downarrow}$	upward and downward effective emissivity
ζ	transformed vertical coordinate
θ_q	wet equivalent potential temperature
θ_{q*}	wet equivalent potential temperature scale, $\theta_{q*} = -(\overline{w'\theta'_q})_s/u_*$
κ	von Kármán's constant
ρ	density
$\Gamma_{d,m}$	dry adiabatic lapse rate and saturated adiabatic lapse rate, respectively
σ	Stefan–Boltzmann constant
σ_E, σ_ϵ	turbulent Prandtl number for E and ϵ, respectively
ϕ	solar zenith angle
$\phi_{m,h}$	dimensionless functions in the surface layer describing the stability corrections
ω	vorticity

Indices

cb	cloud base
ct	cloud top
d	dry air
l	liquid water
L	longwave
m, h	momentum, heat
0	reference state
S	shortwave
s	surface
sat	saturation
v	vapor

Constants

A number of constants have to be evaluated for the turbulence model. The constants $c_{1\epsilon}$, $c_{2\epsilon}$, c_μ, σ_ϵ, σ_E have been taken from Rodi (1980).

The constant c_∞ has been determined from the simulation of the convective boundary layer by Deardorff (1974b), who gives

$$l_\infty \approx 0.8 c_\mu^{3/4} h.$$

Further,

$$l_\infty = c_\infty \frac{\int_0^h z E^{1/2} dz}{\int_0^h E^{1/2} dz} \approx \frac{1}{2} c_\infty h,$$

thus

$$c_\infty \approx 1.6 c_\mu^{3/4}.$$

The value of c_s has been evaluated for a stable layer in which there is a balance between production by shear and consumption by buoyancy and viscous dissipation. This gives a relation between c_s, c_μ, Ri_g and Ri_f,

$$c_s = c_\mu^{1/4} \left(\frac{\mathrm{Ri}_g}{1 - \mathrm{Ri}_f} \right)^{1/2}.$$

We have evaluated c_s for a value of the critical Richardson number $\mathrm{Ri}_g = \mathrm{Ri}_f = 0.3$.

In summary, the values of all the constants as we used them for the turbulence closure are

$$c_{1\epsilon} = 1.44$$

$$c_{2\epsilon} = 1.92$$

$$c_\infty = 0.25$$

$$c_\mu = 0.09$$

$$c_s = 0.36$$

$$\kappa = 0.35$$

$$\sigma_E = 1.0$$

$$\sigma_\epsilon = 1.3.$$

APPENDIX B

Temperature Calculation

In the model, we have used the entropy as a prognostic variable. In order to determine whether a parcel is saturated or unsaturated we need to know the temperature. To be able to calculate the temperature from the definition of θ_q (18), we have to give the relation between the partial saturation vapor pressure and the temperature, $e_{\mathrm{sat}} = e_{\mathrm{sat}}(T)$. We will discuss two relations for $e_{\mathrm{sat}}(T)$. The first is an empirical fit, while the second is a polynomial fit.

An empirical fit is Tetens formula given by Murray (1967)

$$e_{\mathrm{sat}} = e_{so} \exp[a(T - T_t)/(T - b)], \tag{B1}$$

with

$$e_{so} = 610.78$$

$$a = 17.27$$

$$T_t = 273.16\,\mathrm{K}$$

$$b = 35.86$$

in which e_{so} is the partial vapor pressure at the triple point, with temperature T_t. Knowing the values of θ_q, p and q_w, we can use (B1) to solve the temperature from (18). However, the resulting equation for the temperature is an implicit one; therefore, it is a rather lengthy computation to solve.

We can also use a simple polynomial expression for the saturation vapor pressure, given by Iribarne and Godson (1981),

$$\ln e_{\mathrm{sat}} = A - \frac{B}{T}, \tag{B2}$$

with

$$B = \frac{l_v}{R_v},$$

and A is a constant which has to be fitted, for instance at $e_{so} = e_{\mathrm{sat}}(T_t)$. It turns out that for unsaturated air we get an explicit expression for the temperature, whereas for saturated air we get an implicit expression. Therefore, there is a big computational advantage in using the polynomial expression (B2), rather than Eq. (B1).

APPENDIX C

Derivation of Eq. (10)

In this appendix we give a derivation of Eq. (10), which relates the density flux to the θ_q-flux and q_w-flux. We distinguish two different cases: saturated and unsaturated air. First we will give some equations needed (Iribarne and Godson, 1981; Durran and Klemp, 1982):

the entropy equation

$$ds = c_{pd}\left[1 + q_v\left(\frac{c_{pv}}{c_{pd}} - 1\right) + q_l\left(\frac{c_{pl}}{c_{pd}} - 1\right)\right] d\ln T - R_d\left[1 + q_v\left(\frac{1}{\epsilon_r} - 1\right) - q_l\right] d\ln p + \frac{l_v}{T} dq_v, \quad \text{(C1)}$$

the gas law in differential form

$$\frac{dp}{p} = \frac{d\rho}{\rho} + \frac{dT}{T} - \frac{dq_w}{1 - q_w + q_{v/\epsilon_r}} + \frac{dq_{v/\epsilon_r}}{1 - q_w + q_{v/\epsilon_r}}, \quad \text{(C2)}$$

the Clausius–Clapeyron equation

$$\frac{d\ln e_{sat}}{dT} = \frac{l_v}{R_v T^2}, \quad \text{(C3)}$$

the equation for the specific vapor humidity

$$q_v = \frac{\epsilon_r e}{p - e(1 - \epsilon_r)}, \quad \text{(C4)}$$

and the relation between the entropy and θ_q (Pointin, 1984)

$$ds = c_p d\ln\theta_q. \quad \text{(C5)}$$

1. Saturated air

In this case the air is saturated $q_v = q_{vsat}$ and $e = e_{sat}$. Combining (C3) and (C4) gives

$$dq_{vsat} = \left(1 + \frac{1 - \epsilon_r}{\epsilon_r} q_{vsat}\right)\left(\frac{q_{vsat}\epsilon_r l_v}{R_d T^2} dT - q_{vsat}\frac{dp}{p}\right). \quad \text{(C6)}$$

Eliminating q_{vsat}, T and s from (C1), (C2), (C5) and (C6), we obtain

$$\frac{\Gamma_m}{\Gamma_d}\frac{c_p}{c_{pd}} d\ln\theta_q = -\frac{d\rho}{\rho} + \frac{dp}{\rho c_m^2} + \left[\frac{1}{1 - q_w + q_{vsat/\epsilon_r}}\right] dq_w, \quad \text{(C7)}$$

in which

$$\frac{\Gamma_m}{\Gamma_d} = \frac{1 + \dfrac{l_v q_{vsat}}{R_d T} + \dfrac{q_l}{1 + \dfrac{1 - \epsilon_r}{\epsilon_r} q_{vsat} - q_l}\dfrac{l_v q_{vsat}}{R_d T}}{1 + q_{vsat}\left(\dfrac{c_{pv}}{c_{pd}} - 1\right) + q_l\left(\dfrac{c_{pl}}{c_{pd}} - 1\right) + \left(1 + \dfrac{1 - \epsilon_r}{\epsilon_r} q_{vsat}\right)\dfrac{q_{vsat}\epsilon_r l_v^2}{c_{pd} R_d T^2}},$$

$$c_m^2 = c^2\left[\left(\frac{1 + \dfrac{q_{vsat}}{\epsilon_r}\dfrac{1 + \dfrac{1 - \epsilon_r}{\epsilon_r} q_{vsat}}{1 - q_w + q_{vsat/\epsilon_r}}}{1 - q_w + q_{vsat/\epsilon_r}}\right)\frac{c_{pd}}{c_{vd}} - \frac{R_d}{c_{vd}}\frac{\Gamma_m}{\Gamma_d}\left(\frac{1 + \dfrac{1 - \epsilon_r}{\epsilon_r} q_{vsat}}{1 + \dfrac{1 - \epsilon_r}{\epsilon_r}\dfrac{l_v q_{vsat}}{R_d T}}\right)\right]^{-1}, \qquad c^2 = \frac{c_{pd}}{c_{vd}} R_d T.$$

2. Unsaturated air

For unsaturated air $q_v = q_w$. From the equations (C1), (C2) and (C5) we can eliminate T and s. The result can be expressed as

$$C_\Gamma \frac{c_p}{c_{pd}} d\ln\theta_q = -\frac{d\rho}{\rho} + \frac{dp}{\rho c_m^2} + \left[C_\Gamma \frac{l_v}{c_{pd} T} - \frac{\dfrac{1 - \epsilon_r}{\epsilon_r}}{1 + q_{w/\epsilon_r} - q_w}\right] dq_w, \quad \text{(C8)}$$

in which

$$C_\Gamma = \frac{\Gamma_m}{\dfrac{l_v}{c_{pd}}\dfrac{dq_w}{dz} + \Gamma_d} = \left[1 + q_w\left(\frac{c_{pv}}{c_{pd}} - 1\right)\right]^{-1},$$

$$c_m^2 = c^2\left\{\frac{c_{pd}}{c_{vd}}\frac{1}{1 + q_w\left(\dfrac{1 - \epsilon_r}{\epsilon_r}\right)} - \frac{R_d}{c_{vd}}\frac{\Gamma_m}{\Gamma_d + \dfrac{l_v}{c_{pd}}\dfrac{dq_w}{dz}}\right\}^{-1}.$$

3. Saturated and unsaturated air

We can write the resulting equations for saturated (C7) and unsaturated air (C8) in the general form

$$C_{\theta_q}\frac{d\theta_q}{\theta_q} = -\frac{d\rho}{\rho} + \frac{dp}{\rho c_m^2} + C_{q_w} dq_w. \quad \text{(C9)}$$

Neglecting the terms of the order q_v and q_w in C_{θ_q} and C_{q_w}, we can simplify these expressions considerably; the resulting expressions are given in Table 1. Integrating (C9), multiplying it with the vertical velocity perturbation and taking the average, we get

$$C_{\theta_q}\frac{\overline{w'\theta_q'}}{\theta_{q0}} = -\frac{\overline{w'\rho'}}{\rho_0} + \frac{\overline{w'p'}}{\rho_0 c_m^2} + C_{q_w}\overline{w'q_w'}. \quad \text{(C10)}$$

When we neglect the term $\overline{w'p'}$ in (C10), this equation is identical to Eq. (10).

REFERENCES

Albrecht, B. A., R. S. Penc and W. H. Schubert, 1985: An observational study of cloud-topped mixed layers. *J. Atmos. Sci.*, **42**, 800–822.

André, J. C., G. de Moor, P. Lacarrère, G. Therry and R. du Vachat, 1978: Modeling the 24-hour evolution of the mean and turbulent structures of the planetary boundary layer. *J. Atmos. Sci.*, **35**, 1861–1883.

Blackadar, A. K., 1962: The vertical distribution of wind and turbulent exchange in a neutral atmosphere. *J. Geophys. Res.*, **67**, 3095–3102.

Bougeault, Ph., 1981a: Modeling the trade-wind cumulus boundary layer. Part I: Testing the ensemble cloud relations against numerical data. *J. Atmos. Sci.*, **38**, 2414–2428.

——, 1981b: Modeling the trade-wind cumulus boundary layer. Part II: A high-order one-dimensional model. *J. Atmos. Sci.*, **38**, 2429–2439.

——, 1985: The diurnal cycle of the marine stratocumulus layer: A higher-order model study. *J. Atmos. Sci.*, **42**, 2826–2843.

Brost, R., and J. C. Wyngaard, 1978: A model study of the stably-stratified planetary boundary layer. *J. Atmos. Sci.*, **35**, 1427–1440.

Brost, R. A., D. H. Lenschow and J. C. Wyngaard, 1982a: Marine stratocumulus layer. Part I: Mean conditions. *J. Atmos. Sci.*, **39**, 800–817.

——, —— and ——, 1982b: Marine stratocumulus layers. Part II: Turbulence budgets. *J. Atmos. Sci.*, **39**, 818–836.

Businger, J. A., J. C. Wyngaard, Y. Izumi and E. F. Bradley, 1971: Flux-profile relationships in the atmospheric surface layer. *J. Atmos. Sci.*, **28**, 181–189.

Caughey, S. J., B. A. Crease and W. T. Roach, 1982: A field study of nocturnal stratocumulus: II. Turbulence structure and entrainment. *Quart. J. Roy. Meteor. Soc.*, **108**, 125–144.

Chen, C., and W. R. Cotton, 1983: A one-dimensional simulation of the stratocumulus-capped mixed layer. *Bound.-Layer Meteor.*, **25**, 289–321.

Cox, S. K., 1976: Observations of cloud infrared effective emissivity. *J. Atmos. Sci.*, **33**, 287–289.

Daly, B. J., and F. H. Harlow, 1970: Transport equations in turbulence. *Phys. Fluids*, **13**, 2634–2649.

Deardorff, J. W., 1974a: Three-dimensional numerical study of the height and mean structure of a heated planetary boundary layer. *Bound.-Layer Meteor.*, **7**, 81–106.

——, 1974b: Three-dimensional numerical study of turbulence in an entraining mixed layer. *Bound.-Layer Meteor.*, **7**, 199–226.

——, 1976: On the entrainment rate of a stratocumulus-topped mixed layer. *Quart. J. Roy. Meteor. Soc.*, **102**, 563–582.

——, 1980: Stratocumulus-capped mixed layers derived from a three-dimensional model. *Bound.-Layer Meteor.*, **18**, 495–527.

Driedonks, A. G. M., 1982: Models and observations of the growth of the atmospheric boundary layer. *Bound.-Layer Meteor.*, **23**, 283–306.

——, 1986: Current problems in the stratocumulus-topped atmospheric boundary layer. *Mon. Wea. Rev.*

Durran, D. R., and J. B. Klemp, 1982: On the effects of moisture on the Brunt-Väisälä frequency. *J. Atmos. Sci.*, **39**, 2152–2158.

Eskinazi, S., 1975: *Fluid Mechanics and Thermodynamics of our Environment.* Academic Press, 422 pp.

Fravalo, C., Y. Fouquart and R. Rosset, 1981: The sensitivity of a model of low stratiform clouds to radiation. *J. Atmos. Sci.*, **38**, 1049–1062.

Hanson, H. P., 1984: On mixed-layer modeling of the stratocumulus-topped marine boundary layer. *J. Atmos. Sci.*, **41**, 1226–1234.

Harlow, F. H., and P. I. Nakayama, 1967: Turbulence transport equations. *Phys. Fluids*, **10**, 2323–2332.

Iribarne, J. V., and W. L. Godson, 1981: *Atmospheric Thermodynamics.* D. Reidel.

Lenschow, D. H., J. C. Wyngaard and W. T. Pennell, 1980: Mean-field and second-moment budgets in a baroclinic, convective boundary layer. *J. Atmos. Sci.*, **37**, 1313–1326.

Lilly, D. K., 1968: Models of cloud-topped mixed layers under a strong inversion. *Quart. J. Roy. Meteor. Soc.*, **94**, 292–309.

Lumley, J. L., and B. Khajeh-Nouri, 1974: Computational modeling of turbulent transport. *Advances in Geophysics*, Vol. 18A, Academic Press, 169–192.

Mailhot, J., and R. Benoit, 1982: A finite-element model of the atmospheric boundary layer suitable for use with numerical weather prediction models. *J. Atmos. Sci.*, **39**, 2249–2266.

Manton, M. J., 1980: Computations of the effect of cloud properties on solar radiation. *J. Rech. Atmos.*, **14**, 1–16.

Mellor, G. L., and T. Yamada, 1982: Development of a turbulence closure model for geophysical fluid problems. *Rev. Geophys. Space Phys.*, **20**, 851–875.

Moeng, C.-H., and A. Arakawa, 1980: A numerical study of a marine subtropical stratus cloud layer and its stability. *J. Atmos. Sci.*, **37**, 2661–2676.

——, and D. A. Randall, 1984: Problems in simulating the stratocumulus-topped boundary layer with a third-order closure model. *J. Atmos. Sci.*, **41**, 1588–1600.

——, and J. C. Wyngaard, 1985: The structure of a stratus-topped PBL as seen through large-eddy simulation (lecture given at the workshop on the modeling of the CTBL, CSU, Fort Collins).

Murray, F. W., 1967: On the computation of saturation vapour pressure. *J. Appl. Meteor.*, **6**, 203–204.

Nicholls, S., 1984: The dynamics of stratocumulus: Aircraft observations and comparison with a mixed layer-model. *Quart. J. Roy. Meteor. Soc.*, **110**, 783–820.

Oliver, D. A., W. S. Lewellen and G. G. Williamson, 1978: The interaction between turbulent and radiative transport in the development of fog and low-level stratus. *J. Atmos. Sci.*, **35**, 301–316.

Paluch, I. R., 1979: The entrainment mechanism in Colorado cumuli. *J. Atmos. Sci.*, **36**, 2467–2478.

Pointin, Y., 1984: Wet equivalent potential temperature and enthalpy as prognostic variables in cloud modeling. *J. Atmos. Sci.*, **41**, 651–660.

Randall, D. A., J. A. Coakley, Jr., C. W. Fairall, R. A. Kropfli and D. H. Lenschow, 1984: Outlook for research on subtropical marine stratiform clouds. *Bull. Amer. Meteor. Soc.*, **65**, 1290–1301.

Roach, W. T., R. Brown, S. J. Caughey, B. A. Crease and A. Slingo, 1982: A field study of nocturnal stratocumulus: 1. Mean structure and budgets. *Quart. J. Roy. Meteor. Soc.*, **108**, 103–123.

Robert, A. J., 1966: The integration of a low order spectral form of the primitive meteorological equations. *J. Meteor. Soc. Japan*, **44**, 237–244.

Rodi, W., 1980: Turbulence models and their application in hydraulics, IAHR, Delft, The Netherlands.

Schaller, E., and H. Kraus, 1981a: The role of radiation in an inversion-capped planetary boundary layer. Part I: The need for a detailed consideration of radiative processes. *Bound.-Layer Meteor.*, **20**, 485–495.

——, and ——, 1981b: The role of radiation in an inversion-capped planetary boundary layer. Part II: The internally interactive radiative-convective model. *Bound.-Layer Meteor.*, **20**, 497–518.

Schubert, W. H., 1976: Experiments with Lilly's cloud-topped mixed layer model. *J. Atmos. Sci.*, **33**, 436–446.

——, J. S. Wakefield, E. J. Steiner and S. K. Cox, 1979: Marine stratocumulus convection. Part I: Governing equations and horizontally homogeneous solutions. *J. Atmos. Sci.*, **36**, 1286–1307.

Slingo, A., S. Nicholls and J. Schmetz, 1982: Aircraft observations of marine stratocumulus during JASIN. *Quart. J. Roy. Meteor. Soc.*, **108**, 833–856.

Sommeria, G., 1976: Three-dimensional simulation of turbulent processes in an undisturbed trade wind boundary layer. *J. Atmos. Sci.*, **33**, 216–241.

Stage, S. A., and J. A. Businger, 1981a: A model for the entrainment into a cloud-topped marine boundary layer. Part I: Model description and application to a cold-air outbreak episode. *J. Atmos. Sci.*, **38**, 2213–2229.

——, and ——, 1981b: A model for entrainment into a cloud-topped marine boundary layer. Part II: Discussion of model behavior and comparison with other models. *J. Atmos. Sci.*, **38**, 2230–2242.

Stephens, G. L., 1978: Radiation profiles in extended water clouds. II: Parameterizations schemes. *J. Atmos. Sci.*, **35**, 2123–2132.

Tennekes, H., and J. L. Lumley, 1972: A first course in turbulence. MIT Press.

Tripoli, G. J., and W. R. Cotton, 1981: The use of ice-liquid water potential temperature as a thermodynamic variable in deep atmospheric models. *Mon. Wea. Rev.*, **109**, 1094–1102.

Turton, J. D., and S. Nicholls, 1986: A study of the diurnal variation of stratocumulus using a mixed layer model. *Quart. J. Roy. Meteor. Soc.*

Wyngaard, J. C., 1975: Modeling the planetary boundary layer-extension to the stable case. *Bound.-Layer Meteor.*, **9**, 441–460.

——, O. R. Coté and K. S. Rao, 1974: Modeling the atmospheric boundary layer. *Advances in Geophysics*, Vol. 18A, Academic Press, 193–211.

4. TURBULENT STRUCTURE OF A SHEAR-DRIVEN STRATUS-TOPPED ATMOSPHERIC BOUNDARY LAYER: A COMPARISON OF MODEL RESULTS WITH OBSERVATIONS+

Abstract

An observational study of the cloud-topped atmospheric boundary layer (ABL) during a strong gale reveals that the turbulent boundary layer was dominated by shear instead of convection. A one-dimensional ensemble-averaged model is used to study this type of cloud-topped ABL. Turbulence closure is formulated by using an equation for both the turbulent kinetic energy and the viscous dissipation. The radiation model consists of an emissivity model for the longwave radiation and a two-stream model for the shortwave radiation. Both model results and observations indicate that the longwave radiative cooling at cloud top is mainly balanced by entrainment of warm air from above the inversion. A parameterization for the rainfall is included and the effect of this on the liquid water content is studied.

+ Published in Journal of the Atmospheric Sciences, 1988, 45, 2343-2351, with A.G.M. Driedonks as co-author.

1. Introduction

Nicholls and Leighton (1986, hereafter referred to as NL86) discuss results from six flights in marine stratiform cloud-topped boundary layers around the United Kingdom in a variety of conditions. On five of the flights, turbulent mixing in the cloud layer was found to be maintained primarily by convection resulting from longwave radiative cooling at cloud top. As a result of the convection cellular patterns were seen in the top of the cloud layer, which NL86 therefore classified as stratocumulus. However, on one of the flights (flight 564), the cellular patterns associated with convective motions within the cloud were absent. In that case the top of the cloud layer was flat, uniform and featureless, and NL86 therefore classified it as stratus. In this paper we will present a model simulation of this cloud-topped atmospheric boundary layer in order to examine its vertical turbulent structure.

On flight 564 shear-induced mixing dominates throughout the boundary layer. Moreover the shear at cloud top very effectively promotes entrainment of warm air from above the inversion. Together with the subsidence the entrainment more than offsets the longwave radiative cooling at cloud top. As a result no convection is observed and the boundary layer structure is nearly neutral. Very similar conditions were found by Brost et al. (1982 a, b) in a stratocumulus deck off the California coast on 17 June 1976.

2. Model

The model used has been extensively described in Duynkerke and Driedonks (1987) with slight modifications as described in Duynkerke (1988). No tuning has been carried out for this simulation. In the one-dimensional model we have ensemble-averaged equations for the horizontal velocities (u and v), entropy (θ_q) and total water content (q_w). The vertical velocity has to be prescribed. The turbulent fluxes are modeled with the gradient approach in which the exchange coefficient is calculated from the turbulent kinetic energy (E) and the viscous dissipation (ε) the so called E-ε model. In the entropy equation we have heating or cooling due to the radiative-flux divergence. In the radiation model described in Duynkerke and Driedonks (1987), we neglected the radiative-flux divergence outside the cloud layer. Moreover we prescribed the e-folding depth for the shortwave radiative heating. Since then we have

updated the radiation model with a more general model that includes the flux divergence outside the cloud layer. In addition, it explicitly resolves the profile of the shortwave radiative heating within the cloud. The radiation model used will be described below.

2.1 Radiation model

2.1.1 Longwave radiation

We use the emissivity or "grey-body" approximation to calculate the upward ($F^{\uparrow}$) and downward ($F^{\downarrow}$) longwave radiative fluxes (Rodgers 1967):

$$F^{\downarrow} = \int_{z}^{\infty} B(T(z')) \frac{\partial \varepsilon}{\partial z'} (z',z)\, dz', \tag{1a}$$

$$F^{\uparrow} = \int_{z}^{0} B(T(z')) \frac{\partial \varepsilon}{\partial z'} (z,z')\, dz' + B(T_B)\,[1 - \varepsilon(z,0)] \tag{1b}$$

in which B is the Planck function σT^4, $\varepsilon(z,z')$ is the emissivity for corrected mass of absorber $u(z,z')$ corresponding to vertical path from z to z', and T_B is the equivalent blackbody temperature, which we will take as equal to the sea-surface temperature T_S.

The emissivity in (1) is calculated as

$$(1-\varepsilon) = (1 - \varepsilon_v)\,(1 - \varepsilon_{CO_2})\,(1 - \varepsilon_c), \tag{2}$$

in which v stands for vapor, CO_2 for carbon-dioxide and c for cloud. Rodgers (1967) gives suitable schemes for water vapor and CO_2. Welch and Zdunkovski (1976) have discussed a revised scheme for water vapor.
We use eq. (2) with

$$\varepsilon_v = \varepsilon_{v1}(u) + \varepsilon_{v2}\left(\frac{ue}{p_*}\right), \tag{3}$$

in which u is the corrected mass of water vapor absorber

$$u = \left| \int_{z}^{z'} \rho\, q_v\, (p/p_*)^{0.9}\, dz \right| \tag{4}$$

and e is the partial vapor pressure

$$e = \frac{pq_v}{\varepsilon - q_v(\varepsilon-1)} \cdot \tag{5}$$

For $\varepsilon_{v1}(u)$ we have used the scheme presented by Welch and Zdunkovski (1976). The second term in (3), $\varepsilon_{v2}(\frac{ue}{p_*})$ represents the effect of the water vapour dimer within the window region for which we use the parameterization of Stephens and Webster (1979). For $\varepsilon_{CO_2}(u_{CO_2})$ we have used the scheme given by Rodgers (1967) in which

$$u_{CO_2} = \left| \int_z^{z'} 100\ C\ (\frac{\rho}{\rho_*})\ (\frac{p}{p_*})^{0.9} dz \right|, \tag{6}$$

where $C = 330 \times 10^{-6}$ ppm at all levels and u is in cm. atm. For $\varepsilon_c(W)$ we have used the scheme given by Stephens (1978) in which

$$W = \left| \int_z^{z'} \rho q_\ell \, dz \right|. \tag{7}$$

2.1.2 Shortwave radiation

The shortwave radiative fluxes are calculated using a model (SUNRAY) described by Fouquart and Bonnel (1980). Our major departure from Fouquart and Bonnel's parametrization is that we use the δ-Eddington approximation instead of the exponential kernel. The model involves Rayleigh scattering, absorption by atmospheric gases (water vapor, ozone and CO_2) and absorption and scattering by cloud droplets. The cloud radiative properties are defined as in Fouquart and Bonnel (1980) and are based on the optical thickness of a layer (τ).

The optical thickness is calculated from: $\tau = \frac{3W}{2r_e}$, where r_e is the equivalent radius of the droplet distribution (set to 10 μm) and W is the liquid water mass defined in (7). The single scattering albedo of the droplets is given by Fouquart and Bonnel (1980):

$$\omega_o = 0.9989 - 4 \times 10^{-3} \exp(-0.15\ \tau_t), \tag{8}$$

where τ_t is the optical thickness of the whole cloud layer.

3. Synoptic conditions

A weak low-pressure system was situated between the southern tip of Greenland and Iceland at 1200 GMT 13 December 1982. As the accompanying occluded front moved northeastward an unstable wave developed. This can be seen in the surface pressure map at 1200 UTC 14 December shown in Figure 1. From this wave a new low pressure system developed and deepened very rapidly. At 1200 UTC 15 December this new low-pressure system was located just off the west coast of Norway and had reached a pressure of 950 mb at its core (Figure 1). At this time the original low-pressure system is located southwest of Iceland, and it would ultimately merge with the newly developed cyclone. The measurements described by NL86 (case 564) were taken between 1000 and 1512 UTC 15 December 1982 around 50.21°N, 6.38° W. The area of measurement is located in the warm sector of the cyclone, which was strongly influenced by the high-pressure system off the west coast of Spain.

In order to show the vertical structure of the atmosphere around the measuring area we have plotted the radiosonde profiles from Valentia (03953; 51.56°N, 10.15°W), Camborne (03808; 50.13°N, 5.19°W) and Brest (07110; 48.27°N, 4.25°W) at 1200 UTC 15 December (Figure 2). The temperature and dew

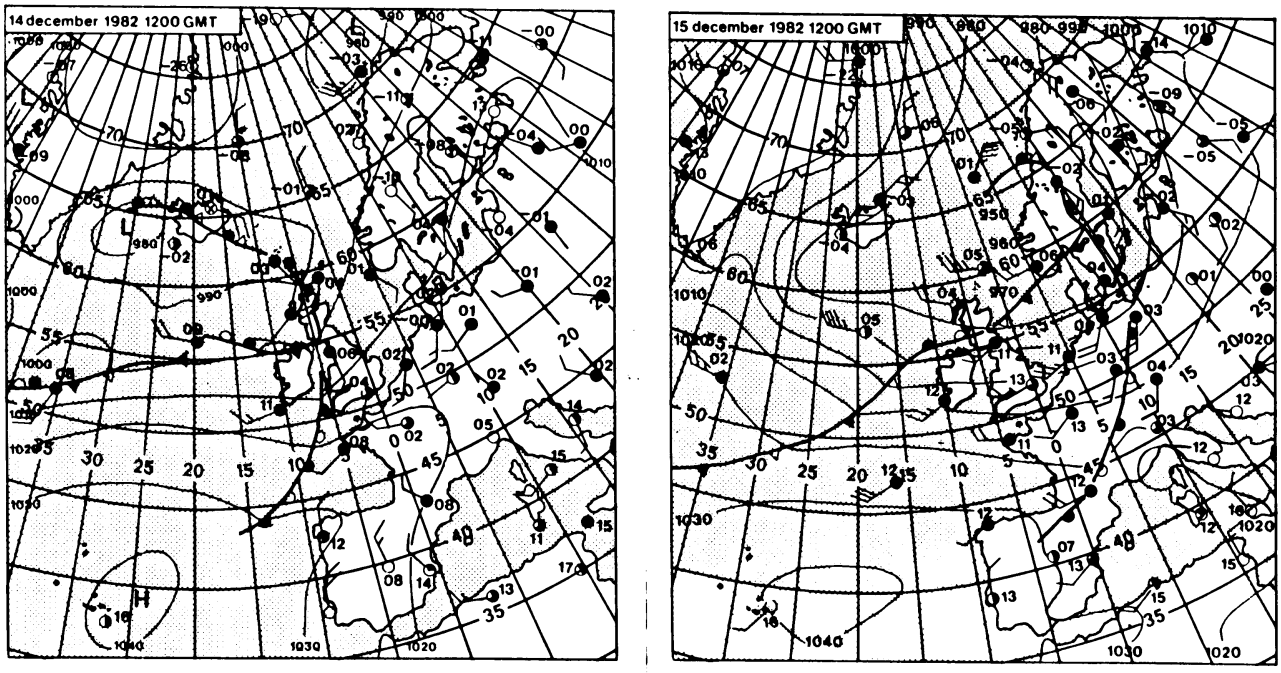

Figure 1. Synoptic surface map for 1200 UTC 14 December 1982 and 1200 UTC 15 December 1982.

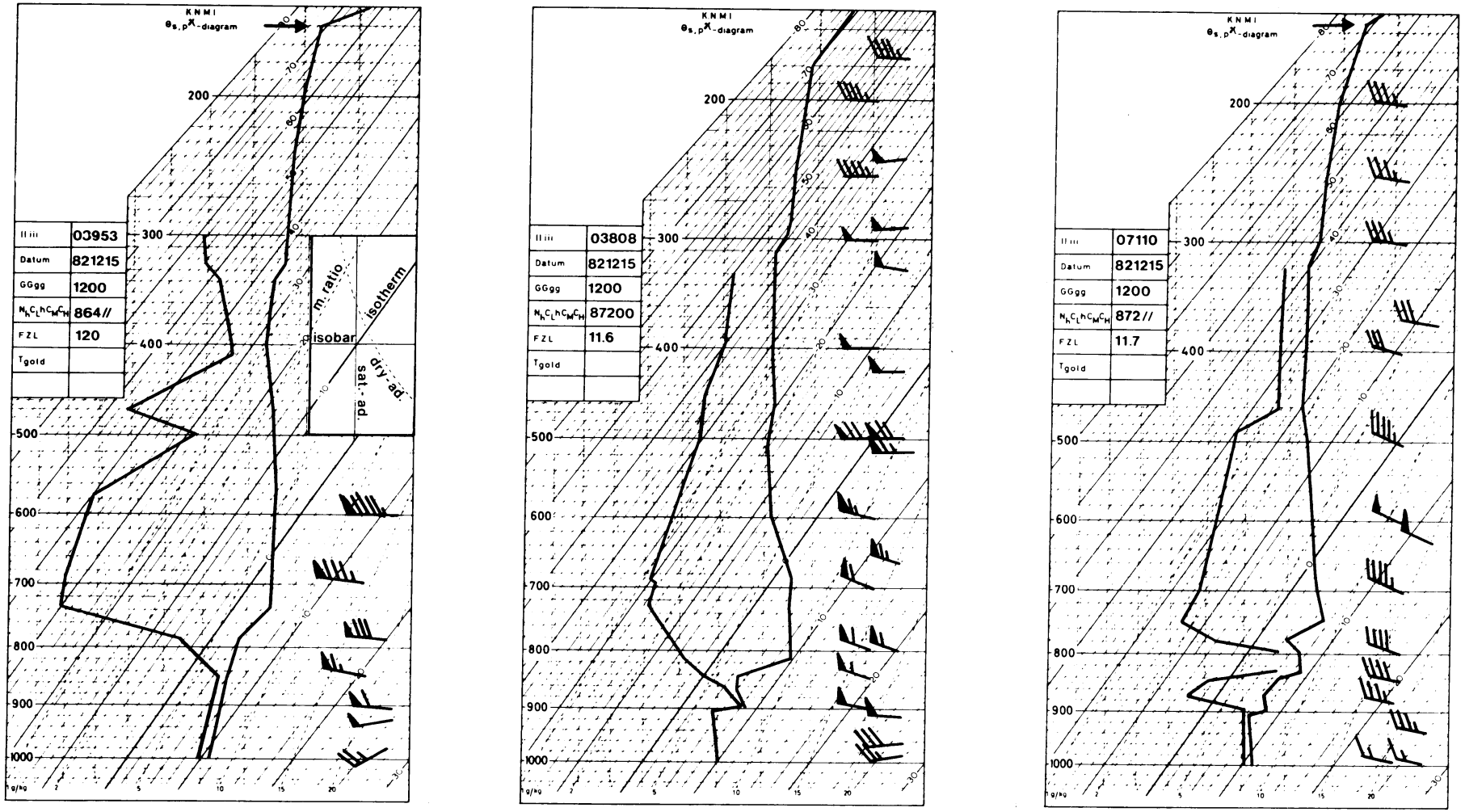

Figure 2. Radiosonde profiles of dewpoint (left) and temperature (right) at 1200 UTC 15 December 1200 GMT for Valentia, Camborne and Brest, respectively.

point profiles at Camborne are very similar to those measured by NL86, except for the maximum in mixing ratio just above the inversion (which might be a measurement error due to the evaporation of water droplets on the radiosonde). In Camborne the surface temperature is 10.4°C whereas NL86 gives a sea surface temperature of 10.3°C. Moreover the radiosonde profile shows an inversion height of about 900 m, whereas NL86 gives 850 m. In Camborne the windspeed at the inversion is 50 knots. At all three stations (Figure 2) the sky was reported to have been completely covered with stratus. The cloud base observed at Camborne was between 100 and 200 m, compared to 180 m observed by NL86. We can therefore conclude that the Camborne radiosonde data are in good agreement with the values observed by NL86 over the sea.

The radiosonde profiles in the nearby stations at Brest and Valentia (Fig. 2), however, show quite a different vertical structure, especially above the boundary layer. We may therefore conclude that the lower atmosphere (up to ~2000 m) in the region of measurement is not horizontally homogeneous on the scale of several hundreds of kilometers.

4. Model results and comparison with observational data

The measurements of case 564 were taken around noon 15 December 1982. The observations show that at this time of year the total shortwave absorption inside the cloud is quite small (~15W/m^2). The air is slightly warmer than the sea causing a virtual heat flux ($\rho c_p \overline{w'\theta'_v}$) at the surface of about -20 W/m^2. Due to the stable stratification near the surface no convection from the sea surface, is generated. Although the observations show a strong longwave radiative cooling (78 W/m^2) at cloud top, no convection is observed in the cloud layer.

NL86 note that in case 564 shear production dominates throughout the depth of the boundary layer. This is a result of the strong winds in the boundary layer (~30 m/s), with little variation up to the atmospheric boundary layer (ABL) height where quite strong jumps occurred. The locally strong wind shear generated significant entrainment of warm air from above the inversion. Together with the subsidence the entrainment warming balances the longwave radiative cooling at cloud top, and the buoyancy flux is negative throughout the boundary layer (no convection). Cloud top processes were therefore hardly felt farther down in the ABL, and as a result the ABL showed a near-neutral

structure, in which shear production was almost locally balanced by dissipation.

The model simulation was set up to see whether this type of turbulence structure could be simulated. The run was done for a latitude of 50°N and longitude of 0°W. In the neutral boundary layer the time scale $\frac{2\pi}{f}$ (~15 hours) is dominant. In order to get winds that are fairly stationary in the boundary layer, we will present model results after a simulation time of 24 hours. The model run was started at local noon 15 December. We initialized the model with values close to those observed by NL86. A divergence of $1.1 \times 10^{-5} s^{-1}$ was applied to limit the rise of the mean cloud top. The initial wind components u and v were set equal to their geostrophic values of 30 and -8 m/s, respectively. The inversion height was set to the observed value of 850 m. Below the inversion we initialized θ_q = 304.5 K, and above the inversion θ_q = 312.5 K and $q_w = 7.4 - 8 \times 10^{-4} z$ g/kg (z in m) up to the model top. The sea surface temperature was set at T_s = 283.3 K, the specific humidity was set equal to its saturated value at the surface $q_w = q_{vsat}(T_s)$ and the surface pressure was 1009 mb. The roughness length was determined from Charnock's relation $z_o = \alpha \frac{u_*^2}{g}$ with α = 0.014 (Haltiner and Williams 1980), which gives $z_o = 8 \times 10^{-4}$ m.

The u and v wind profiles after a simulation time of 24 hours are plotted in Figure 3 together with the observed values from NL86. It can be

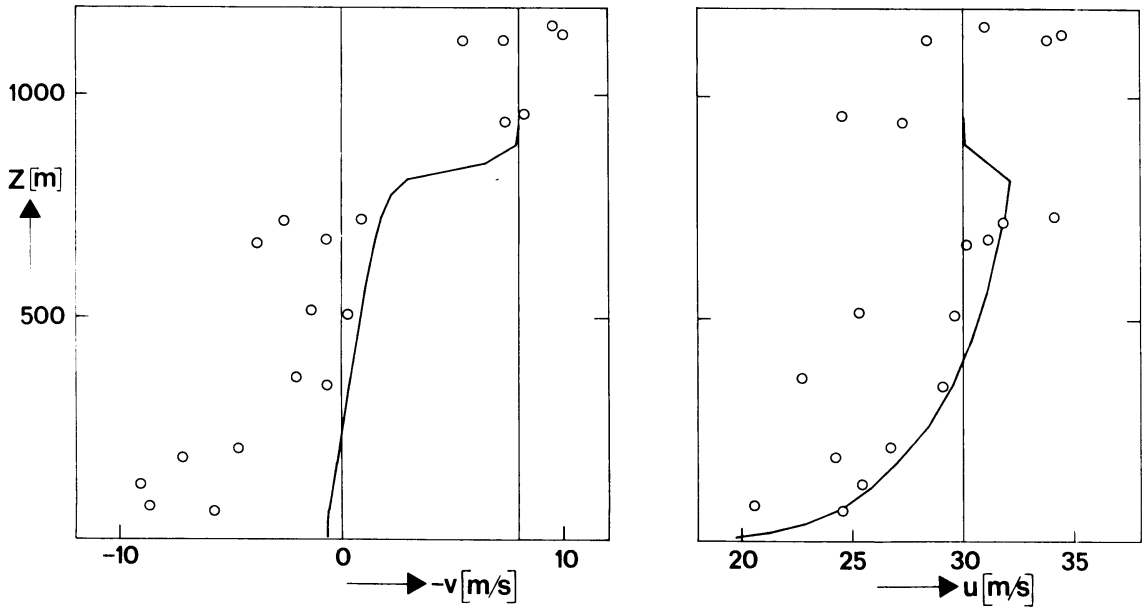

Figure 3. Comparison of observed (circles) and modeled (thick lines) wind speed. Thin lines are initial conditions.

seen that the v-component of the wind is rather well mixed throughout the ABL. At the inversion the model gives jumps in the wind $\Delta v \approx -6$ m/s and $\Delta u \approx -2$ m/s compared to observed values of -6 m/s and -3 m/s, respectively. The observations indicate a slightly larger turning of the wind close to the surface, which might be due to the inhomogeneity mentioned in section 3.

In Figure 4 and 5 the observed, initial and calculated profiles of T, q_w and q_ℓ are shown together with the observations. The initial temperature difference between the sea surface and the air just above is about 1°C. The model results give a Monin-Obukhov length L = 1550 m and thus the stability has only a small effect on the turbulence due to the extremely high wind speed. At the inversion there is a temperature jump of about 6°C. Due to the applied subsidence a net warming takes place above the inversion. The predicted liquid water content (Figure 5) is about twice as large as the observed liquid water content. Later it will be shown that this discrepancy can be explained by taking gravitational droplet settling into account (section 4.1). In Table 1 we have compared the calculated longwave and shortwave radiative fluxes above and below the stratus layer with both the observed values and the values calculated with the model used by NL86. The model gives a net cooling of 67 W/m^2 over the whole cloud layer due to longwave radiation compared to an observed value of 70 W/m^2. The calculated absorption of shortwave radiation equals 15 W/m^2 (Table 1). As discussed above, in this case the longwave radiative

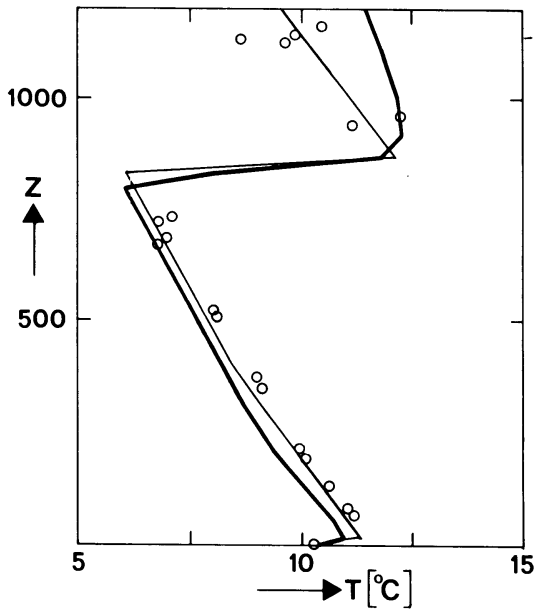

Figure 4. As in Figure 3 but for temperature.

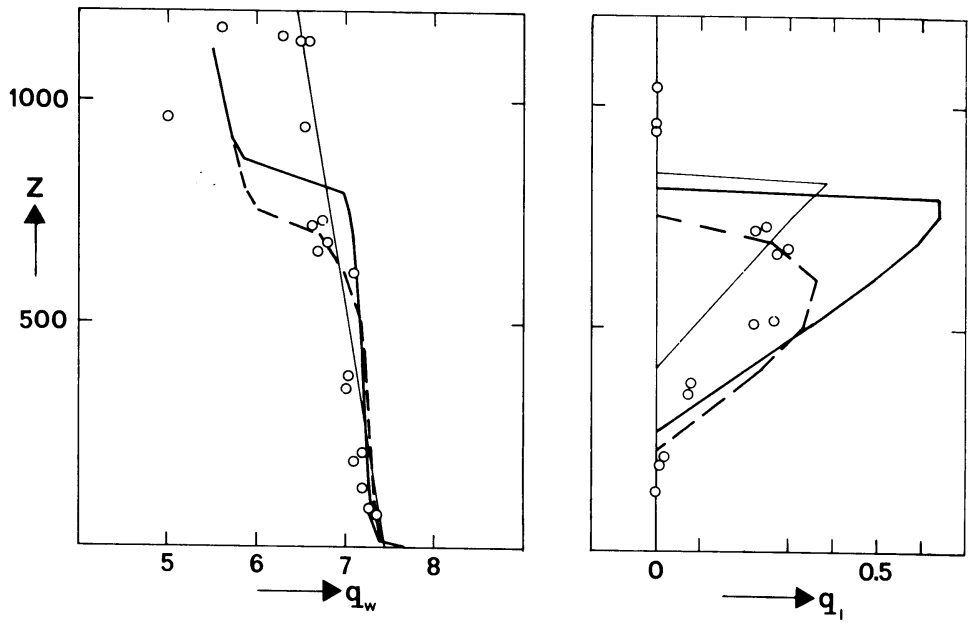

Figure 5. As in Figure 3 but for the specific water content (q_w) and the specific liquid water content (q_ℓ). The dashed lines are model results in which gravitational droplet settling has been taken into account.

	observed (NL86)	model (NL86)	present model
$F_L^{\uparrow +}$	345	354	349
$F_L^{\downarrow +}$	267	246	277
$F_L^{\uparrow -}$	366	362	363
$F_L^{\downarrow -}$	358	357	358
$F_L^{\uparrow +} - F_L^{\uparrow -}$	-21	-8	-14
$F^{\downarrow +} - F^{\downarrow -}$	-91	-111	-81
$F_L^{+} - F_L^{-}$	70	103	67
$F_S^{-} - F_S^{+}$	-19	17	15

Table 1. Cloud longwave and shortwave properties: observations and model results of Nicholls and Leighton (1986); results with present model.

cooling at the cloud top is not promoting convection because it is locally balanced by the entrainment and subsidence of warm air. We will demonstrate this by showing some vertical profiles of turbulence quantities and discuss their effect on the structure of the ABL.

Profiles of the calculated stresses are compared with the observed values in NL86 in Figure 6. The zonal component of the stress decreases linearly with height up to the inversion. By considering the zonal component of the momentum equation

$$f(v-v_g) = \frac{\partial \overline{u'w'}}{\partial z} \quad , \tag{9}$$

it follows that $(v-v_g)$ should be constant within the mixed layer as can be seen in Figure 3. Integrating (9) from $z = z_o$ to above the inversion and assuming that $v-v_g$ is constant throughout the mixed layer, we get: $\Delta v = -\frac{u_*^2}{fh}$. Both the $\overline{uw}$ and $\overline{vw}$ profiles are very similar to those observed by Nicholls (1985) (during the JASIN experiment), which are representative for the near-neutral ABL. In those cases the boundary layer was nearly neutral, and its growth was inhibited by a stable lapse rate aloft. This has been extensively discussed in Duynkerke (1988). In Figure 6 we have also plotted the corresponding values for $\frac{zf}{u_*}$, which show that the depth of the boundary

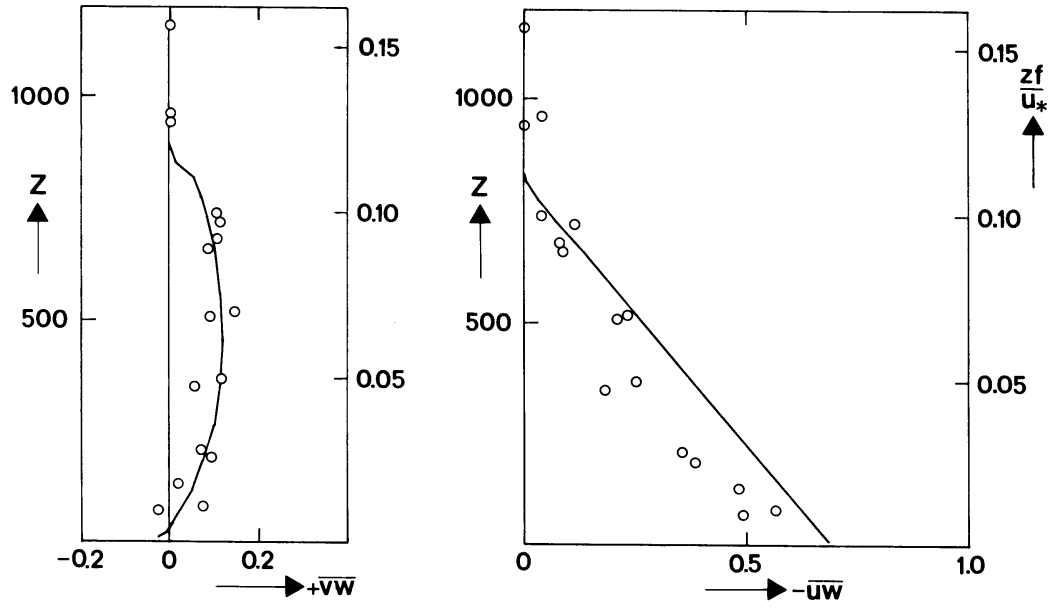

Figure 6. Comparison of observed (circles) and calculated (curves) momentum fluxes.

layer is about 0.11 u_*/f, whereas Nicholls (1985) found a depth of approximately 0.2 u_*/f. This lower boundary layer depth may be a result of the stronger inversion in this case.

Observations similar to those of Nicholls (1985) have been made by Grant (1986), who found a boundary layer depth of about 0.1 u_*/f. The observed boundary layer height and turbulent fluxes in case 564 are thus in good agreement with values observed in other near-neutral ABL's.

The terms in the turbulent kinetic energy equation are shown in Figure 7. Throughout the entire boundary layer, the shear production (S) is almost locally balanced by viscous dissipation (D), whereas the buoyancy term (B) and transport of TKE (T) are small. As a result, a neutral ABL is formed. Near the inversion the shear production has a local maximum due to the velocity jumps shown in Figure 3. This causes an enhanced entrainment of warm air from above the inversion. Figure 8 shows the calculated TKE-profile and the measured $\overline{w^2}$-profile (we have no data for $\overline{u}^2$ and $\overline{v}^2$), both made dimensionless with u_*^2 and plotted as a function of z/h in which h = 0.11 u_*/f. If convection due to longwave radiative cooling at cloud top were present the $\overline{w}^2$-profile would show a maximum inside the cloud layer (NL86). However, both the

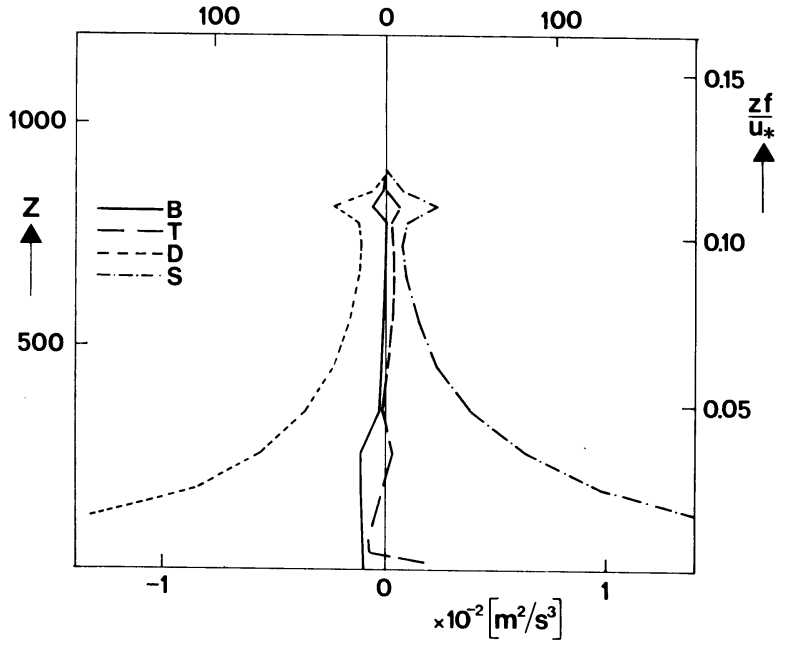

Figure 7. The calculated turbulent kinetic energy budget: B buoyancy production; T turbulent transport; D viscous dissipation; S shear production.

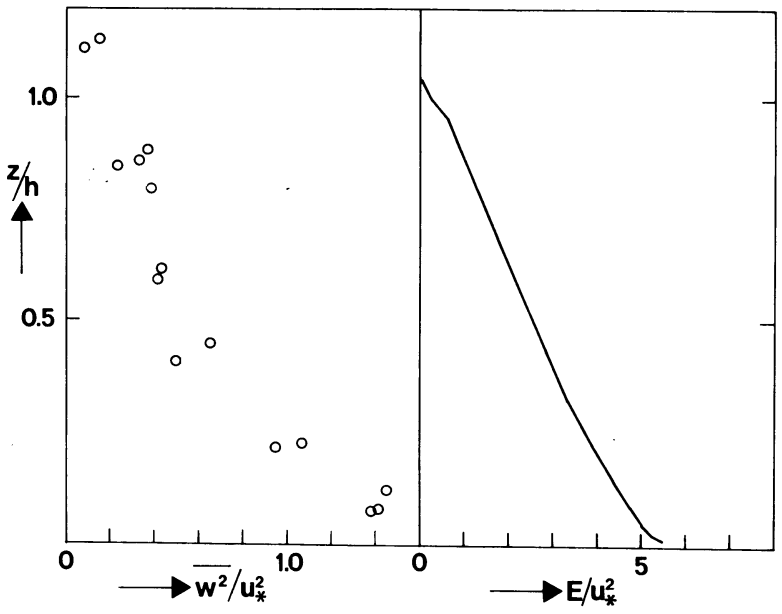

Figure 8. Vertical velocity variance measurements (circles) and calculated turbulent kinetic energy as a function of height.

calculated TKE-profile and the measured $\overline{w}^2$-profile decrease continuously with height and thus reveal that the structure of the ABL is neutral, as found by Nicholls (1985) and Grant (1986).

The observed virtual temperature flux data are compared with the calculated profile in Figure 9. Both observations and calculations show that the

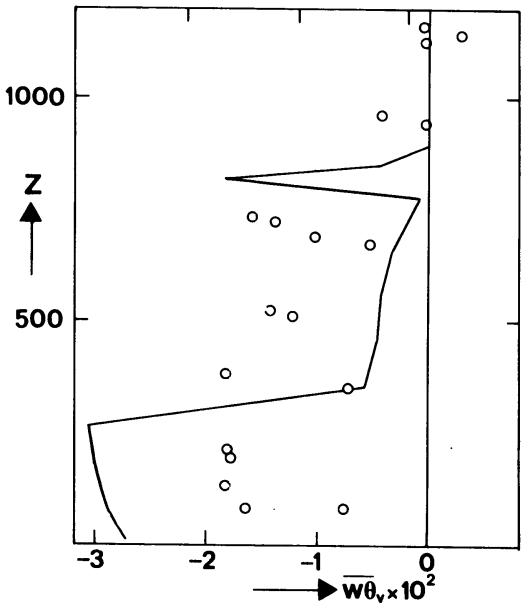

Figure 9. As in Figure 6 but for the virtual temperature flux.

boundary layer is slightly (Figure 7) stable up to the inversion. The calculated profile shows much more vertical structure than the observations: in the cloud $\overline{w\theta}_v$ is small with minima near the inversion and below cloud. Due to the horizontal variations in the boundary layer depth and the horizontal averaging used to obtain the observational fluxes, it is almost impossible to resolve the minimum in the virtual temperature flux near cloud top. From this minimum, according to both the model and the observational results, it seems that the cloud top in the model is slightly higher than in the observations.

In the model the boundary layer depth is almost constant in time, therefore the entrainment velocity (w_e) equals the subsidence velocity at cloud top which has a value of 0.9 cm s^{-1}. From the observations, NL86 estimated the entrainment velocity to be about 1.2 cm s^{-1}, with an uncertainty of 30% to 50%. The entrainment velocity calculated with the model is thus somewhat smaller than the value estimated from observations, but within the uncertainty interval.

The calculated virtual temperature flux (Figure 9) at the surface ($\approx -2.7\times10^{-2}$ Kms^{-1}) is smaller than the observed value ($\approx -1.8\times10^{-2}$ Kms^{-1}). This might be a result of the fact that the $\overline{w\theta}_v$-flux at the surface is very sensitive to the value of the prescribed sea surface temperature. From the radiation thermometer NL86 estimated the sea surface temperature to be 283.3 ±0.5 K. We used T_s = 283.3 K. An increase of the sea surface temperature of about 0.3 K is sufficient to obtain the observed virtual temperature flux in the model. The influence of stability on the turbulence, however remains small, as discussed above. In Figure 10 both calculated and observed moisture fluxes are shown. The observations show considerable scatter from which no clear conclusions can be drawn. The calculated profile indicates that the input of moisture from the sea surface is about as large as the entrainment of dry air from above the inversion. As a result the turbulent flux is constant throughout the boundary layer and thus the value of q_w in the ABL does not change due to turbulence.

The net longwave radiative flux, net shortwave radiative flux, and wet equivalent potential temperature flux ($\overline{w'\theta'}_q$) are displayed in Figure 11. The longwave radiative cooling at the cloud top is mainly balanced by entrainment ($\overline{w'\theta'}_q$) and subsidence (not shown). Therefore, the cooling at cloud top does not generate a positive buoyancy flux (no convection!) (Figure 9).

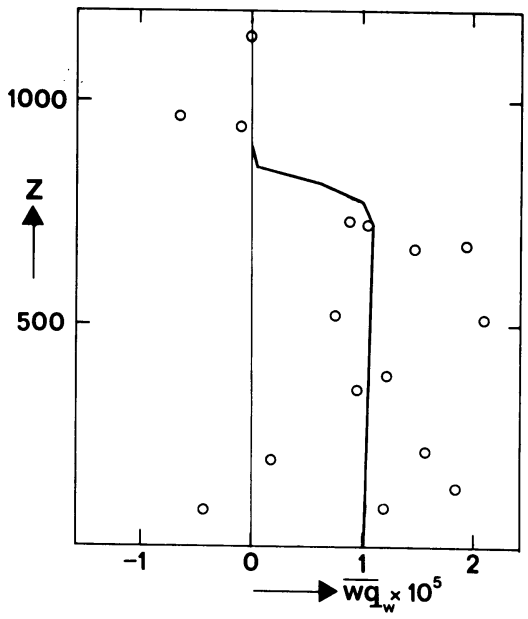

Figure 10. As in Figure 6 but for the total water flux.

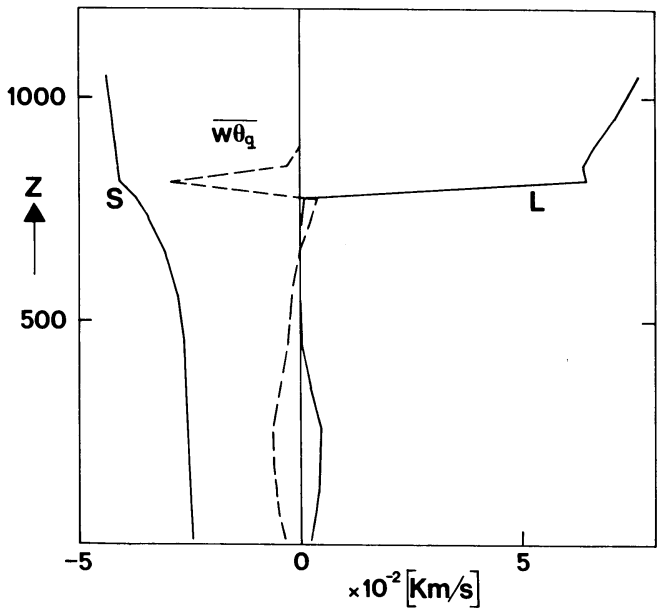

Figure 11. The profiles of the net longwave radiative flux L, net shortwave radiative flux S, and $\overline{w'\theta'_q}$ flux.

4.1 The effect of rainfall rate

From the preceding comparison between the calculations and observations made above, we can conclude that the model can simulate the observed structure of case 564 quite well. One of the clearest differences was that the model predicted a liquid water content twice as high as the observed value. Here we will show that this might be due to the gravitational settling of droplets, which was not included in the model until now. In case 564 the air mass is of maritime origin so, that the droplet concentration is very small (N~35 cm^{-3}) and the mean volume radius of the droplets is quite large (r_v ~ 20 μm). The cloud-top rainfall rate observed in NL86 was large (1.7 x 10^{-5} ms^{-1}) and of the same order as the observed moisture flux (Figure 10). If we include the effect of gravitational settling of droplets, the equation for q_w becomes

$$\frac{\partial q_w}{\partial t} = - \frac{\partial \overline{w'q'_w}}{\partial z} - \frac{\partial \widetilde{w_T q_\ell}}{\partial z} - w \frac{\partial q_w}{\partial z}, \tag{10}$$

where $\widetilde{w_T q_\ell}$ is the gravitational settling (or rainfall rate) following Brost et al. (1982b):

$$\widetilde{w_T q_\ell} = - \frac{\rho_\ell}{\rho_o} \int_o^\infty w_T(r) \, \frac{4}{3}\pi r^3 n(r) dr. \tag{11}$$

The fall speed of a droplet of radius r is represented by w_T. Over a wide range of radii ($r \leq 40$ μm), w_T can be parameterized as: $w_T = w_o r^2$, with w_o = 1.27 x $10^8 m^{-1}s^{-1}$ (Stokes flow). The number of drops per unit volume in the radius interval r to r + dr is n(r). If we employ the size distribution (Hansen and Travis 1974)

$$n(r) = \frac{N_o}{(ab)^{\frac{1-2b}{b}} \, \Gamma\left(\frac{1-2b}{b}\right)} \, r^{\left(\frac{1-3b}{b}\right)} \exp\left(-\frac{r}{ab}\right), \tag{12}$$

in which N_o in m^{-3} is the number of particles per unit volume, a the effective radius (r_e), b the dimensionless variance and Γ is the gamma function. If we use Stokes flow and (12) in (11) we get

$$\widetilde{w_T q_\ell} = - \left(\frac{\rho_\ell}{\rho_o} \frac{4}{3}\pi \, (1-b)(1-2b)\right)^{-2/3} w_o (1+2b)(1+b) \, \frac{q_\ell^{5/3}}{N_o^{2/3}}. \tag{13}$$

With b~0.1 equation (13) gives, $\widetilde{w_T q_\ell} = - 1 \times 10^6 \, \frac{q_\ell^{5/3}}{N_o^{2/3}}$ ms^{-1}. This seems a

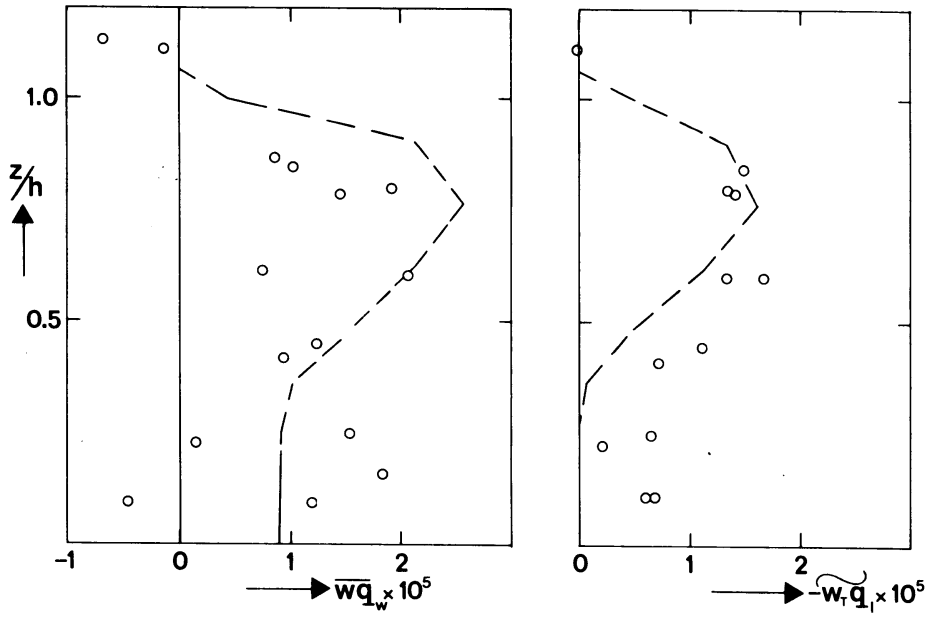

Figure 12. Comparison of observed (circles) and calculated (dashed lines) fluxes: the flux of total water substance $\overline{w'q'_w}$; gravitational settling of droplets $\widetilde{w_T q_l}$.

reasonable parameterization for the rainfall rate for smaller droplets ($r \lesssim 40$ μm).

For larger droplets (which also determine the rainfall rate below cloud) we need another expression, which will be much more complicated because it depends on the details in the droplet distribution for large r. Moreover the Stokes flow will no longer hold. Because of the complexity we have not accounted for this effect. Therefore we will not get any drizzle below cloud.

We have made the same model run as before but have now included the parameterization for the gravitational droplet settling (13) in the equation for q_w (10). Observational data (Nicholls 1984; NL86) indicate that the droplet concentration N_o is approximately independent of height. Therefore, we have taken N_o in (13) to be constant and equal to the observed value $N_o = 35 \times 10^{+6}$ m^{-3} (NL86). In Figure 12 we have compared the calculated turbulent moisture flux $\overline{w'q'_w}$ and the rainfall rate $\widetilde{w_T q_l}$ with the observed fluxes. With N_o constant, we get from (13) that the rainfall rate (Figure 12) is thus very similar to the liquid water profile: the value of $-\widetilde{w_T q_l}$ increases from cloud base upwards and has a maximum just below cloud top. From (10) it follows that above the maximum in the rainfall rate q_w will decrease due to droplet settling, whereas below the maximum in $-\widetilde{w_T q_l}$, q_w will increase.

Because q_w is almost well-mixed throughout the boundary layer, $\overline{wq}_w + \widetilde{w_T q_\ell}$ varies approximately linearly (here nearly constant) with height. This means that the turbulent transport $\overline{wq}_w$ will partially compensate the changes due to droplet settling. In Figure 5 we have drawn the calculated q_w and q_ℓ profiles, which show that, due to the gravitational droplet settling, the liquid water content has been reduced quite drastically. The calculated maximum liquid water content (~0.35 g/kg) is now just slightly larger than the observed value (~0.3 g/kg).

The liquid water content will thus be significantly reduced due to the gravitational droplet settling. However, the gravitational droplet settling has little effect on the other results discussed here. Because there will be enough liquid water to ensure that the cloud radiates as a blackbody, the longwave radiative cooling at cloud top will remain almost unchanged. Moreover, the dynamics of this stratus layer are so dominated by shear that the results discussed in this paper (except, of course, for the liquid water content), will remain almost unchanged if gravitational droplet settling is included.

5. Conclusions

Observations on flight 564 (NL86) made in a strong gale show that the boundary layer was dominated by shear-driven mixing instead of convective mixing, despite the fact that the longwave radiative cooling at cloud top was quite large (~78 W/m^2). Both model results and observations indicate that the radiative cooling near cloud top is mainly balanced by entrainment of warm air from above the inversion. The entrainment is enhanced because of velocity jumps at the inversion. In addition, the model results show that part of the longwave radiative cooling is balanced by subsidence, which warms the air in and above the inversion. In case 564 the net result of longwave radiative cooling, entrainment, and subsidence warming is that the buoyancy flux is negative throughout the boundary layer. The buoyancy term, however, is small compared to the shear production term, and as a result a near-neutral ABL is formed. It is found that the observed turbulent structure compares well with other observations of the near-neutral ABL (Grant 1986; Nicholls 1985).

The largest discrepancy between the model results and observations is that the model tends to overpredict the liquid water content. It is shown that

the prediction of the liquid water content can be improved by including gravitational droplet settling, which was important in case 564 because the air was of maritime origin. In this kind of air, the droplet concentration is small and the droplets are relatively large, resulting in a significant flux of water due to gravitational settling.

Acknowledgments

We would like to thank H.R.A. Wessels for discussions on the microphysical part of the work and H.L. Pan for reading the manuscript. A version of the original shortwave radiation program was kindly supplied by L. Smith and J.J. Morcrette when one of us (P.G.D.) was visiting Colorado State University. We are also grateful to S. Nicholls for supplying us with the experimental data on flight 564.

References

Brost, R.A., Lenschow, D.H. and J.C. Wyngaard, 1982a: Marine stratocumulus layer. Part I: Mean conditions. J. Atmos. Sci., 39, 800-817.

Brost, R.A., Lenschow, D.H. and J.C. Wyngaard, 1982b: Marine stratocumulus layers. Part II: Turbulence budgets. J. Atmos. Sci., 39, 818-836.

Duynkerke, P.G., 1988: Application of the E-ε turbulence closure model to the neutral and stable atmospheric boundary layer. J. Atmos. Sci, 45, 865-880.

Duynkerke, P.G. and A.G.M. Driedonks, 1987: A model for the turbulent structure of the stratocumulus-topped atmospheric boundary layer. J. Atmos. Sci., 44, 43-64.

Fouquart, Y. and B. Bonnel, 1980: Computations of solar heating of the earth's atmosphere: A new parameterization. Beitr. Phys. Atmos., 53, 35-62.

Grant, A.L.M., 1986: Observations of boundary layer structure made during the 1981 KONTUR experiment. Quart. J. Roy. Meteor. Soc., 112, 825-841.

Haltiner, G.J. and R.T. Williams, 1980: Numerical prediction and dynamic meteorology. Wiley and Sons, 477 pp.

Hansen, J.E. and L.D. Travis, 1974: Light scattering in planetary atmospheres. Space Sci. Rev., 16, 527.

Nicholls, S., 1984: The dynamics of stratocumulus: aircraft observations and comparison with a mixed layer-model. Quart. J. Roy. Meteor. Soc., 110, 783-820.

Nicholls, S., 1985: Aircraft observations of the Ekman layer during the Joint Air-Sea Interaction Experiment. Quart. J. Roy. Meteor. Soc., 111, 391-426

Nicholls, S. and J. Leighton, 1986: An observational study of the structure of stratiform cloud sheets: Part I: Structure. Quart. J. Roy. Meteor. Soc., 112, 431-460.

Rodgers, C.D., 1967: The use of emissivity in atmospheric radiation calculations. Quart. J. Roy. Meteor. Soc., 93, 43-54.

Stephens, G.L., 1978: Radiation profiles in extended water clouds. Part II: Parameterizations schemes. J. Atmos. Sci., 35, 2123-2132.

Stephens, G.L., and P.J. Webster, 1979: Sensitivity of radiative forcing to variable cloud and moisture. J. Atmos. Sci., 36, 1542-1556.

Welch, R. and W. Zdunkowski, 1976: A radiation model of the polluted atmospheric boundary layer. J. Atmos. Sci., 33, 2170-2184.

5. THE DIURNAL VARIATION OF A MARINE STRATOCUMULUS LAYER: A MODEL SENSITIVITY STUDY[+]

Abstract

A one-dimensional model which has previously been tested against observational data is used to study the diurnal variation of a marine stratocumulus layer. The influence of the shortwave radiative heating during different seasons on the decoupling of the cloud layer from the sub-cloud layer is studied. Results for a typical winter and summer situation are presented. It is shown that the decoupling can strongly affect the surface energy balance, suggesting that it is important to resolve the diurnal variation. Finally a sensitivity study of the model for initial and boundary conditions is presented.

+ Submitted to Monthly Weather Review.

1. Introduction

Wilson and Mitchell (1986) have shown that a poor representation of the variations in cloud amounts through the day and their influence on the radiative fluxes can degrade the performance of a general circulation model and could lead to large-scale changes in the climate simulation. They conclude that if the effect of clouds are to be properly included a diurnal cycle is necessary. Clouds affect the radiation balance at the top of the atmosphere in two ways: they reflect a larger part of the solar radiation than the underlying surface and the outward infrared flux to space is decreased. The solar contribution is efective only during the day so a realistic model should include the diurnal variation of cloud and radiation. Moreover it is necessary to include the diurnal cycle in order to investigate possible changes in surface climate, such a maximum and minimum temperatures.

Model studies on the diurnal cycle of a stratocumulus layer have been made by Turton and Nicholls (1986) and Bougeault (1985). Bougeault (1985) used a third-order turbulence closure model to reconstruct a realistic stratocumulus-topped ABL over the ocean starting from large-scale information only. On a time scale of a few days the solution converged to a quasi-equilibrium state. The absorption of solar radiation induced a strong diurnal cycle in the cloud deck. The main effect of this shortwave heating is that cloud base undergoes significant height variation rising during day-time and descending during night-time. This variation of cloud thickness is mainly the result of the formation of a stable zone just below cloud base (decoupling). This turns off the mixing and thereby the moisture supply from the surface to the stratocumulus layer, and as a result the liquid water content decreases.

Turton and Nicholls (1986) adapted a mixed-layer model to include the separation of the cloud layer from the sub-cloud layer. This is done by placing a constraint on the buoyancy flux at cloud base, so as to limit the amount of work that can be done against negative buoyancy. Once a threshold value is reached, the layer which was previously well-mixed from the surface to cloud top, is allowed to separate in two independently driven layers. This criterion is verified against observational data (e.g. Nichols and Leighton, 1986). Turton and Nicholls (1986) showed that the inclusion of separation leads to a stronger diurnal variation in cloud structure, with cloud thinning during the morning (after decoupling) and thickening in the late afternoon and night. The tendency for the layers to become decoupled is shown to be promoted

by significant shortwave absorption by the cloud and small surface buoyancy fluxes. Therefore, at mid-latitudes we expect the decoupling being more likely in summer than in winter.

With the synoptic reports from 1971 till 1981, Warren et al. (1986) have made a global distribution of total cloud cover and cloud type amounts over land. It turns out that stratus, stratocumulus and fog ("sky obscured" fog) together have the greatest average coverage of any low cloud type. In order to illustrate some of their findings we have presented some of the data for three regions (north-west Scotland, south-west England, and the Netherlands) around the North Sea in Table 1.

In all areas stratus, stratocumulus and fog ("sky obscured" fog) together, contribute most to total cloud coverage. The average frequency of occurrence around the North Sea is about 65% with an amount of about 70% when present. As a result the average cloud amount, which is the product of the two former quantities, is about 45%. With the aid of the 3 hourly synoptic reports Warren et al. (1986) have also quantified the diurnal variation in cloud cover. They examined the amplitude and phase of the first Fourier component (24-hour period) of the mean diurnal cycle. From Table 1 it is clear that the variations in cloud cover is quite small (small amplitude), this might of course be due to the low resolution (in octas) of the synoptic reports. More pronounced is the clear maximum around dawn.

We have developed a one-dimensional model which includes turbulence and radiation. In Duynkerke and Driedonks (1987, 1988) we compared the model with observational data (Nicholls, 1984; Brost et al., 1982a,b; Nicholls and Leighton, 1986) which were made under totally different conditions. In these papers we concluded that the model reproduces the observational data quite well. In this paper we will concentrate on the diurnal variation of a stratocumulus layer. At present no experimental data are available on the development of a stratocumulus layer in time.

The purpose of this paper is to study the diurnal cycle of a mid-latitude marine stratocumulus layer during different seasons. Observational data (Nicholls, 1984; Nicholls and Leighton, 1986) show that the virtual buoyancy flux at the surface, in the presence of a stratocumulus layer, is quite small. Therefore, in those cases the turbulence in the ABL is mainly driven by longwave radiative cooling at cloud top. For example, this was the case for five of the six flights discussed in Nicholls and Leighton (1986). If the solar elevation is large enough also the shortwave radiative heating

NW-Scotland	Frequency of occurrence (%)	Amount when present %	Average cloud amount (%)	Diurnal cycle	
				Amplitude (%)	Phase
DJF	75	68	51	3.0	3
MAM	71	67	48	4.7	3
JJA	77	68	52	5.0	4
SON	72	65	47	3.2	3
SW-England					
DJF	78	76	59	2.2	4
MAM	67	72	48	4.1	5
JJA	68	70	47	4.4	6
SON	71	70	50	2.8	5
Netherlands					
DJF	69	82	57	2.6	5
MAM	53	75	40	4.4	5
JJA	52	71	37	4.9	6
SON	58	74	43	3.6	6

Table 1. The coverage of stratus, stratocumulus and fog ("sky obscured") together, during the period 1971-1981 for three regions around the North Sea from Warren et al. (1986). The phase is defined as the local time in the morning of maximum cloud amount.

inside the cloud layer may be important. Nicholls (1984) made observations in a stratocumulus layer over the North Sea which showed that the combined effect of shortwave heating, longwave cooling and entrainment is that the cloud layer is heated more than the sub-cloud layer. As a result a slightly stable zone is formed near cloud base which prevents the ABL from being well mixed from the surface up to the cloud top. However, the cloud layer and sub-cloud layer are separately both being well mixed. This is called decoupling. In section 4 we will study the effect of the shortwave radiation on the decoupling as a function of the time of the year. Moreover it will be shown the diurnal cycle (decoupling) has important consequences for the net radiative fluxes at the surface. A good representation of the diurnal cycle is thus important for the surface climate (Wilson and Mitchell, 1986).

For the prediction of boundary layer clouds with mesoscale models (Reiff et al., 1986) it is important to know how sensitive the model results are for initial and boundary conditions. In section 5 we will study the influence of the initial moisture profile, the divergence and the sea-surface temperature on the predicted profiles.

2. Model

The model has been described in detail in Duynkerke en Driedonks (1987, 1988) and Duynkerke (1988). In the one-dimensional model we have ensemble-averaged equations for the horizontal velocity (u and v), the wet equivalent potential temperature (θ_q) and the total water content (q_w). The vertical velocity has to be prescribed. The turbulent fluxes are modeled with the gradient approach in which the exchange coefficient is calculated from the turbulent kinetic energy (E) and the viscous dissipation (ε), the so-called E-ε model. This is discussed in detail in Duynkerke (1988). In the entropy equation we have heating or cooling due to the radiative flux divergence. We have a model for both longwave and shortwave radiation.

For the longwave radiation we use the emissivity or "grey-body" approximation to calculate the longwave radiative flux. The effect of water vapour, carbondioxyde and liquid water on the emissivity is taken into account. The shortwave radiative fluxes are calculated with a two-stream approximation. The shortwave model includes Rayleigh scattering, absorption by atmospheric gases (water vapour, ozone and CO_2) and absorption and scattering

by cloud droplets. Further details on the radiation model are given in Duynkerke and Driedonks (1988).

3. Initial conditions

We have used the same initial and boundary conditions as Turton and Nicholls (1986) which are given in Table 2. Except for above the boundary layer where they used $\frac{\partial q_w}{\partial z}$ = 2.9 g kg^{-1} km^{-1} whereas we have set the gradient of q_w equal to zero. Turton and Nicholls (1986) have included this gradient to obtain an increase of q_w (due to subsidence) above the boundary layer. From radiosonde profiles it can be seen that this increase was much more a result of advection.

h(m)	1120	$\frac{\partial q_w}{\partial z}$ (g kg^{-1} km^{-1})	0
Θ_q (K)	296.1	T_s (K)	284.5
$\Delta \Theta_q$ (K)	0.9	U_g (ms^{-1})	0
$\frac{\partial \Theta_q}{\partial z}$ (K km^{-1})	7.3	V_g (ms^{-1})	-7
q_w (g kg^{-1})	5.4	albedo	0.05
Δq_w (g kg^{-1})	-3.5	divergence (s^{-1})	3 x 10^{-6}

Table 2. Initial values for model integrations.

The initial conditions are based on aircraft observations made on 16 November, 1983 between 1650 and 2100 GMT off NW Scotland as reported by Nicholls and Leighton (1986) (flight 624). At this time a high pressure system is located between England and Greenland (Figure 1). In the measuring area, indicated in the Figures 1 and 2 with a sign off NW Scotland, the wind is due north with a speed of about 7 m/s. The sky was reported to be completely covered with stratocumulus. The horizontal extent of the stratocumulus cloud field can be seen from the infrared satellite picture of 1832 GMT (Figure 2), which is just in the middle of the measuring period. Because the wind is due north, we have shown in Figure 3 the radiosonde profiles at Stornoway (58.13 N

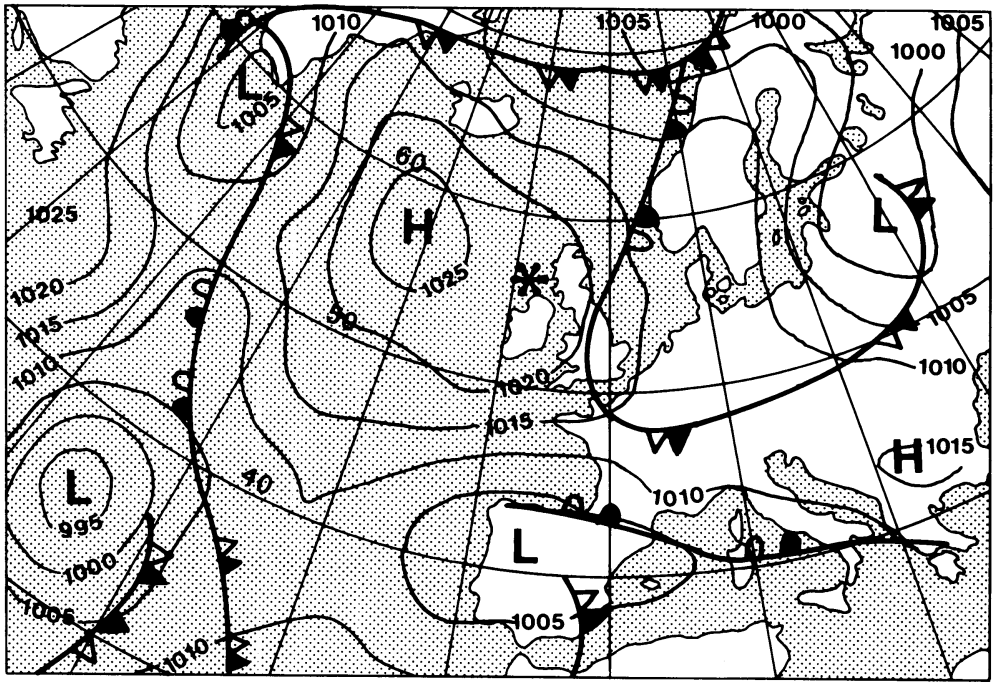

Figure 1. Synoptic surface map for 17 November 1983 (0000 GMT). The sign north-west of Scotland indicates the observational area on flight 624 (Nicholls and Leighton, 1986).

6.19 W) to illustrate the vertical structure. Note that due to its location these are very little influenced by land surfaces. The synoptic reports at Stornoway indicate that the sky is completely covered with stratocumulus, with a cloud base between 300 and 600 m. From the radiosonde profiles we see that the dew point is less than the temperature throughout the ABL. The radiosonde profiles therefore do not indicate clouds present whereas from the synoptic reports and satellite picture it is obvious that clouds are present. In section 5 we will study the sensitivity of the predicted (12 and 24 h in advance) profiles on the initial temperature and moisture profiles and the boundary conditions such as sea-surface temperature and divergence.

The model calculations are made at a latitude of 56° N and a roughness length $z_o = 2 \times 10^{-4}$ m is used. For the simulations in sections 4 and the "standard" run in section 5 we have used the initial and boundary conditions as given in Table 2.

Figure 2. NOAA infrared satellite picture on 16 November 1983 at 1832 GMT.

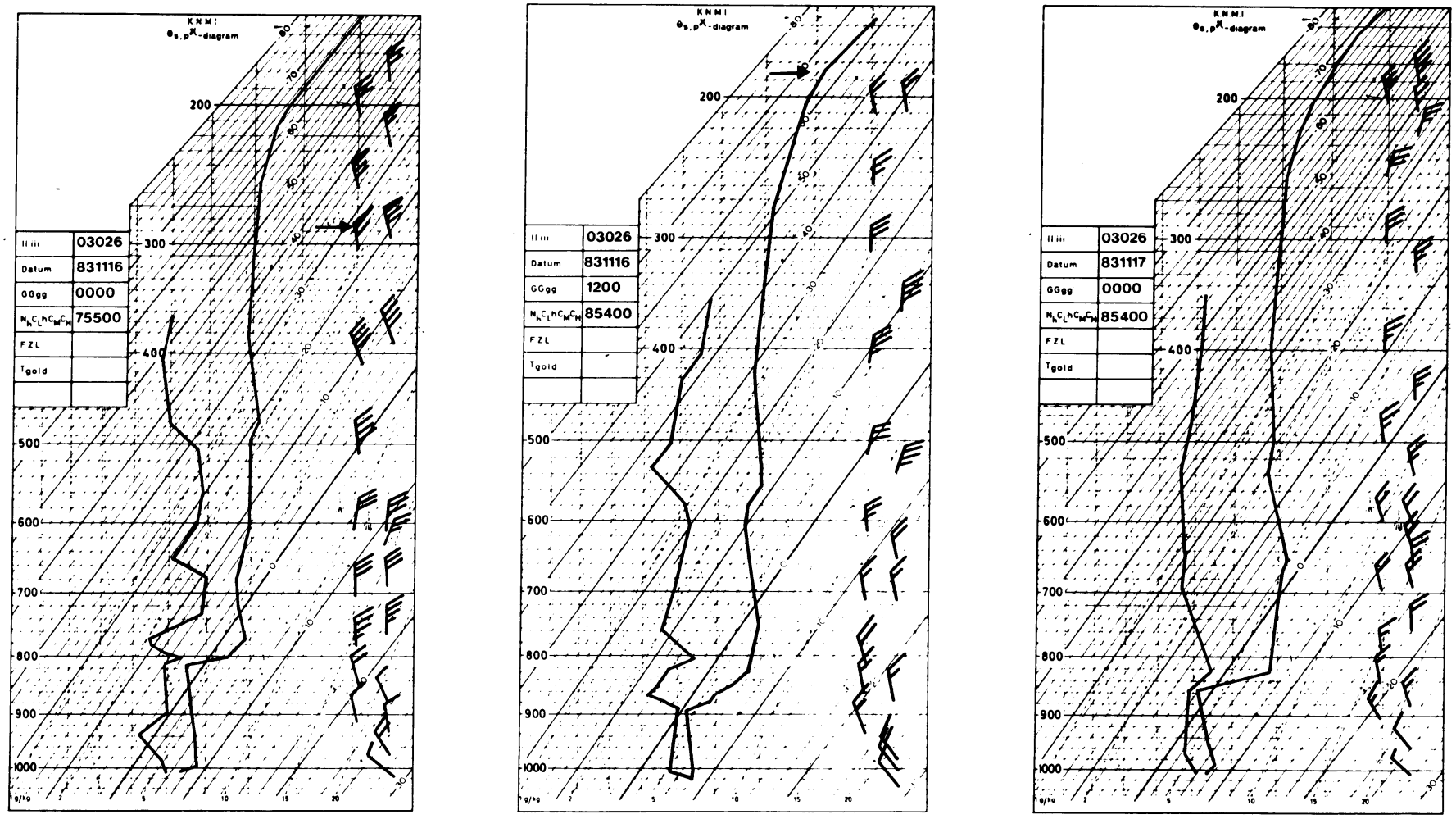

Figure 3. Radiosonde profiles of dew point (left) and temperature (right) at Stornoway (58.13° N 6.19° W) on 16 (0000 and 1200 GMT) and 17 November (0000 GMT) 1983.

4. Seasonal dependence of diurnal variation

At first we have made a simulation with conditions appropriate to the day of the observations (16 November) which is typial for a winter situation. These results are discussed and compared with observations in section 4.1. In section 4.2 we will present results for the 1 July which is typical for a mid-latitude summer situation. We will compare some of our results with the results from the mixed-layer model developed by Turton and Nicholls (1986). This is an interesting comparison because in their model the decoupling is diagnosed while in our model the decoupling is explicitly calculated. In section 4.3 we will show in which time of the year the decoupling is most likely to happen. The sensitivity of the predicted profiles (12 and 24 hours in advance) to the inital profiles and boundary conditions will be discussed in section 5.

4.1 Winter case

Results form an integration with a solar angle appropriate to 16 November are shown in Figure 4. Little diurnal variation is present in both

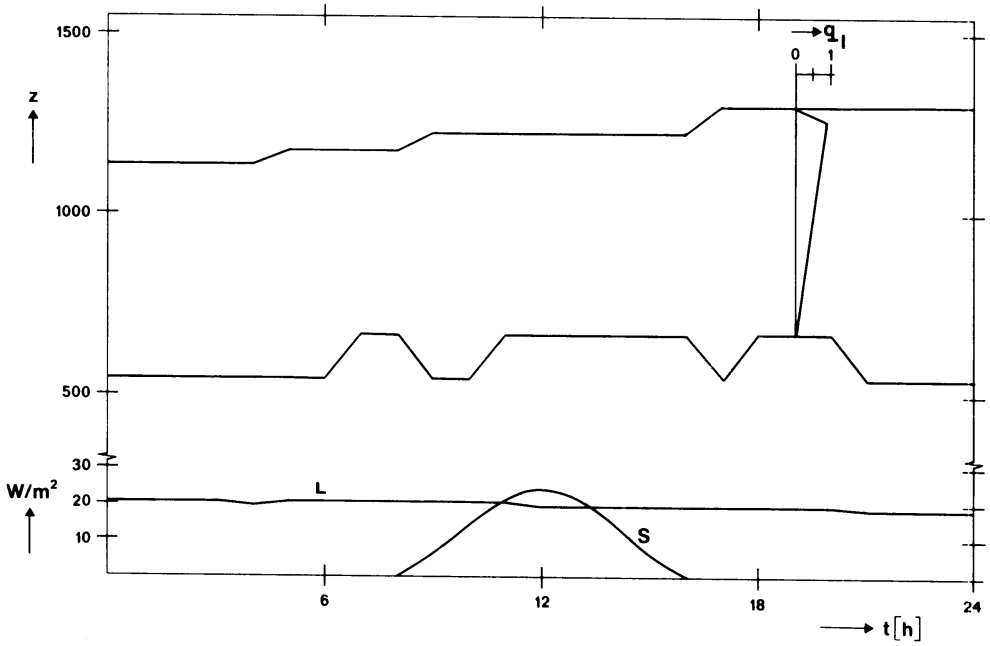

Figure 4. In the upper part of the Figure the variation of cloud top and cloud base as a function of time and the liquid water profile (q_ℓ) at t = 1900 h. In the lower part the net longwave (L) and shortwave (S) radiative fluxes at the surface.

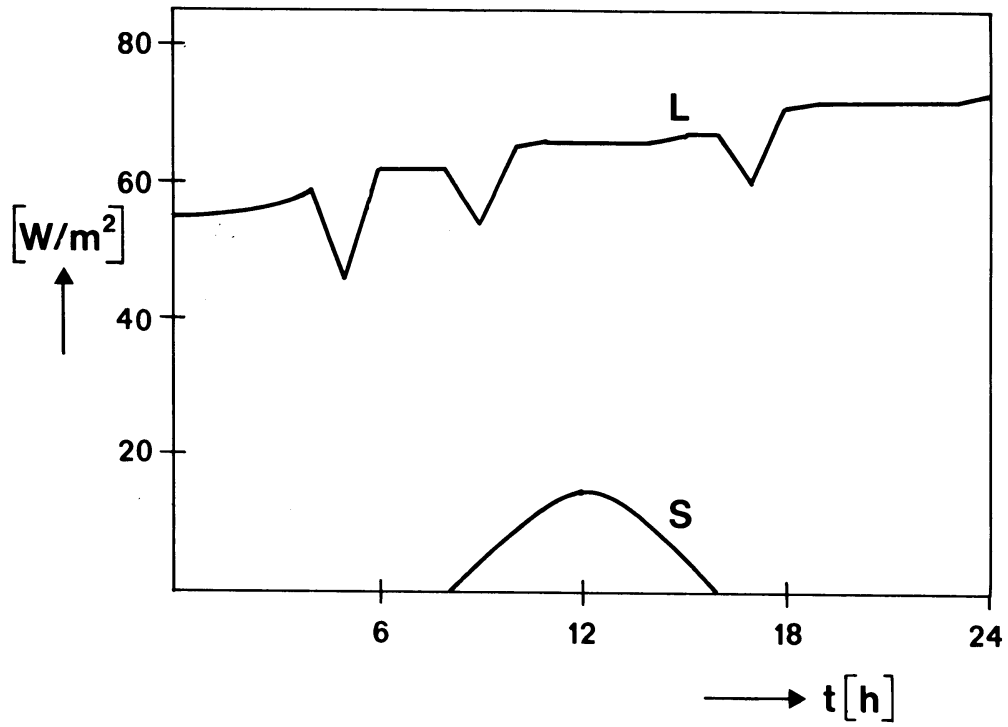

Figure 5. The net longwave (L) and shortwave (S) radiative flux over the whole cloud layer as a function of time.

cloud base and cloud top because of the weak solar flux. In Figure 5 we have plotted the total absorption of both longwave and shortwave radiation over the cloud layer. The longwave radiation thus cools the cloud layer by about 65 W/m^2 whereas the shortwave radiative heating has a maximum of about 15 W/m^2. Therefore the effect of the shortwave radiation can be neglected compared to the longwave cooling.

The Monin-Obukhov length (L) at the surface is about -60 m with a virtual buoyancy flux of ~ 13 W/m^2. In Figure 6 we have compared the calculated virtual buoyancy flux profile (at 19 h) with the observational data of Nicholls and Leighton (1986). Both observations and calculations show that most of the buoyancy production is concentrated within the cloud layer. Except for a shallow layer near the surface, where wind shear is important, the turbulence is driven by longwave radiative cooling at cloud top. The longwave radiative cooling is in this case strong enough to promote mixing all the way down to the sea-surface. A "quasi-equilibrium" state is reached in which the longwave cooling in the cloud is balanced by heating from the sea-surface and entrainment. In Figure 5 we have also drawn the net longwave and shortwave radiation at the surface. The longwave cooling is constant and about 20 W/m^2 whereas the shortwave heating varies as a function of time with a maximum of

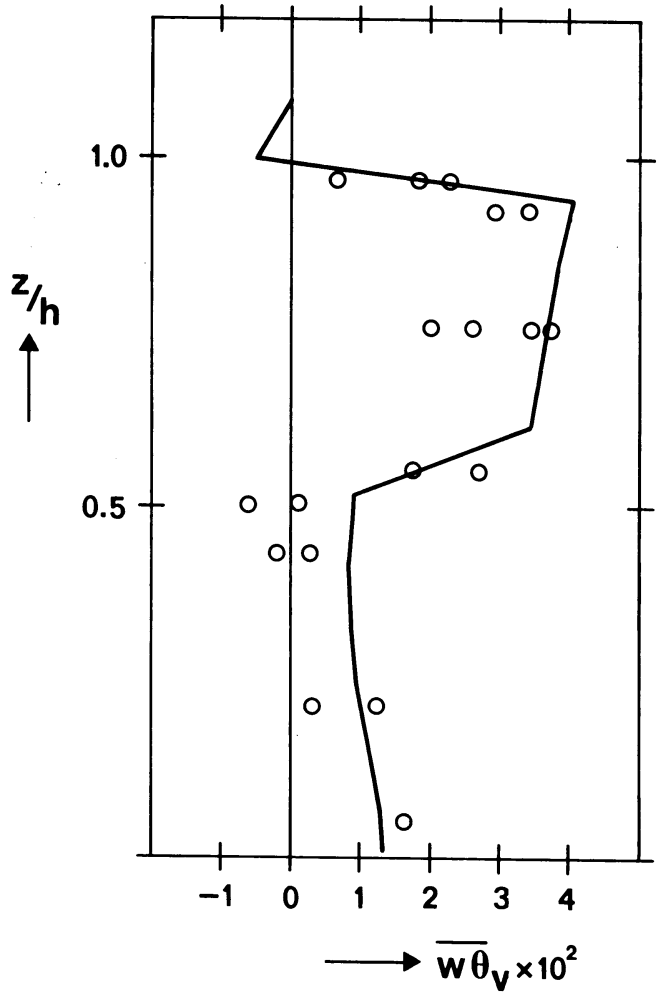

Figure 6. The virtual buoyancy flux as a function of dimensionless height: circles are observations (flight 624) and the full line is the calculated profile at t = 19 h.

about 25 W/m^2 around noon. Finally in Table 3 we have compared the observed and calculated upward and downward longwave radiative fluxes at cloud top and cloud base. The downward flux at the top of the model was set to a value so that the calculated downward flux at cloud top was approximately equal to the observed downward flux. The calculated fluxes are then in good agreement with the observed fluxes.

	NL obs.	NL mod.	t=19h
$F_L^{\uparrow+}$	326	327	330
$F_L^{\downarrow+}$	243	226	240
$F_L^{\uparrow-}$	351	347	352
$F_L^{\downarrow-}$	336	326	334
$F_L^{\uparrow+} - F_L^{\uparrow-}$	-25	-20	-22
$F_L^{\downarrow+} - F_L^{\downarrow-}$	-93	-100	-94
Net loss	68	80	72

Table 3. Cloud longwave radiative properties at cloud top (+) and cloud base (-): observed (NL stand for Nicholls and Leighton (1986)) and modelled.

4.2 Summer case

Figure 7 shows results for a simulation with the same initial and boundary conditions except that the radiation calculations are now performed for 1 July. The cloud top height increases steadily but slowly with time. Whereas, cloud base undergoes height variations of several hundreds of meters, rising during day-time and descending during night-time. This variation is induced by the formation of a stable zone near cloud base. This stable zone is a result of the effect that the shortwave heating which is of the same order as the longwave cooling in the cloud layer (Figure 8). Together with the heating due to entrainment this will make that the cloud layer is heated more than the sub-cloud layer such that a stable layer can be formed near cloud base. The stable layer will prevent the moisture to be transported from the surface to the cloud layer. This lack of moisture supply together with the heating of the cloud layer will increase the height of cloud base and decrease the liquid water content rapidly (Figure 7). Because in the sub-cloud layer turbulent mixing is supported by shear and buoyancy the moisture supply into the mixed-layer goes on (Figure 11). As a result cumulus clouds my form just

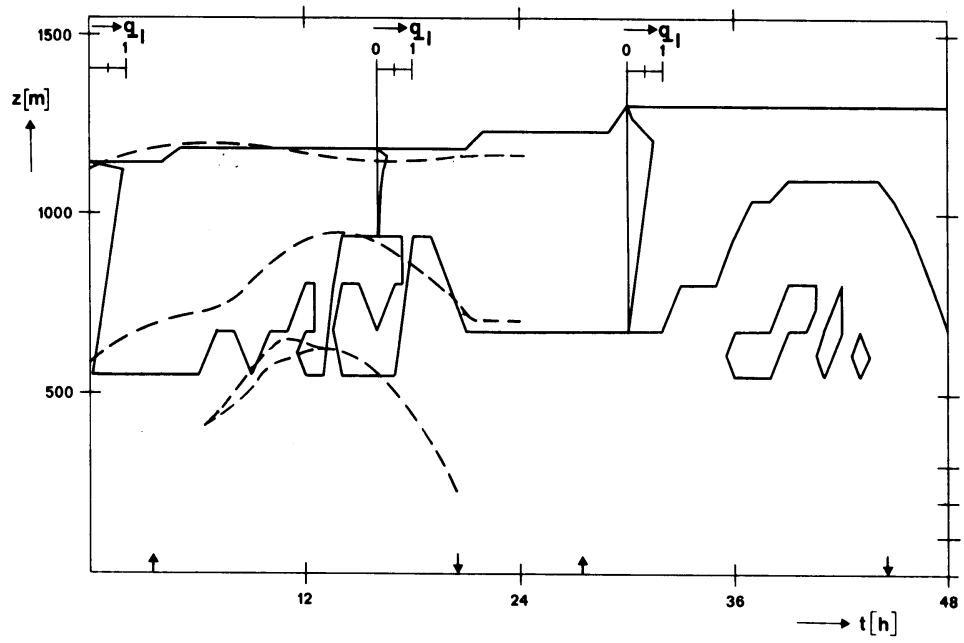

Figure 7. The height variation of cloud top and cloud base as a function of time for the summer case. Full line are model results and dashed line results of Turton and Nicholls (1986).

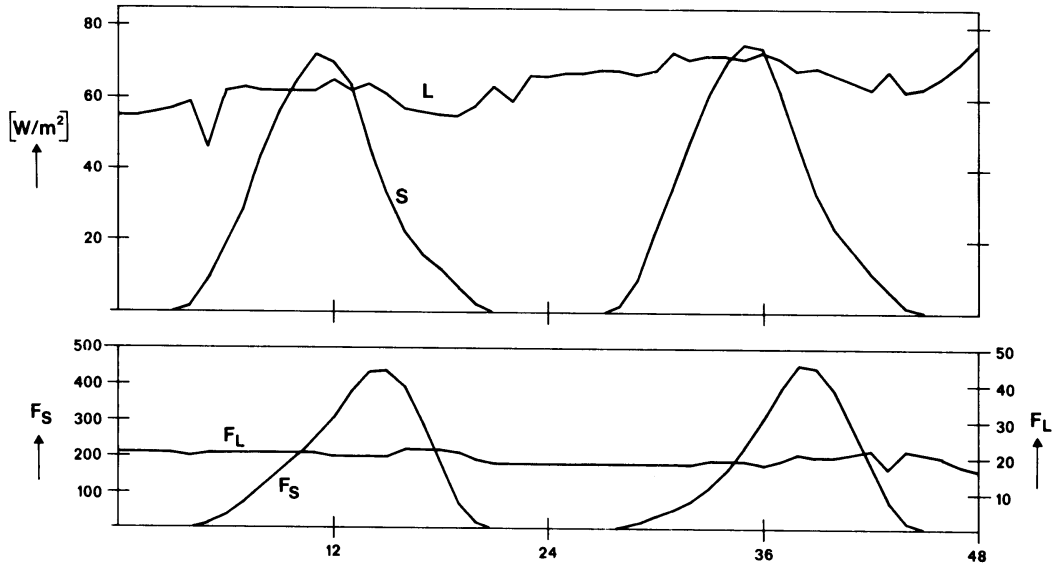

Figure 8. The net longwave (L) and shortwave (S) radiative fluxes over the whole cloud layer (upper) and at the surface (lower) for the summer case.

below the stable layer (Figure 7) which is also observed by Nicholls et al. (1983).

The results from the mixed-layer model of Turton and Nicholls (1986) are also shown in Figure 7. Qualitatively their results agree well with ours: the cloud top height is nearly constant whereas cloud base rises quickly in the morning and descends during the late afternoon. In the mixed-layer model the decoupling tends to start somewhat earlier than in our model.

In Figure 8 we have also shown the net longwave and shortwave radiative fluxes at the surface. The net longwave flux is constant and about 20 W/m^2, the net shortwave flux varies as a function of time and has a maximum of about 450 W/m^2. This large net shortwave flux at the surface is the result of the thinning of the cloud during day-time. In the afternoon the cloud is thin and

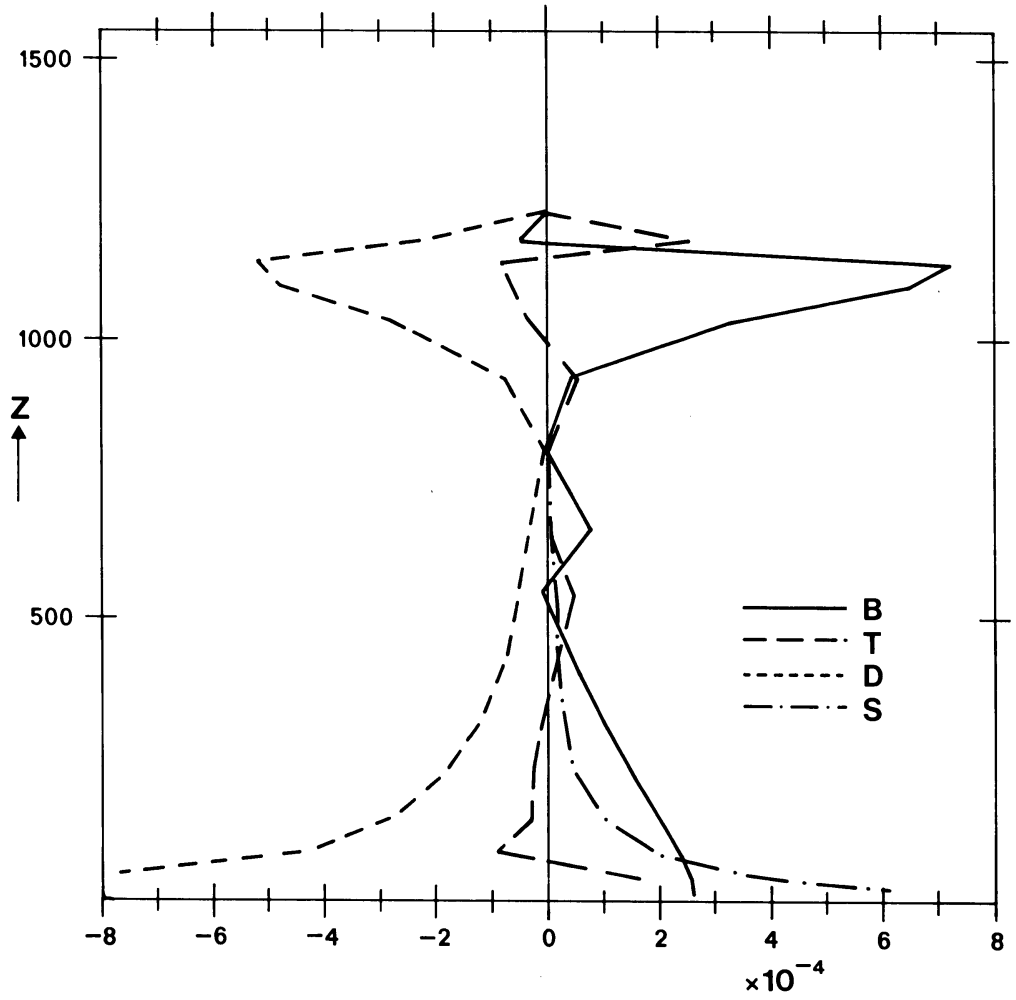

Figure 9. The terms in the turbulent kinetic energy budget as a function of height for the summer case at t = 16 h: B buoyancy, T transport, D dissipation and S shear production.

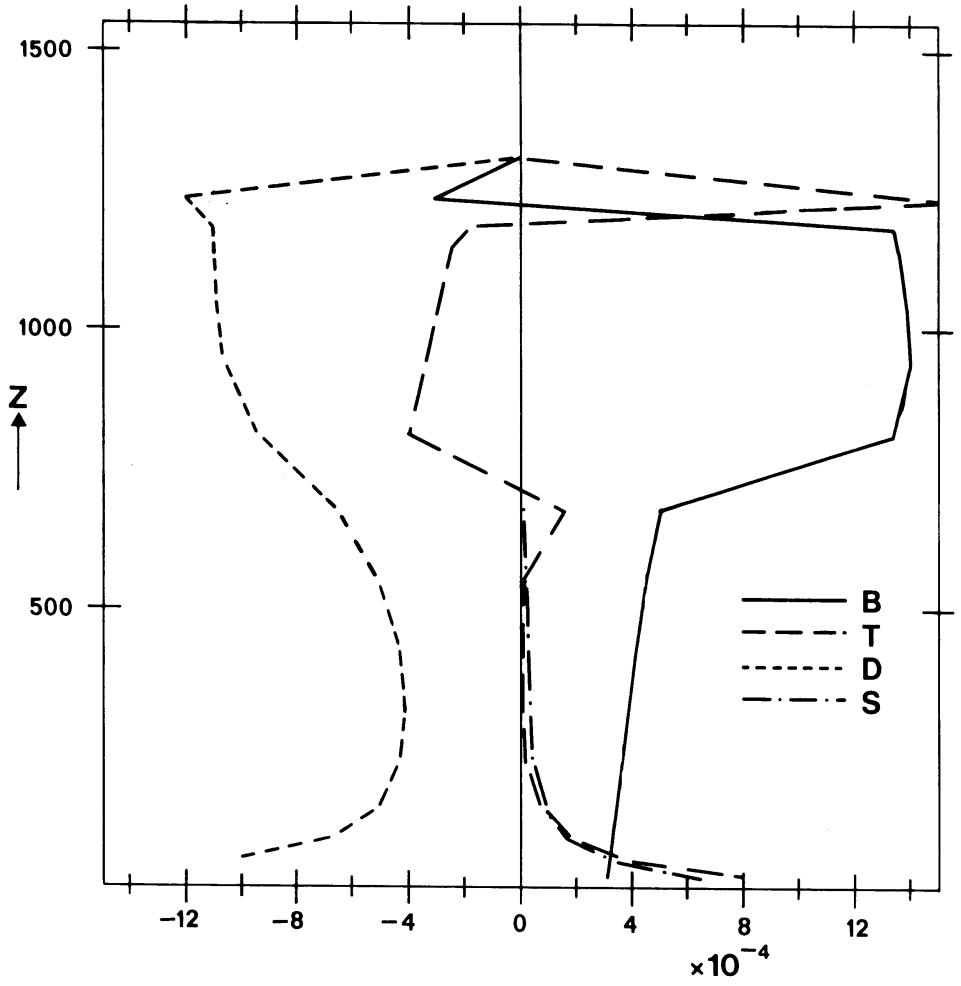

Figure 10. Same as Figure 9 but then at t = 28 h.

has a small liquid water content (Figure 7). As a result the transmittance of the cloud layer is large (Manton, 1980). The strong diurnal variation in cloud thickness thus significantly changes the surfce energy balance. A thinner cloud is much more transmissive for short wavelengths, but is still optically thick at longer wavelengths. The net longwave flux at the surface therefore hardly changes while the net shortwave flux is increased. These results suggest that it is important to resolve the diurnal variation of a stratocumulus layer in large scale models. This result is very similar with the results obtained by Wilson and Mitchell (1986) who have shown that the simulation of climate in a GCM will be degraded if the diurnal cycle is not adequately resolved.

The vertical structure of the turblent fluxes (e.g. Figure 11) undergoes a diurnal modification forced by the decoupling. The terms in the turbulent kinetic energy budget have been shown in Figures 9 and 10 at t = 16 and 28 h,

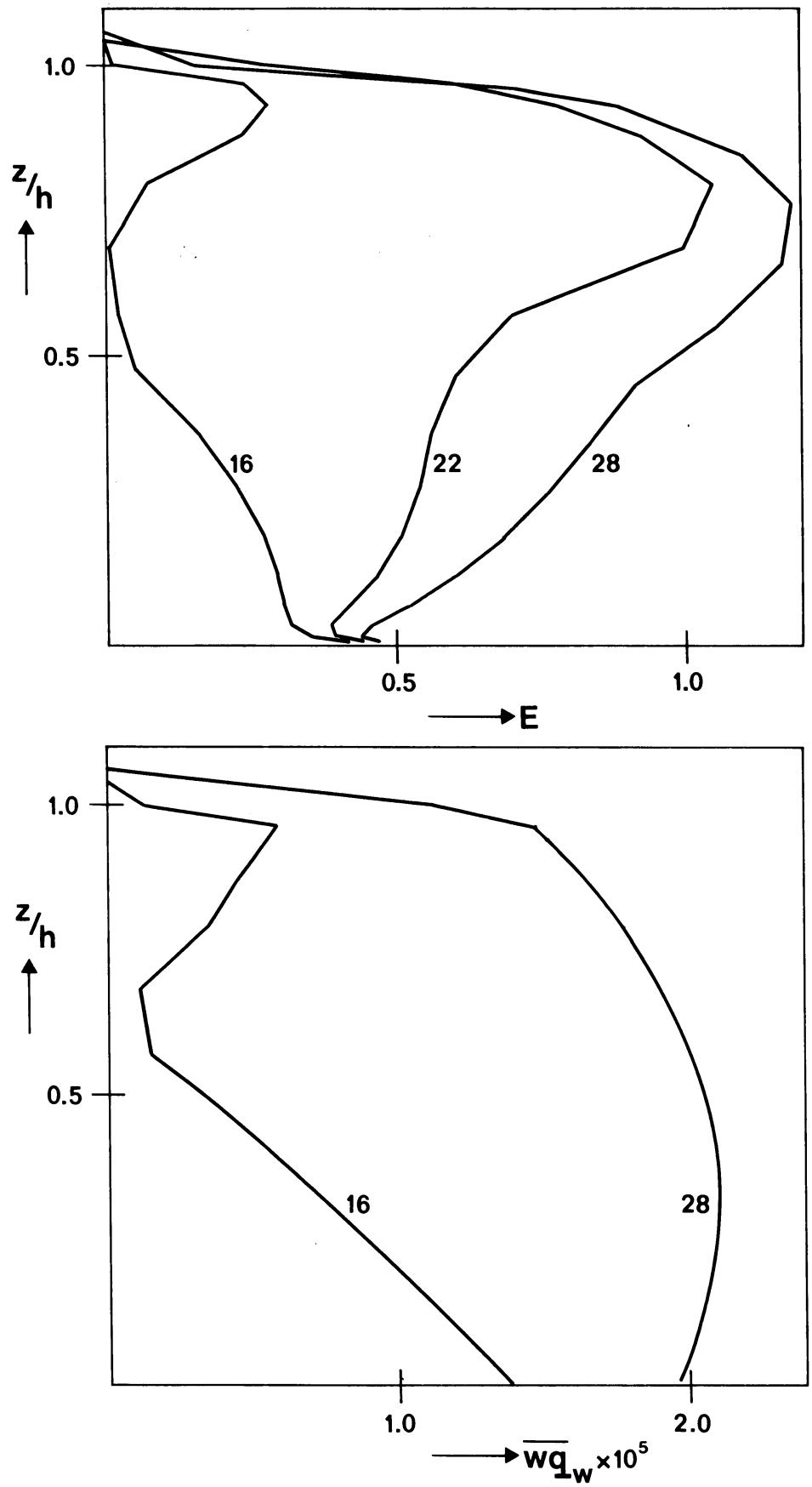

Figure 11. The turbulent kinetic energy (upper) at t = 16, 22 and 28 h and the total moisture flux (lower) at t = 16 and 28 as a function of dimensionless height for the summer case.

respectively. In the late afternoon the buoyancy flux is positive in the thin cloud layer, is slightly negative near cloud base (except for the peak due to the cumulus cloud) and positive in the layer near the surface. From Figure 11 it is clear that the turbulent kinetic energy shows a clear minimum near cloud base and that the turbulent moisture flux is zero within this layer. Thus as a result of the turbulence q_w increases in the layer near the surface due to the moisture input from the sea-surface whereas in the cloud layer q_w decreases due to the entrainment of dry air from above the inversion. The buoyancy term in the TKE-equation is being balanced by the viscous dissipation. The transport term transfers turbulent kinetic energy from the cloud layer both into the entrainment region and the stable layer near cloud base. During the night the turbulence is dominated by longwave radiative cooling at cloud top. This will tend to destabilize the whole ABL so that mixing will extend down to the surface (E in Figure 11). This will redistribute the moisture surplus present in the layer close to the surface (brought in during the day) over the whole ABL. As a result the cloud thickens rapidly, i.e. cloud base height decreases. This redistribution process can be clearly seen in the total moisture flux (Figure 11): in the lower part of the ABL the gradient is positive and thus q_w decreases whereas in the upper part of the ABL the gradient is negative and thus q_w increases. Due to the cloud thickening and the absence off shortwave absorption the integrated buoyancy flux increases (Figure 10) and therefore the TKE-level increases (Figure 11).

4.3 Seasonal dependance of decoupling

From sections 4.1 and 4.2 it is clear that at mid-latitude (here 56° N) the decoupling of the cloud layer from the sub-cloud layer is present in the summer case, but not in the winter case. For this latitude and initial conditions we have made runs during different seasons. We have used two criteria to diagnose the decoupling: the first is when the total moisture flux starts to deviate significantly from being linear throughout the ABL, the second is when the TKE below cloud base is less than 20% of the maximum TKE in the cloud layer. These results are shown in Figure 12. The decoupling is clearly present from April till August with the most pronounced decoupling (20% cirterion) present during the afternoon.

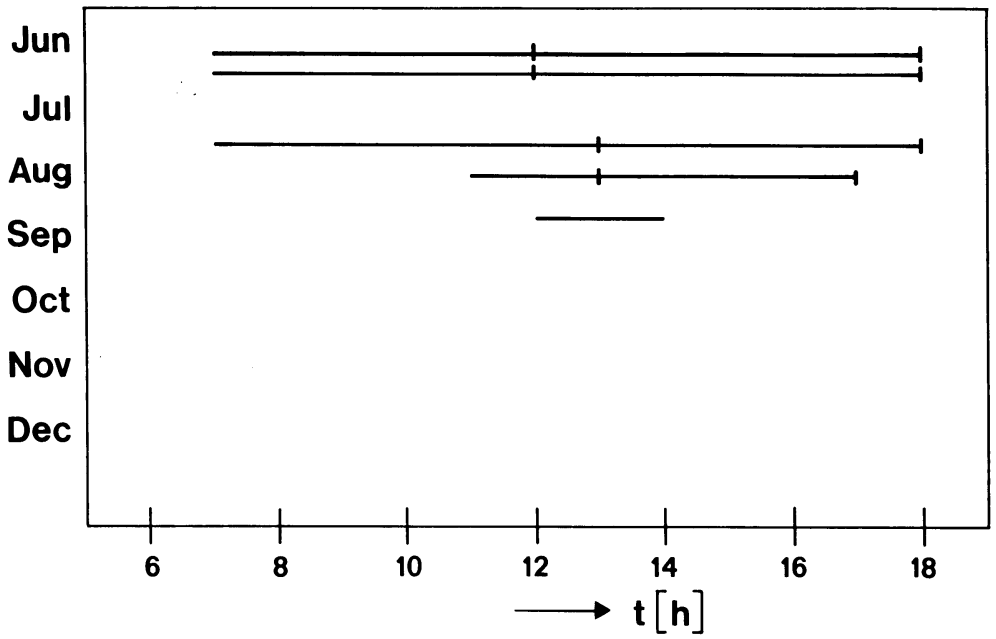

Figure 12. The decoupling as a fuction of the time of the day during different months: full line from moisture flux criterion: ⟷ E below cloud base less than 20% of maximum in cloud layer.

5. Sensitivity analysis

In this section we will investigate the sensitivity of the model results for the initial and boundary conditions. In section 3 we have discussed typical radiosonde profiles through a stratocumulus-topped ABL from which it was clear that due to measuring errors these profiles did not show a stratocumulus deck present. However, from synoptic reports and satellite pictures it was clear that the sky was completely covered with stratocumulus.

The initial fields in forecast models are obtained from ground based stations, radiosondes and satellites. For the vertical thermodynamic structure of the atmosphere, especially over land, mostly radiosonde data have been used up to now. For example, in the Air Mass Transformation (AMT) approach (Reiff et al., 1984) the vertical thermodynamic structure in the source area is obtained from several observations of nearby radiosonde stations. This initial vertical profile is advected along trajectories and can change under the influence of subsidence and surface fluxes. Here we will not consider the

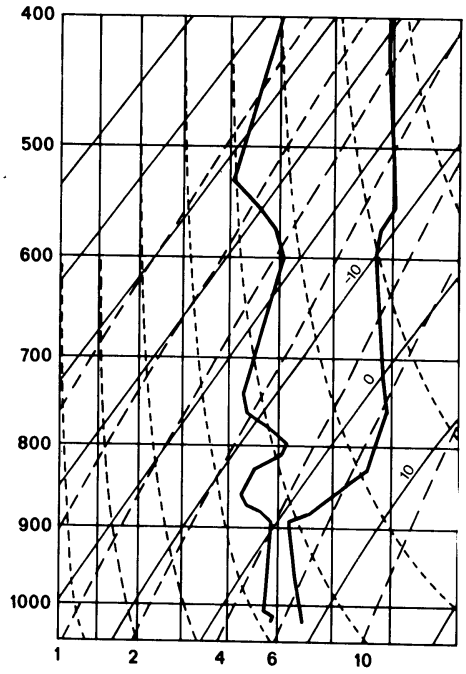

Figure 13. Radiosonde profile of dew point (left) and temperature (right) in the observational area (56.10° N, 8.46° W) composed from three nearby radiosondes by a method described in Reiff et al. (1984).

trajectory part. In Figure 13 we have shown the vertical profile in the observational area (56.10° N, 8.46° W) which is composed from the radiosonde profiles at the stations 03026 (58.22° N, 6.32° W), 04018 (63.97° N, 22.60° W) and 99183 (57.00° N, 20.00° W) by a method described in Reiff et al. (1984). The radiosonde profile is thus clearly not saturated near cloud top, this is mainly a result of the fact that the specific humidity is significantly underestimated (about 1 g/kg at cloud top). In this section we will investigate the influence of (measuring) errors in the initial data on the quality of the forecast.

We will present results for 1 July at t = 17 and t = 24 h which are representative for results during the late afternoon in which decoupling is present and results during the night in which the turbulence is mixing throughout the ABL, respectively. Profiles of the specific liquid water content will be presented, so that cloud top, cloud base and the amount of liquid water in the cloud are clearly indicated. The standard run is thus the same as the summer simulation discussed in section 4.2. In this section we will study how sensitive the model results are for small changes in initial and boundary conditions. Here we will present changes in the initial total

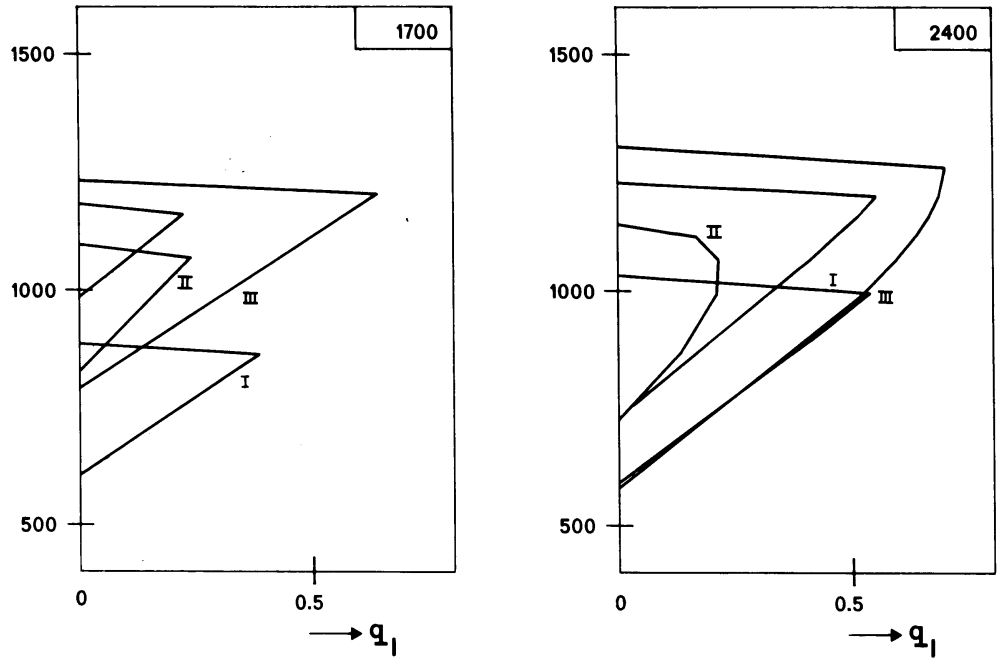

Figure 14. Liquid water profiles at 17 h and 24 h for 1 July for different initial values of q_w in the boundary layer: standard run; I q_w = 4.4 g kg^{-1}; II q_w = 4.9 g kg^{-1}; III q_w = 5.9 g kg^{-1}.

specific water content (q_w) in the boundary layer (Figure 14), in the initial total specific water content above the ABL (Figure 15), in the sea-surface temperature (Figure 16) and in the value of the applied divergence (Figure 17).

If we increase the initial q_w in the boundary layer the cloud thickness increases and therefore also the integrated buoyancy production increases (see Figure 6). Due to the increased buoyancy production also the entrainment increases and as a result the cloud top height rises faster. This corresponds to case III in Figure 14. If the initial q_w in te ABL is decreased compared to the standard value (case II in Figure 14) the opposite is happening. If the initial value of q_w is decreased far enough, initially no cloud will be present (case I), as in the radiosonde profile. Also in this case I ultimately a cloud will be formed but with a much lower cloud top initially. In Figure 15 we have shown results for different initial values of q_w above the ABL. Increasing the total water content above the ABL will, due to entrainment, increase the liquid water content of the cloud. Case III, with the highest initial value of q_w above the ABL, the cloud top is somewhat lower due to the lower entrainment rate. The larger amount of water vapor above the ABL

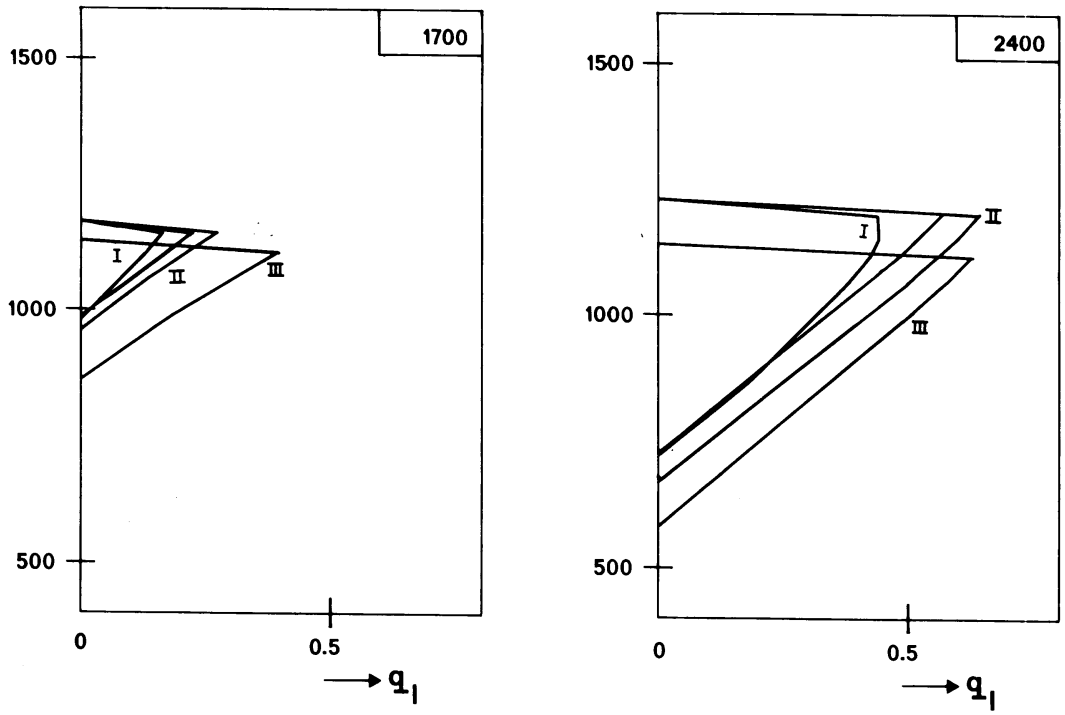

Figure 15. Liquid water profiles at 17 h and 24 h for 1 July for different initial values of q_w above the boundary layer: standard run; I q_w = 1.5 g kg^{-1}; II q_w = 2.3 g kg^{-1}; III q_w = 3.1 g kg^{-1}.

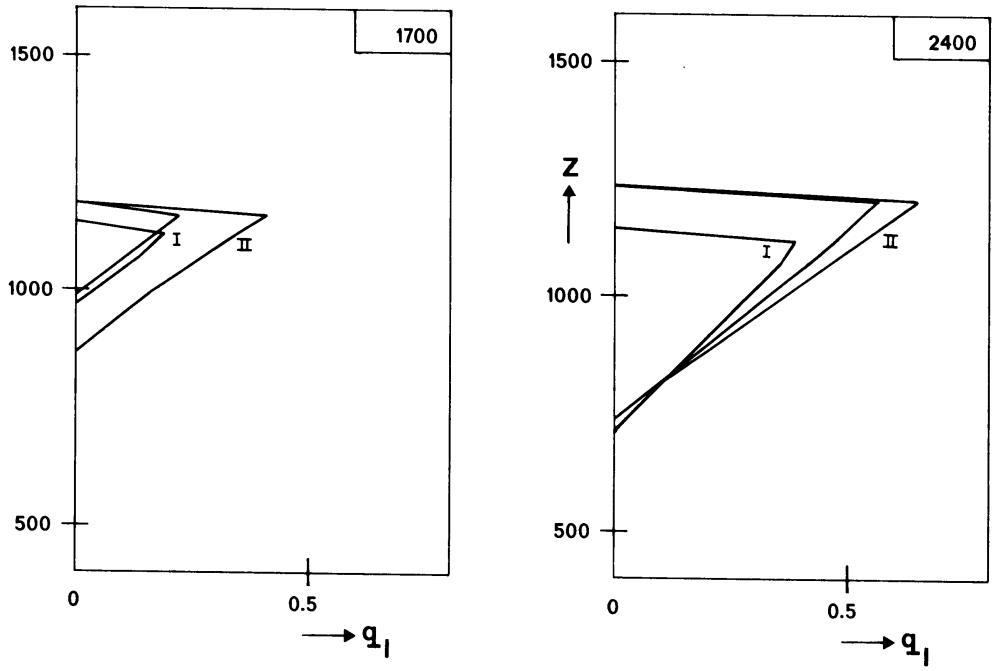

Figure 16. Liquid water profiles at 17 h and 24 h for 1 July for different sea surface temperatures; standard run; I T_s = 283.5 K; II T_s = 285.5 K.

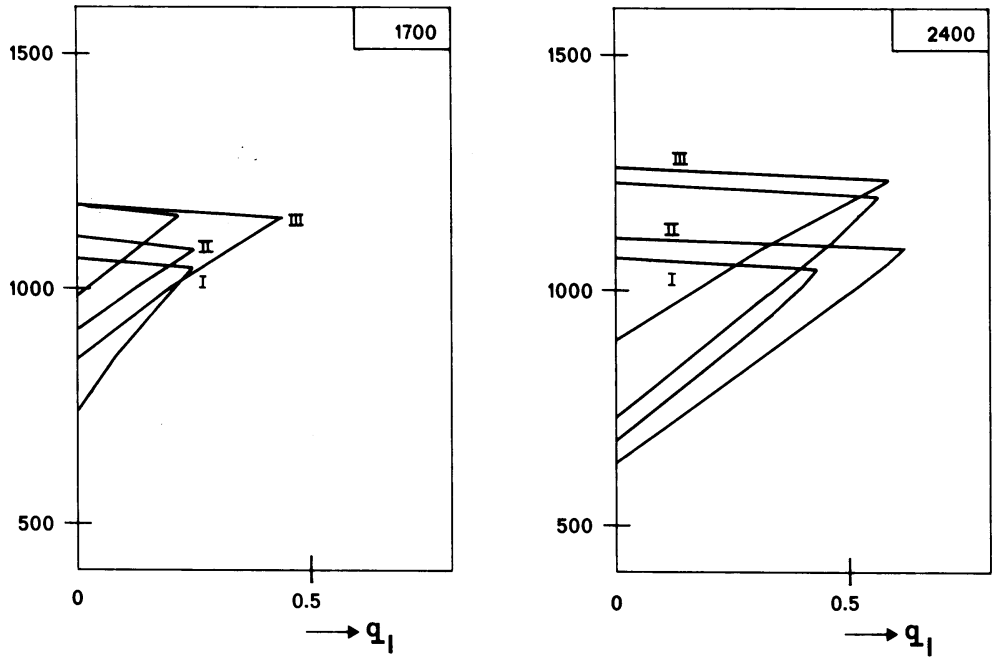

Figure 17. Liquid water profiles at 17 h and 24 h for 1 July for different values of the divergence: standard run; I 5 x 10^{-6} s^{-1}; II 4 x 10^{-6} s^{-1}; III 2 x 10^{-6} s^{-1}.

compared to the standard run, increases the downward longwave radiative flux above cloud top. Because the upward longwave radiative flux remains nearly the same the cloud top radiative cooling decreases. As a result the turbulence level and thus the entrainment rate decreases. In Figure 16 we have shown the results for three different sea-surface temperatures. For the standard run T_s = 284.5 K. Case I and II are results for a run with the sea-surface temperature one degree lower, respectively higher. Due to the reduced buoyancy flux at the surface in case I the entrainment is smaller and as a result the cloud top height is lower than for the standard run. In Figure 17 we have shown the liquid water content profiles for different divergences applied. The effect of increasing the divergence is that the cloud top height decreases.

The general conclusion of the sensitivity study is that the predicted profiles are in general not very sensitive to the applied boundary conditions and initial conditions. This gives good hope for including boundary layer clouds in forecast models.

6. Conclusions

The diurnal simulation of a typical marine stratocumulus layer at mid-latitudes with a one-dimensional model has shown that the turbulent mixing was maintained primarily by convection driven by radiative cooling at cloud top. This is also supported by observational data of Nicholls and Leighton (1986) who observed this to be the case in five out of six cases.

At larger solar elevations (during summer at mid-latitudes) the shortwave heating is of the same magnitude as the longwave cooling which makes that during day-time a stable layer is formed near cloud base. The stable layer prevents the turbulence from mixing the whole ABL, the cloud layer and sub-cloud layer are separately still being rather well-mixed. Because there is (almost) no exchange between the two layers we call this decoupling. Due to the decoupling the moisture input from the sea-surface can only be distributed over the sub-cloud layer, and not over the cloud layer, together with the entrainment of drier air and heating of the cloud layer the cloud is thinning very rapidly. The cloud top height remains nearly constant over the period of one day whereas the cloud base rises quickly during the morning and descends during the afternoon.

The strong diurnal variation in cloud thickness, which will at mid-latitudes only be present during summer, changes the surface energy balance significantly. A thinner cloud has a much higher transmittance for shortwave radiation than a thick cloud, whereas at larger wavelengths the cloud will still be optically thick. The net shortwave flux at the surface is thus significantly increased whereas the net longwave flux at the surface hardly changes. This suggests that it is important to include the diurnal variation of stratocumulus in climate models.

We have made a sensitivity study of the model for initial and boundary conditions. Here we have shown results for small changes in the initial moisture profile (in and above the boundary layer), sea-surface temperature and subsidence. From the sensitivity study we can conclude that the results are not very sensitive for the initial and boundary conditions, which gives good hope for including boundary layer clouds in forecast models.

It should be stressed that in this paper we have only considered stratocumulus clouds over sea and not over land. In a future study we hope to investigate a stratocumulus layer over land. This will be much more complicated due to the direct influence of the net radiation on the latent and sensible heat flux at the surface.

Acknowledgements

The author thanks A.A.M. Holtslag and A.C.M. Beljaars for their helpful discussions and comments and M. Kaltofen for preparing the paper.

References

Brost, R.A., D.H. Lenschow, and J.C. Wyngaard, 1982a: Marine stratocumulus layer. Part I: Mean conditions. J. Atmos. Sci., 39, 800-817.

Brost, R.A., D.H. Lenschow, and J.C. Wyngaard, 1982b: Marine stratocumulus layers. Part II:Turbulence budgets. J. Atmos. Sci., 39, 818-836.

Bougeault, Ph., 1985: The diurnal cycle of the marine stratocumulus layer: A higher-order model study. J. Atmos. Sci., 42, 2826-2843.

Duynkerke, P.G., and A.G.M. Driedonks, 1988: The turbulent structure of a shear-driven stratus-topped atmospheric boundary layer: A comparison of model results with observations. J. Atmos. Sci., 45, 2343-2351.

Duynkerke, P.G., 1988: Application of the E-ε turbulence closure model to the neutral and stable atmospheric boundary layer. J. Atmos. Sci., 45, 865-880.

Duynkerke, P.G., and A.G.M. Driedonks, 1987: A model for the turbulent structure of the stratocumulus-topped atmospheric boundary layer, J. Atmos. Sci., 44, 43-64.

FIRE, the First ICCP Regional Experiment, 1983. Research Plan. Available from the National Climate Program Office, Room 108, 11400 Rockville Pike, Rockville MD 20852, USA.

Manton, M.J., 1980: Computations of the effect of cloud properties on solar radiation. J. Rech. Atmos., 14, 1-16.

Nicholls, S., B. Brümmer, F. Fiedler, A. Grant, T. Hauf, G. Jenkins, C. Readings, and N. Shaw, 1983: The structure of the turbulent atmospheric boundary layer. Phil. Trans. R. Soc. Lond., A 308, 291-309.

Nicholls, S, and J. Leighton, 1986: An observational study of the structure of stratiform cloud sheets: Part I. Structure. Quart. J. Roy. Met. Soc., 112, 431-460.

Nicholls, S., 1984: The dynamics of stratocumulus: aircraft observations and comparison with a mixed layer-model. Quart. J. Roy. Met. Soc., 110, 783-820.

Reiff, J., D. Blaauboer, H.A.R. de Bruin, A.P. van Ulden and G. Cats, 1984: An air mass transformation model for short-range weather forecasting. Mon. Wea. Rev., 112, 393-412.

Reiff, J., A.G.M. Driedonks, and A.A.M. Holtslag, 1986: Report of the workshop on boundary layer models in short range weather forecasting. Scientific report = Wetenschappelijk rapport, WR 86-4. KNMI, P.O. Box 201, 3730 AE De Bilt, The Netherlands.

Turton, J.D., and S. Nicholls, 1986: A study of the diurnal variation of stratocumulus using a mixed layer model, Quart. J. Roy. Met. Soc., 113, 969-1009.

Warren, S.G., C.J. Hahn, J. London, R.M. Chervin, and R.L. Jenne, 1986: Global distribution of total cloud cover and cloud type amounts over land. NCAR/TN 273 + STR, p. 234. National Center for Atmospheric Research, Boulder, Co.

Wilson, C.A., and J.B.E. Mitchell, 1986: Diurnal variation and cloud in a general circulation model. Quart. J. Roy. Met. Soc., 112, 347-369.

I Application of the $E - \epsilon$ Turbulence Closure Model to the Neutral and Stable Atmospheric Boundary Layer ✱

P. G. DUYNKERKE

Free University, Amsterdam, The Netherlands

(Manuscript received 6 April 1987, in final form 19 August 1987)

ABSTRACT

In the $E - \epsilon$ turbulence model an eddy-exchange coefficient is evaluated from the turbulent kinetic energy E and viscous dissipation ϵ. In this study we will apply the $E - \epsilon$ model to the stable and neutral atmospheric boundary layer. A discussion is given on the equation for ϵ, which terms should be included and how we have evaluated the constants. Constant cooling rate results for the stable atmospheric boundary layer are compared with a second-order closure study. For the neutral atmospheric boundary layer a comparison is made with observations, large-eddy simulations and a second-order closure study. It is shown that a small stability effect can change the neutral atmospheric boundary layer quite drastically, and therefore, it will be difficult to observe a neutral boundary layer in the atmosphere.

1. Introduction

In this study we will apply the $E - \epsilon$ model, in which an eddy-exchange coefficient is evaluated from the turbulent kinetic energy E and the viscous dissipation ϵ, to the stable and neutral atmospheric boundary layer (ABL). The use of the $E - \epsilon$ model in engineering flows is now quite standard (Rodi, 1980). This popularity raises the question whether it could also be used for modeling the ABL, especially for flows in which the length scale cannot be prescribed in advance; for instance, under circumstances in which there are internal production processes of turbulent kinetic energy in the boundary layer, such as phase changes, radiative heating and radiative cooling in clouds (Duynkerke and Driedonks, 1987). Another application of the $E - \epsilon$ model is the flow over irregular terrain, in which a length scale is no longer determined by local (surface) characteristics (Rao et al., 1974; Beljaars et al., 1983).

In higher-order closure studies the use of the ϵ-equation has also become standard (Wyngaard et al., 1974; Zeman and Lumley, 1979; André et al., 1979). However, very little new insight in the ϵ-equation has been gained since the early work of Harlow and Nakayama (1967). Besides the frequent use of an ϵ-equation in higher-order closure studies we are aware of only a few applications of the $E - \epsilon$ model to atmospheric boundary-layer problems (Lee and Kao, 1979; Mason and Sykes, 1980; Detering and Etling, 1985a,b).

Lee and Kao (1979) combined the equations for E and ϵ to derive an equation for the eddy-exchange coefficient K. The constants used in this equation for K can be directly calculated from the constants used in the equation for E and ϵ. However, Lee and Kao (1979) divided the constants, which they proposed for the ϵ-equation, by 25 before calculating the constants in the equation for K. The reason and implications of this change are not clear to us. Mason and Sykes (1980) studied the dynamics of large-scale, horizontal roll vortices in the neutral ABL with an $E - \epsilon$ model. They concluded that the model results were completely stable for all perturbations, due to the anomalous high eddy-exchange coefficient obtained with the $E - \epsilon$ model. Similar results (too large K) were obtained by Detering and Etling (1985a) while simulating the neutral ABL.

Detering and Etling (1985a) compared their model results for the neutral ABL with the "Leipzig Wind Profile" (Mildner, 1932; Lettau, 1950, 1957) and concluded that both the eddy-exchange coefficient and the boundary layer height were much too large. Therefore, Detering and Etling (1985a) modified the ϵ-equation by making one of the constants a function of lf/u_*, which is the ratio of a turbulent length scale (l) and the depth of the neutral ABL (u_*/f). Qualitatively, this is analogous to a diagnostic length scale formulation in which l is proportional to u_*/f (Blackadar, 1962). Therefore, we think there is no real advantage in using their prognostic equation for ϵ above a diagnostic length scale. Moreover, we will show that the "Leipzig Wind Profile", which Detering and Etling (1985a) used to tune their model for the neutral case, is not representative for the truly neutral ABL, but some stability effect must be important. This was already noticed by Lettau (1950): "In the same air mass, the 1400 UTC sounding at the aerological station Lin-

Corresponding author address: P. G. Duynkerke, Royal Netherlands Meteorological Institute, P.O. Box 201, 3730 AE de Bilt, The Netherlands.

© 1988 American Meteorological Society

✱Published in Journal of the Atmospheric Sciences, 1988, 45, 865-880

denberg (less than 100 miles from Leipzig) showed a rather uniform lapse rate of −0.65°C/100 m in the layer under consideration, which corresponds to an increase of potential temperature of 0.35°C/100 m."

Recently, Nicholls (1985) presented an observational study of the Ekman layer over sea during the Joint Air–Sea Interaction Experiment. The conditions were described as near neutral and barotropic. Nicholls (1985) concluded that in the absence of a low level inversion a well-mixed Ekman layer is observed on each occasion, which is limited to a height of $0.2u_*/f$.

Model simulations of the truly neutral ABL have been made by Deardorff (1972), Wyngaard et al. (1974) and Mason and Thomson (1986). Deardorff (1972) presented model results of a large-eddy simulation of the neutral ABL. He made two model runs, with model top at $0.45u_*/f$, and u_*/f, respectively. From the results of Deardorff (1972) it is clear that the height of the neutral ABL is somewhere between $0.45u_*/f$ and u_*/f. However, most of the results he presents are for the run with the lower model top and therefore these data cannot be trusted completely. Wyngaard et al. (1974) used a second-order closure model to simulate the neutral ABL and obtained a boundary layer height of $0.7u_*/f$. Recently, Mason and Thomson (1986) made a very detailed study of the neutral ABL with their large-eddy model; they found a boundary layer height of about $0.6u_*/f$ (their B10 case) for the neutral ABL.

The observational data (Lettau, 1950; Nicholls, 1985) thus show a boundary layer height of about $0.2u_*/f$, whereas the model results (Deardorff, 1972; Wyngaard et al., 1974; Mason and Thomson, 1986) show a boundary layer height of about $0.6u_*/f$. We will take the model results of Deardorff (1972), Wyngaard et al. (1974) and Mason and Thomson (1986) as representative for the truly neutral ABL, and with these data we will compare our model results for the neutral ABL (section 3b1). As noticed already by Lettau (1950) and Nicholls (1985) it will be difficult to observe this truly neutral boundary layer in the atmosphere. The differences between the experimental results in the near-neutral ABL and the theoretical solution of the truly neutral ABL reflects the presence of a weakly stable layer above the mixed layer in the observations. For instance, the potential temperature profiles presented by Nicholls (1982) show a neutral profile up to a certain height with a stable potential temperature gradient of 1 to 2 K km^{-1} aloft.

In order to reproduce the "Leipzig Wind Profile" and the observations of Nicholls (1985) we have initialized the model with a stable potential temperature gradient of 1 and 2 K km^{-1}, respectively. The model was run for 24 hours while the surface heat flux was kept zero. At the end of the simulation a neutral layer had formed up to a certain height, with a stable lapse rate above. In section 3b2 we have compared these model results with the observational data of Lettau (1950) and Nicholls (1982, 1985). Before using our model under conditions with arbitrary stratification we will first compare our model results with the model results of Wyngaard (1975) and Brost and Wyngaard (1978, 1979) on the stable ABL (section 3a).

2. Model description

In this section we will discuss the model, which is used in a one-dimensional horizontally homogeneous version. The ensemble-averaged equations for the horizontal velocities and the potential temperature are given in section 2a. In these equations the vertical velocity has been set equal to zero. The $E-\epsilon$ model is introduced in section 2a1, in which a full discussion is given on the equation for the viscous dissipation (ϵ).

In section 2a2 we show how we have determined the constants in the turbulence closure. Finally, section 2b gives details on the boundary conditions used.

a. Governing equations

We consider a horizontally homogeneous flow, with the mean velocities (u, v) in the (x, y) direction and mean potential temperature θ governed by

$$\frac{\partial u}{\partial t} = -\frac{\partial \overline{u'w'}}{\partial z} + f(v - v_g), \tag{1a}$$

$$\frac{\partial v}{\partial t} = -\frac{\partial \overline{v'w'}}{\partial z} - f(u - u_g), \tag{1b}$$

$$\frac{\partial \theta}{\partial t} = -\frac{\partial \overline{w'\theta'}}{\partial z}. \tag{1c}$$

Here f is the Coriolis parameter, (u_g, v_g) the geostrophic wind in the (x, y) direction, and primed quantities denote turbulent fluctuations.

1) TURBULENCE CLOSURE

For the fluxes in Eq. (1) a gradient transfer approach is taken:

$$-\overline{u'w'} = K\frac{\partial u}{\partial z}, \tag{2a}$$

$$-\overline{v'w'} = K\frac{\partial v}{\partial z}, \tag{2b}$$

$$-\overline{w'\theta'} = K\frac{\partial \theta}{\partial z}. \tag{2c}$$

The closure problem is now shifted to determining the distribution of K. In this paper the exchange coefficient will be determined from the turbulent kinetic energy (E) and the viscous dissipation of turbulent kinetic energy (ϵ) as

$$K = c_\mu E^2/\epsilon \tag{3}$$

in which c_μ is a constant and both E and ϵ have to be

determined from their modeled equations. This turbulence closure is called the $E - \epsilon$ model.

The turbulent kinetic energy equation in one-dimensional form reads

$$\frac{\partial E}{\partial t} = \underbrace{-\overline{u'w'}\frac{\partial u}{\partial z} - \overline{v'w'}\frac{\partial v}{\partial z}}_{S} + \underbrace{\frac{g}{\theta_0}\overline{w'\theta'}}_{B} \underbrace{- \frac{\partial}{\partial z}\left(\overline{w'E'} + \frac{\overline{p'w'}}{\rho_0}\right)}_{T} - \underbrace{\epsilon}_{D}, \quad (4)$$

in which p is the pressure. The momentum flux and heat flux are closed by (2). The transport term in (4) is modeled as

$$-\left(\overline{w'E'} + \frac{\overline{p'w'}}{\rho_0}\right) = \frac{K}{\sigma_E}\frac{\partial E}{\partial z}, \quad (5)$$

in which σ_E is the turbulent Prandtl number for E.

The equation for ϵ is the most difficult to model. At high Reynolds number ϵ is equal to the kinematic viscosity times the mean-square vorticity fluctuations ($\overline{\omega_i'\omega_i'}$). Tennekes and Lumley (1972) show that at sufficiently high Reynolds numbers there is a balance between the generation of $\overline{\omega_i'\omega_i'}$ due to vortex stretching and the destruction of $\overline{\omega_i'\omega_i'}$ due to viscosity. The next terms in order are the rate of change, advection and turbulent transport of $\overline{\omega_i'\omega_i'}$. Other terms are of higher order and can be neglected.

The transport term in the ϵ-equation is modeled with the gradient assumption

$$-\overline{w'\epsilon'} = \frac{K}{\sigma_\epsilon}\frac{\partial \epsilon}{\partial z}, \quad (6)$$

in which σ_ϵ is the turbulent Prandtl number for ϵ. The generation and destruction in the ϵ-equation, which are the biggest terms, are the most difficult to model. However, as pointed out by Tennekes (1985), the spectral energy flux and therefore the dissipation rate is determined by the dynamics at the large-scale end of the spectrum. Thus, ϵ is determined by the terms which produce the TKE. This idea was also used by Lumley and Khajeh-Nouri (1974) to parameterize the generation and destruction terms in the ϵ-equation. Using their parameterization for the generation and destruction we get

$$\frac{\partial \epsilon}{\partial t} = -\frac{\partial}{\partial z}\overline{w'\epsilon'} + \frac{\epsilon}{E}(c_{1\epsilon}P - c_{2\epsilon}\epsilon), \quad (7)$$

in which P is the production of turbulent kinetic energy. In their second-order closure study Wyngaard et al. (1974) have applied (7) with success to the neutral and convective ABL by using for P

$$P = S + B, \quad \text{with} \quad c_{1\epsilon} = 1.5, \quad c_{2\epsilon} = 2.0, \quad (8a)$$

so that the term between brackets in (7) becomes

$$(c_{1\epsilon}P - c_{2\epsilon}\epsilon) = (1.5S + 1.5B - 2\epsilon). \quad (8b)$$

This will be called the standard ϵ-equation. Moreover, Wyngaard (1975) applied the ϵ-equation to the stable boundary layer; in that case he used

$$(c_{1\epsilon}P - c_{2\epsilon}\epsilon) = (1.75S + 0.5B + 1\frac{B^2}{\epsilon} - 2\epsilon). \quad (9)$$

In order to clarify the difference between (8) and (9) we have drawn the terms $(1.5B/\epsilon)$ and $(0.5B/\epsilon + B^2/\epsilon^2)$ as a function of B/ϵ in Fig. 1. Thus, if $B > 0$ the expressions are almost equivalent. However, for $B < 0$ the influence of the buoyancy term (B) on the production term (P) in (9) is small. Therefore, in the range of interest ($-0.25 < B/\epsilon < 1$), the quadratic form in B [Eq. (9)] can be approximated by max(0, B). This was already used by Duynkerke and Driedonks (1987). The buoyancy term is thus only included in P if it is really a production term and is set to zero if it is a destruction term.

From the results on the neutral ABL in section 3b we will see that the transport term also can be an important source term in the turbulent kinetic energy budget (Mason and Thomson, 1986). Moreover, from the results in section 3b1 and the results of Detering and Etling (1985) it is clear that (9) does not give the correct results for the neutral ABL. From this we concluded that the transport term (T) should also be included in P in (7). We did this analogous to the buoyancy term. As a result P reads

$$P = S + \max(0, B) + \max(0, T). \quad (10)$$

In the next section we will evaluate the values of the constants used in the turbulence closure.

2) EVALUATION OF CONSTANTS

In the neutral surface layer, the two largest terms in (4) are S and D. Thus $S = D$ is a reasonable assumption which with (2) and (3) gives $c_\mu = (u_*^2/E)^2$. Panofsky and Dutton (1984) give a list of estimates of the ratio

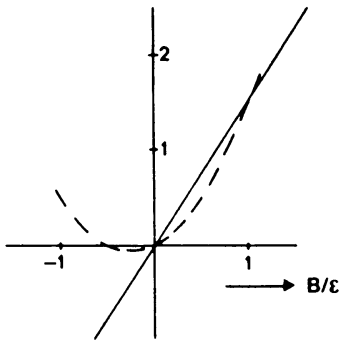

FIG. 1. The terms $(1.5B/\epsilon)$ (solid line) and $(0.5B/\epsilon + B^2/\epsilon^2)$ (dashed line) as a function of B/ϵ.

of standard deviations of velocity components to friction velocity, with an average of $E = 5.5u_*^2$; this gives $c_\mu = 0.033$.

In the equation for ϵ (7) three unknown constants appear: $c_{1\epsilon}$, $c_{2\epsilon}$ and σ_ϵ. The constant $c_{2\epsilon}$ is, as usual, based on the decay of grid turbulence. For the decay of grid turbulence Eqs. (4) and (7) reduce to

$$u\frac{\partial E}{\partial x} = -\epsilon, \quad u\frac{\partial \epsilon}{\partial x} = -c_{2\epsilon}\frac{\epsilon^2}{E}. \tag{11}$$

The exact solution of (11) is (Reynolds, 1974)

$$E/E_0 = \left(1 + \frac{x}{a}\right)^{-n}, \quad \frac{\epsilon}{\epsilon_0} = \left(1 + \frac{x}{a}\right)^{-(n+1)}, \tag{12}$$

with

$$n = \frac{1}{c_{2\epsilon} - 1}, \quad a = \frac{nuE_0}{\epsilon_0},$$

in which the index 0 indicates the value for $x = 0$. Measurements on the decay of neutral isotropic turbulence give values for n from 1 up to 1.4 (Monin and Yaglom, 1975). Reynolds (1974) proposed a simple model for the energy spectrum ($E(k)$) during the decay of isotropic turbulence. This model is only likely to work when the large-scale structure is devoid of any scales, i.e., when the large-scale energy is uniformly distributed over all wave vectors. This means that the spectrum tensor $\phi_{ii}(\mathbf{k})$ is the same at all $\mathbf{k}$ low wavenumbers and the three-dimensional energy spectrum function $E(k)$ is proportional to k^2. On this basis Reynolds (1974) got $n = 6/5$. This is a good average of all the experimental results (Monin and Yaglom, 1975). Therefore, we take $n = 6/5$ to fix $c_{2\epsilon}$, which gives with (12) $c_{2\epsilon} = 1.83$.

Next, we want to determine $c_{1\epsilon}$. Harris et al. (1977) and Tavoularis and Corrsin (1981) have studied a nearly homogeneous turbulent shear flow. A shear generator in a wind tunnel was used to create both turbulence and a uniform velocity gradient. The shear generator consisted of parallel channels of equal width with adjustable internal resistances. If no shear was present the turbulence would decay as described above. However, when a shear was applied there was continuous production of turbulent kinetic energy. This is described by Eqs. (4) and (7) as

$$u\frac{\partial E}{\partial x} = S - \epsilon, \quad u\frac{\partial \epsilon}{\partial x} = (c_{1\epsilon}S - c_{2\epsilon}\epsilon)\frac{\epsilon}{E}, \tag{13}$$

in which

$$S = c_\mu \frac{E^2}{\epsilon}\left(\frac{\partial u}{\partial z}\right)^2$$

and here $\partial u/\partial z$ is a constant. The full solution of (13) is rather complicated (Duynkerke and Nieuwstadt, 1988). Therefore, we will only give the solution for the ratio of E and ϵ:

$$e = E/\epsilon = \frac{\beta}{\alpha}\left\{\frac{c_0 e^{2\alpha\beta x} - 1}{1 + c_0 e^{2\alpha\beta x}}\right\}, \tag{14}$$

with

$$\beta^2 = \frac{c_{2\epsilon} - 1}{u}, \quad \alpha^2 = \frac{\hat{c}}{u}(c_{1\epsilon} - 1),$$

$$\hat{c} = c_\mu\left(\frac{\partial u}{\partial z}\right)^2, \quad c_0 = \frac{\beta/\alpha + e_0}{\beta/\alpha - e_0}.$$

For e_0 the value of e at $x = 0$. In the experimental results of Harris et al. (1977) and Tavoularis and Corrsin (1981) c_0 is large (~ 16), so that (14) reduces to

$$E/\epsilon = \beta/\alpha,$$

$$E/E_0 = e^{\gamma x}, \quad \epsilon/\epsilon_0 = e^{\gamma x}, \tag{15}$$

with

$$\gamma = \frac{\epsilon}{uE}\left(\frac{S}{\epsilon} - 1\right),$$

$$\frac{S}{\epsilon} = \frac{c_{2\epsilon} - 1}{c_{1\epsilon} - 1}.$$

This exponential increase (15) of E has also been found by Tavoularis (1985) using totally different arguments. From the experimental data of Harris et al. (1977) and Tavoularis and Corrsin (1981) we get that S/ϵ is a constant (independent of x) and equals 1.8. We had found already that $c_{2\epsilon} = 1.83$; this gives with (15) $c_{1\epsilon} = 1.46$.

Another way to tune the value of $c_{1\epsilon}$ is in a stably stratified flow in which the Richardson number has reached its critical value (Ri_c). In that case the transport terms and the rate of change in (4) and (7) can be neglected and thus reduce to

$$S + B - \epsilon = 0, \quad c_{1\epsilon}S - c_{2\epsilon}\epsilon = 0, \tag{16a}$$

which gives

$$c_{1\epsilon} = c_{2\epsilon}(1 - \mathrm{Ri}). \tag{16b}$$

From (16b) it is clear that the constants $c_{1\epsilon}$ and $c_{2\epsilon}$ determine the value of a critical Richardson number. With our values for $c_{1\epsilon}$ and $c_{2\epsilon}$ this gives $\mathrm{Ri}_c = 0.2$.

Finally the constant σ_ϵ in (6) has to be determined. In the neutral surface layer the transport term in the turbulent kinetic energy equation (4) is negligible, so that shear production equals viscous dissipation. Using this ($S = \epsilon$) in the equation for ϵ (7), in which the transport term is not negligible, one finds (Rodi, 1980)

$$\sigma_\epsilon = \frac{\kappa^2}{c_\mu^{1/2}(c_{2\epsilon} - c_{1\epsilon})}. \tag{17}$$

With the von Kármán constant $\kappa = 0.4$ this gives $\sigma_\epsilon = 2.38$. The only constant which is not fixed yet is σ_E, in (5). We take it as 1.

b. *Boundary conditions*

In order to calculate the turbulent fluxes near the surface we use the Monin–Obukhov similarity theory to relate the fluxes to the vertical gradients in the surface layer. For the similarity functions (ϕ) we took the func-

tion proposed by Dyer (1974). In the stable region the similarity function for momentum and heat are the same:

$$\phi = 1 + 5\frac{z}{L}. \tag{18}$$

The solution of the turbulent kinetic energy equation and the ϵ-equation requires specification of E and ϵ or their fluxes near the surface. We prescribed the values of E and ϵ at the first level above the surface (André et al., 1978):

$$E = c_\mu^{-1/2}u_*^2,$$
$$\epsilon = u_*^3\left\{\frac{\phi}{\kappa z} - \frac{1}{\kappa L}\right\}. \tag{19}$$

The surface boundary condition for ϵ is based on the fact that in the atmospheric boundary layer viscous dissipation balances shear production and buoyancy.

3. Results

a. *The stable ABL: Constant cooling rate results*

In this section we will study the quasi-stationary stable boundary layer. Here quasi-stationary means that the potential temperature is allowed to decrease with time but that other characteristic parameters (u_*, θ_*, L, etc.) are independent of time. This also means that the profiles of mean variables, fluxes and other turbulent quantities, made dimensionless with appropriate scaling parameters, should be independent with time.

Wyngaard (1975) integrated a full second-order turbulence model and demonstrated that the stable ABL could approach a steady state after 2–8 h, depending on the specified constant cooling rate at 1 m. He found that the boundary layer height (h) obeyed Zilitinkevich's similarity relation

$$h = d\left(\frac{u_* L}{f}\right)^{1/2}, \tag{20}$$

with $d = 0.22$. This low value of $d = 0.22$ compared to the more usual value of 0.4 (Garratt, 1982) is due to the constants specified in the ϵ-equation. The constants used by Wyngaard (1975) are given in Eq. (9). From the discussion given in section 2a2 it follows that these values specify a critical Richardson number of 1/8; this can also be seen in his Fig. 7. Nieuwstadt (1983) derived a formula for d as function of the von Kármán constant and the critical Richardson number

$$d^2 = (3)^{1/2}\kappa\,\mathrm{Ri}_c. \tag{21}$$

From (21) it can be seen that the too low value for the critical Richardson number (Wyngaard, 1975, used $\mathrm{Ri}_c = 1/8$) gives a too low value for d.

Brost and Wyngaard (1978, 1979) simplified the second-order closure model of Wyngaard (1975) considerably by neglecting time derivatives, Coriolis terms and triple correlations. Instead of using an equation for ϵ they parameterize ϵ as $E^{3/2}/l$, where they specify the turbulent length scale l. As noted by Fitzjarrald (1979) these simplified equations can be rewritten in the form of an eddy-exchange coefficient formulation. Brost and Wyngaard (1979) found that d varied from 0.37 to 0.51 for cooling rates from 0.2 to 6 K h^{-1}.

We generated four cases with our model by applying cooling rates of 0.2, 0.5, 1 and 2 K h^{-1} at the surface. This is somewhat different from Wyngaard (1975) and Brost and Wyngaard (1978, 1979) because they have applied the cooling rate at $z = 1$ m. As in Brost and Wyngaard (1979) we took $G = 10$ m s^{-1} and $z_0 = 0.01$ m. In Table 1 we compare the quasi-steady state results after 10 h for the four different cooling rates with the results of Brost and Wyngaard (1979).

In this study, as in Wyngaard (1975) and Brost and Wyngaard (1979), h is taken as the height at which the stress is 5% of its surface value. This definition of h is used because it is difficult to determine h from the potential temperature profile. From this definition of h we find that d varies between 0.43 and 0.45 and is thus nearly constant. Moreover our model results show nearly the same values of α (the angle between the surface wind and the geostrophic wind) and h/L as those of Brost and Wyngaard (1979). Because Brost and Wyngaard (1979) have used the flux-profile relations of Businger et al. (1971) and we have used the flux-profile relations of Dyer (1974) their values of u_*

TABLE 1. For 10 h after transition and different constant cooling rates, boundary layer depth h, Monin–Obukhov length L, friction velocity u_*, surface vertical potential temperature heat flux Q_0, cross isobar angle α, stability parameter h/L and the constant d in Zilitinkevich's Eq. (20).

	0.2 K h^{-1}		0.5 K h^{-1}		1 K h^{-1}		2 K h^{-1}	
	Present	BW (1979)	Present	BW (1979)	Present	BW (1979)	Present	BW (1979)
h	329	194	182	127	115	86	71	55
L	195	120	77	48	36	23	16	9.9
u_*	0.31	0.23	0.27	0.20	0.23	0.176	0.19	0.147
Q_0	−0.0112	−0.0084	−0.0190	−0.0139	−0.0251	−0.0189	−0.0305	−0.024
α	27	29	33	34	38	38	43	42
h/L	1.7	1.6	2.4	2.6	3.2	3.7	4.4	5.6
d	0.45	0.37	0.43	0.41	0.43	0.43	0.44	0.46

and Q_0 are approximately 25% lower than ours. As a result both the values of L and h we find are much higher. However, the Zilitinkevich relation (20) still holds very well, with an average value for d of 0.44.

Figure 2 shows the wind spiral, made dimensionless by u_*, after 10 h for a cooling rate of 1 K h^{-1}. In Fig. 3 we have plotted the temperature profiles for the four different cooling rates as a function of height. The temperature differences, made dimensionless with the temperature difference at the surface, as a function of z/h show that for the higher cooling rates the cooling is penetrating up to larger z/h values, due to the lower values of h/L. The temperature profile (1 K h^{-1}) presented by Brost and Wyngaard (1978) shows a very similar structure.

Next we will discuss some turbulence quantities. Figure 4 shows the turbulent kinetic energy as a function of height. This profile is similar to the profile observed in the neutral ABL (Fig. 10). In Fig. 5a we have compared our stress profiles with the stress profiles of Wyngaard (1975). It is not clear why the stresses of Wyngaard (1975) do not sum to 5% at $z = h$, because this is his definition of the boundary layer h. The heat flux profiles (Fig. 5b) show a slight curvature at the top of the boundary layer, analogous to the results of Brost and Wyngaard (1978), with a maximum cooling rate at the ground.

Brost and Wyngaard (1978) found that the profile of the eddy diffusivity for momentum is well represented by

$$\frac{K_m}{\kappa u_* h} = \frac{\frac{z}{h}\left(1 - \frac{z}{h}\right)^{1.5}}{1 + 4.7\left(\frac{z}{h}\right)\left(\frac{h}{L}\right)}, \qquad (22)$$

whereas the ratio K_h/K_m averages about 1.2.

In Fig. 6 we have compared (22) with our model results which illustrates a good agreement between both results. In Fig. 7 we have shown the profile of the Richardson number, which shows that the Richardson number equals its critical value throughout almost the whole boundary layer; for $z/h > 1$ the Richardson number exceeds its critical value and near the surface $\mathrm{Ri} < \mathrm{Ri}_c$ due to the high shear production. This kind of behavior was already observed by Nieuwstadt (1983, 1984) and Garratt (1982).

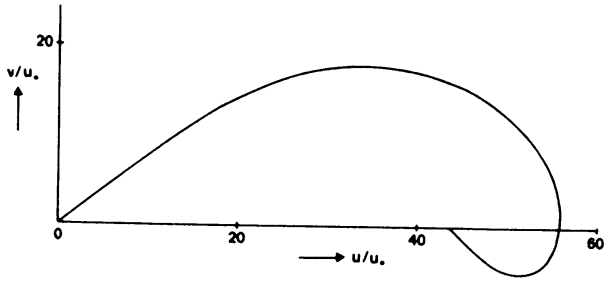

FIG. 2. The dimensionless wind spiral 10 h after transition, for a cooling rate of 1 K h^{-1}.

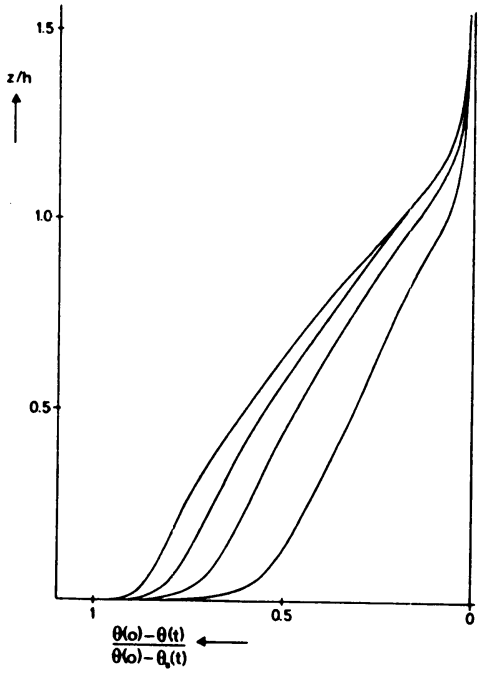

FIG. 3. For 10 h after transition the dimensionless temperature rofile as a function of z/h, from right to left, for a cooling rate of 0.2, 0.5, 1 and 2 K h^{-1}, respectively.

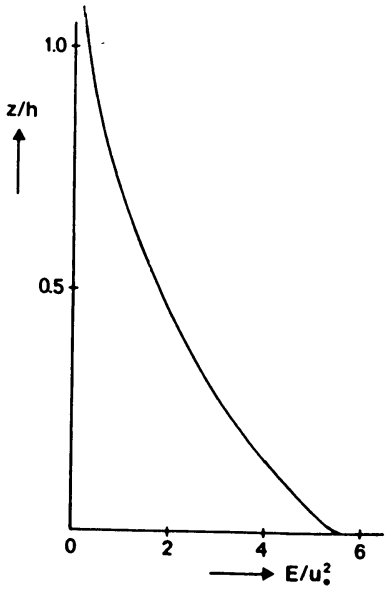

FIG. 4. The turbulent kinetic energy (E) as a function of height.

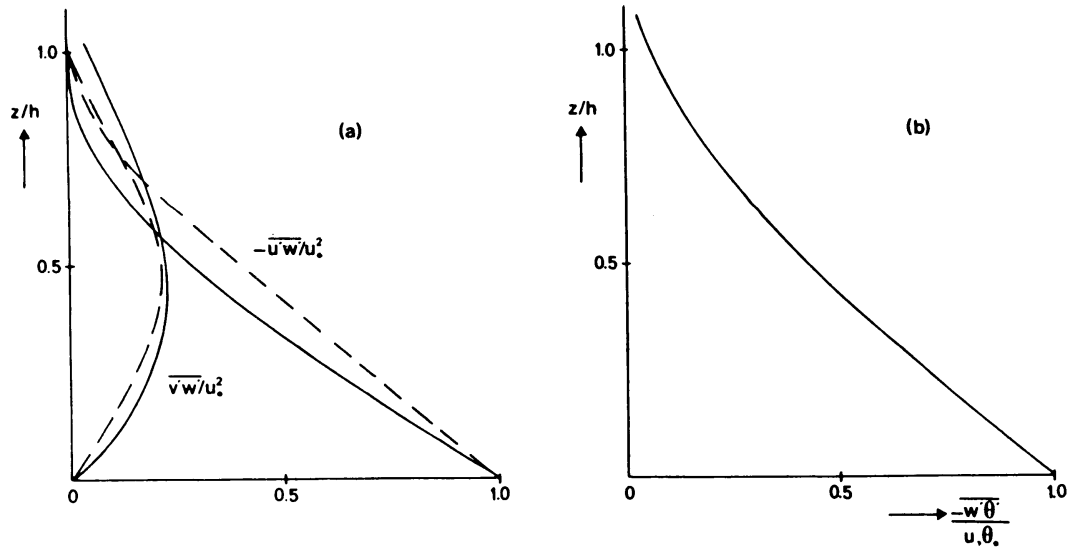

FIG. 5. The profiles of the (a) momentum flux and (b) heat flux as a function of height: our results (solid line), results of Wyngaard (1975) (dashed line).

We can conclude that with our $E - \epsilon$ model we can reproduce the results of Wyngaard (1975) and Brost and Wyngaard (1978, 1979) very well. Essential in obtaining these results is the critical Richardson behavior introduced in the ϵ-equation. This could be reached by including a term max(0, B) instead of B in the production term. Although something similar was already done by Wyngaard (1975), using a quadratic function

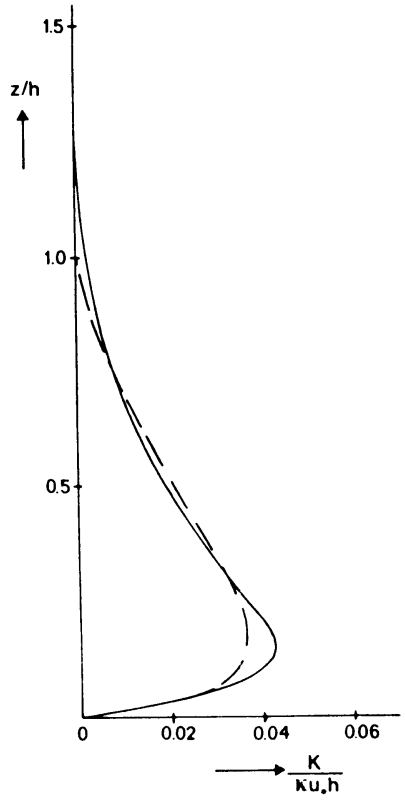

FIG. 6. Comparison of Brost and Wyngaard's (1978) (dashed) eddy diffusivity and our model results (solid).

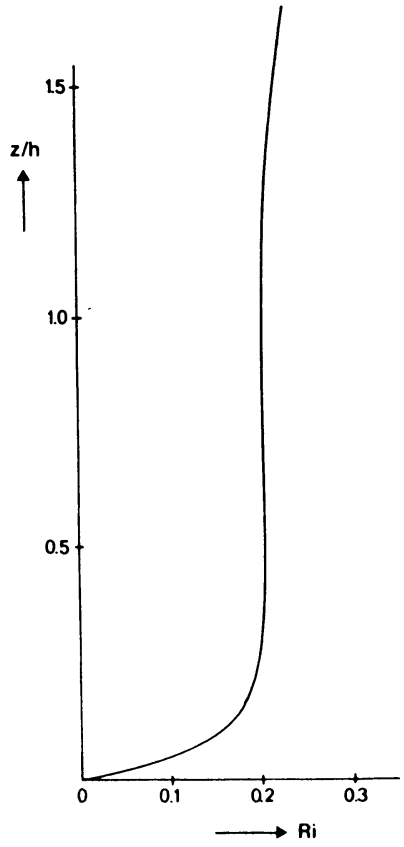

FIG. 7. Variation of the Richardson number with height.

in B (see section 2a), he did not explain the necessity of this clearly.

b. The neutral ABL

In the neutral ABL the heat flux is, by definition, identical to zero. In a model this condition can be easily satisfied. However, in this section we will demonstrate that in the atmosphere a boundary layer with neutral stratification can hardly ever be observed. Therefore, observational data presented as representative for the neutral ABL (Nicholls, 1985; "Leipzig Wind Profile") are in fact influenced by (a slightly stable) stratification.

In our model we have used a prognostic equation for the viscous dissipation ϵ, which is analogous to a prognostic equation for the turbulent length scale l. However, it is also possible to diagnose a length scale. For instance, based on observations Blackadar (1962) proposed a length scale as

$$l = 2.7 \times 10^{-4} G/f, \tag{23}$$

which is similar to the length scale used by Detering and Etling (1985a):

$$l = 6.3 \times 10^{-3} u_*/f. \tag{24}$$

However, prescribing a length scale with (23) or (24) means that the boundary layer height is determined by the value of the constant.

In order to circumvent this problem Detering and Etling (1985a) used an $E - \epsilon$ model for the neutral ABL. They modified the constant $c_{2\epsilon}$ [Eq. (7)] in such a way that the model results fit the "Leipzig Wind Profile". Detering and Etling (1985a) did this by making $c_{2\epsilon}$ a function of lf/u_*, with l proportional to $E^{3/2}/\epsilon$. It is clear that this modification is more or less the same as diagnosing a length scale by (24) and therefore, there is no real advantage in using the ϵ-equation above a diagnostic length scale (24).

In this section we will present model results for the truly neutral and near-neutral ABL over sea (Nicholls, 1985). We have taken $z_0 = 2 \times 10^{-4}$ m and $G = 10$ m s^{-1} and all the results shown are for a simulation time of 24 h. In section 3b1 we will compare our model results with the large-eddy simulations by Deardorff (1972) and Mason and Thomson (1986) and the higher-order closure study by Wyngaard et al. (1974) of the neutral ABL. In section 3b2 we will initialize the model with a stable potential temperature gradient of 1 and 2 K km^{-1} and set the surface heat flux to zero. The resulting profiles will be compared with the observational data of Nicholls (1982, 1985) and the "Leipzig Wind Profile" (Mildner, 1932; Lettau, 1950).

1) COMPARISON WITH MODEL RESULTS ON THE NEUTRAL ABL

Application of the standard $E - \epsilon$ model [Eq. (7)] to the neutral ABL gave the same unrealistic results as Detering and Etling (1985a) found. The eddy-exchange coefficient and the length scale increase linearly with height up to the model top, as shown in Figs. 8 and 9. In Fig. 8 we have also plotted the K-profiles of Wyngaard et al. (1974). We see that in the upper part of the boundary layer our eddy-exchange coefficients are much higher than those of Wyngaard et al. (1974). As a result, the boundary layer height extends up to the model top, which can be seen from the turbulent kinetic energy profile in Fig. 10. This boundary layer height is too high compared with the model results of Deardorff (1972), Mason and Thomson (1986) and Wyngaard et al. (1974), which are also shown in Fig. 10.

This discrepancy between our model results and the other model results is due to the fact that at the top of the neutral boundary layer the transport term is an important source term in the turbulent kinetic energy equation, whereas in the standard ϵ-equation the transport term as a source term is neglected. The fact that the transport term is important in the upper part of the neutral boundary layer can be seen from the TKE budget of the large-eddy simulation of Mason and Thomson (1986), which is shown in Fig. 11. In almost the whole neutral ABL the shear production and viscous dissipation are an order of magnitude larger than the transport term, except above $\sim 0.3 u_*/f$ where the transport term assumes increasing importance. This gave us the idea to include the transport of TKE as a production term in the ϵ-equation (7). Analogous to the buoyancy term we only included it when the transport term was positive (10). However, from the simulation of the neutral and stable boundary layer no conclusion could be reached about what to do in regions in which the transport term is negative, because

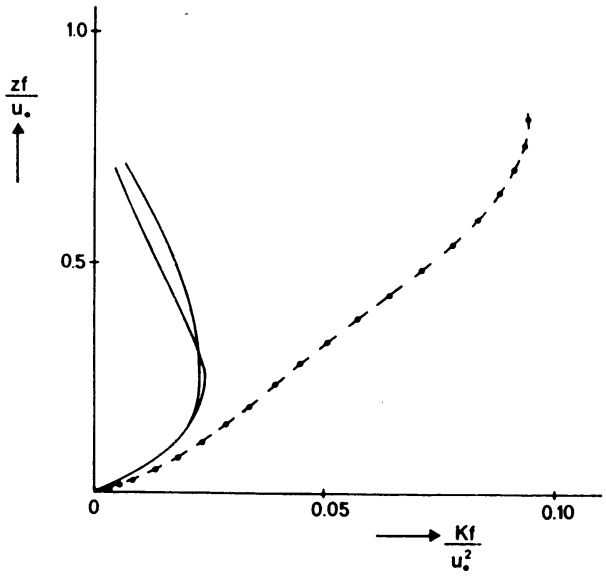

FIG. 8. Vertical distribution of eddy viscosity in the neutral atmospheric boundary layer for standard $E - \epsilon$ model (dashed) and the results of Wyngaard et al. (1974) (solid).

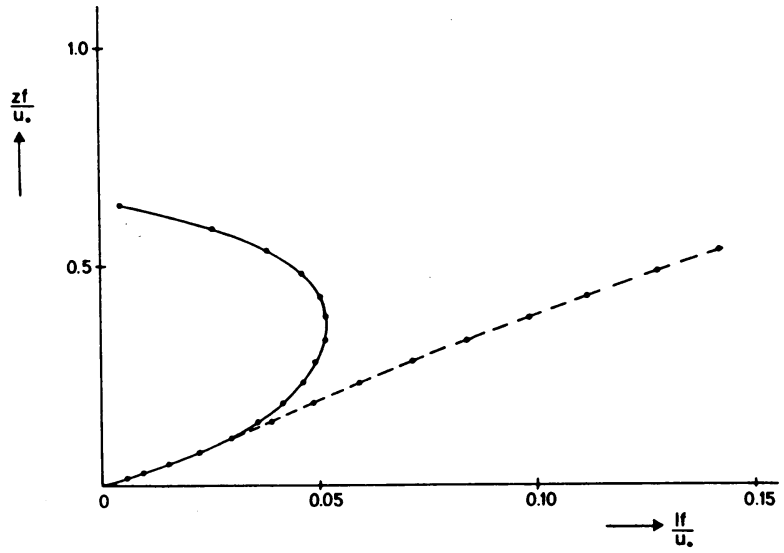

FIG. 9. The length scale as a function of height for the standard (dashed) and modified (solid) $E - \epsilon$ model.

in those regions the shear production and viscous dissipation were an order of magnitude larger.

We will now discuss the results of the modified $E - \epsilon$ model in which the transport term (T) has been included in the production term (P) in the ϵ-equation (7). In Fig. 10 we have compared the TKE profile with the other model results, the observations of Nicholls (1985) and measurements on a boundary layer in a wind tunnel (Hinze, 1975). Extensive measurements on turbulence quantities in the boundary layer of a wind tunnel have been made, many of which have been summarized by Hinze (1975). Because we expect some similarity between turbulence quantities in a wind tunnel boundary layer and the ABL, we have made some comparison, especially, in the case of quantities which cannot be so easily measured in the atmosphere. In order to do so we have set the boundary layer height in the wind tunnel equal to $0.5u_*/f$. We see that our turbulent kinetic energy profile is nearly identical to that of Deardorff (1972), Wyngaard et al. (1974) and

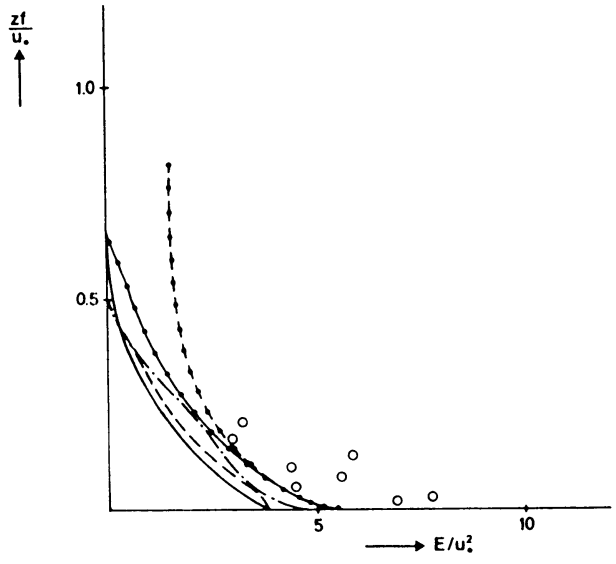

FIG. 10. The vertical profile of turbulent kinetic energy, neutral case: observations of Nicholls (1985) (O); standard $E - \epsilon$ (dashed with dot); modified $E - \epsilon$ (solid with dot); Deardorff (1972) (dashed); Wyngaard et al. (1974) (solid); Hinze (1975) (dot-dashed).

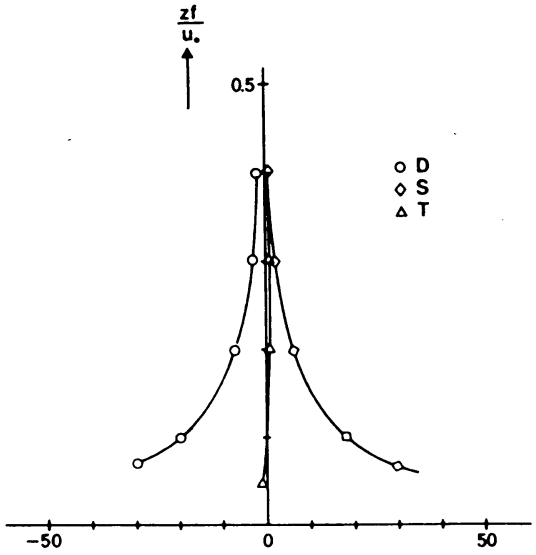

FIG. 11. Balance of terms in the turbulent kinetic energy equation for the neutral boundary layer (Mason and Thomson, 1986: B10 case).

the laboratory data (Hinze, 1975), whereas the values observed by Nicholls (1985) are somewhat higher. The higher values of the turbulent kinetic energy in the atmosphere might be a result of the fact that there is a significant contribution from larger scales ($\geq u_*/f$) as can be seen in the measured velocity spectra in Nicholls (1985).

In Fig. 12 we have shown the dimensionless wind profiles as a function of zf/u_*. We see that our results compare rather well with the profiles of Wyngaard et al. (1974). The profiles of Deardorff (1972) are somewhat different due to the too low model top used during his run ($z_i = 0.45u_*/f$). Here, we see that there is a big difference between the model results and observational data. As mentioned already, this is due to the fact that the observations do not represent a neutral ABL as can be seen from the observed temperature profiles of Nicholls (1982). This will be discussed further in the next section. In Fig. 13 we have compared the stress profiles with the observations of Nicholls (1985). We see that especially the resemblance in $\overline{v'w'}$ is very poor.

In Fig. 14 we have compared the computed eddy-exchange coefficient profiles with the profiles of Deardorff (1972), Wyngaard et al. (1974) and the laboratory data (Hinze, 1975). We see that the values agree rather well and moreover, the maxima show up at the same height. In Fig. 15 we have compared the computed TKE budget with the values measured by Nicholls (1985). We see that the shear production (S) and dissipation agree rather well, but the measured transport term (T) is an order of magnitude larger than the computed transport term. If we compare the TKE budget calculated with the $E - \epsilon$ model with the TKE budget of Mason and Thomson (1986) we see that the agreement is excellent. Moreover, from the TKE budget it is clear why it will be hard to observe a neutral boundary layer in the atmosphere. At about $0.25u_*/f$ the production of turbulent kinetic energy becomes small and therefore a weak stable stratification can make the turbulence die out. This will be discussed in the next section.

Before turning to the observations we will test the Rossby number similarity (Tennekes, 1973) of this model. According to this theory, the geostrophic drag coefficient (u_*/G) and the cross-isobar angle (α) should be functions of the surface Rossby number ($\mathrm{Ro} = G/fz_0$) only. We varied the Rossby number by varying z_0 and have plotted u_*/G and α as a function of Ro in Fig. 16. We have also shown the results of Mason and Thomson (1986) (B10 case) and Deardorff (1972). The results of Wyngaard et al. (1974) (for $\kappa = 0.4$) are not shown because they are nearly identical to those of Mason and Thomson (1986). If we compare the computed u_*/G and α (Fig. 16) with observational data (Tennekes, 1973) we see that the values of u_*/G agree rather well whereas the observed values of α are somewhat larger. We believe this is due to the sensitivity of the cross-isobar angle on stability and in the observational data some stability will be always important.

2) Comparison with observations on the nearly neutral ABL

In section 3b1 we have shown that there is a difference between observational data on the near-neutral

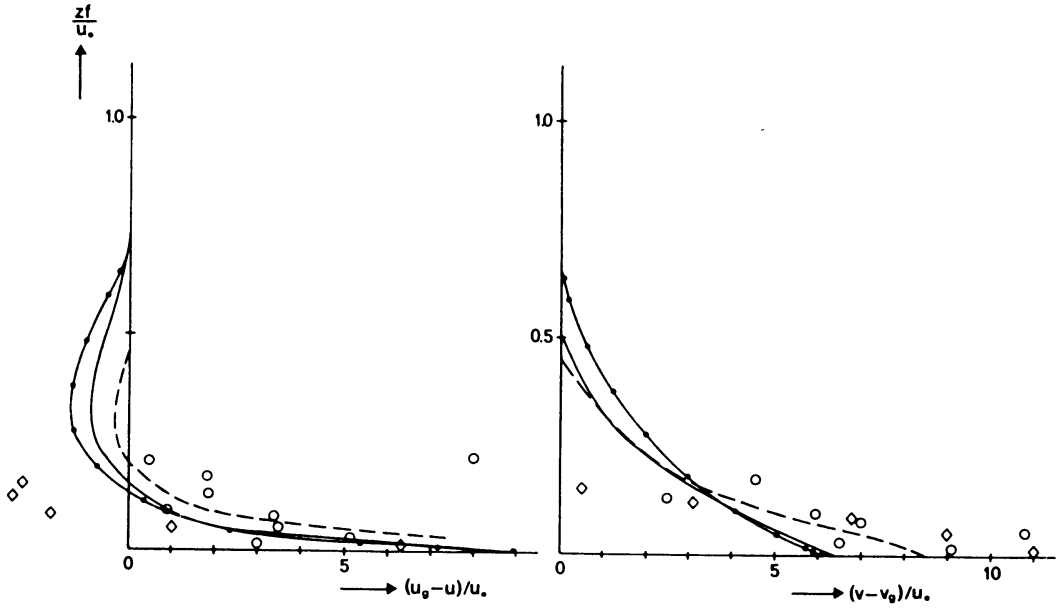

FIG. 12. Nondimensional wind defect profiles: Nicholls (1985) (O); Lettau (1950) (◇); modified $E - \epsilon$ (solid with dot); Deardorff (1972) (dashed); Wyngaard et al. (1974) (solid).

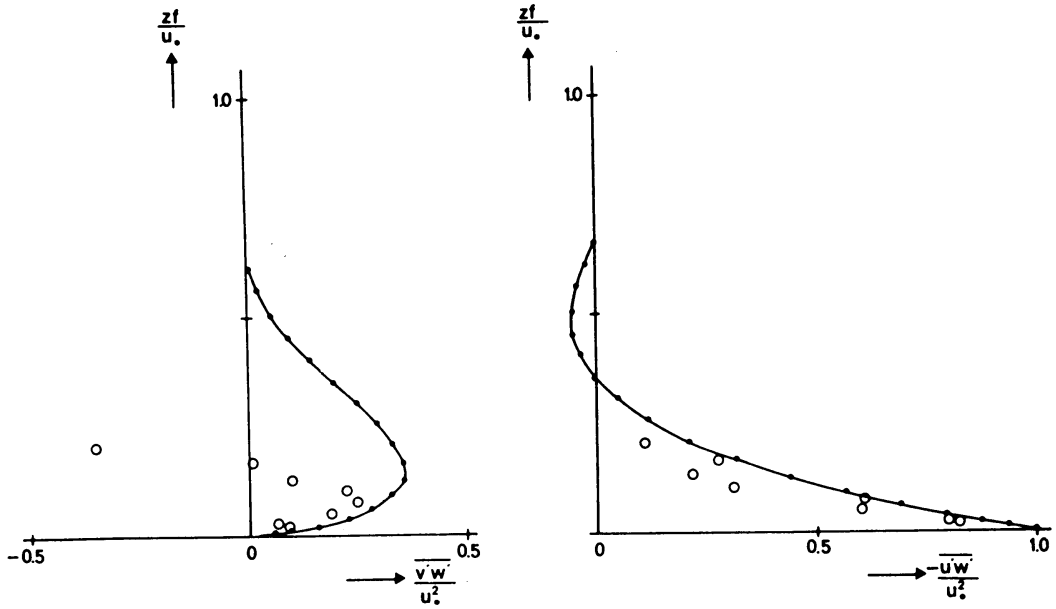

FIG. 13. Nondimensional momentum flux profiles: Nicholls (1985) (open circles); modified $E - \epsilon$ (solid line).

ABL and model results of the truly neutral ABL. Especially, there is a big difference between observed ($h \sim 0.2u_*/f$) and calculated ($h \sim 0.6u_*/f$) boundary layer height. This discrepancy can be directly explained by the TKE budget of the neutral ABL, as shown in Fig. 15. Above $\sim 0.25u_*/f$ the production term becomes small and in the real atmosphere a small stability will prevent the layer from being turbulent. The measured potential temperature profiles (Nicholls, 1982, 1985) show a neutral layer up to $z \sim 0.2u_*/f$ with a slightly stable region above (potential temperature gradient of 1 to 3 K km^{-1}). Thus the neutral boundary layer is inhibited to grow higher by a stable lapse rate aloft and this we will simulate in this section.

The model was initialized with a stable lapse rate of 1 and 2 K km^{-1}, respectively, as shown in Fig. 17. We have run the model for 24 hours during which the surface heat flux was set equal to zero. The final potential

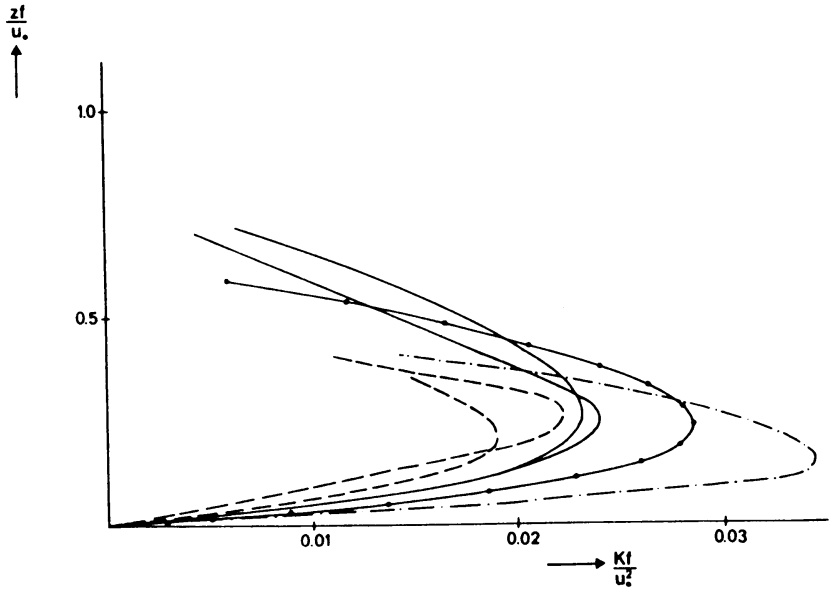

FIG. 14. Vertical distribution of eddy-exchange coefficient in the neutral boundary layer: Hinze (1975) (dot-dashed); modified $E - \epsilon$ (solid with dot); Deardorff (1972) (dashed); Wyngaard et al. (1974) (solid).

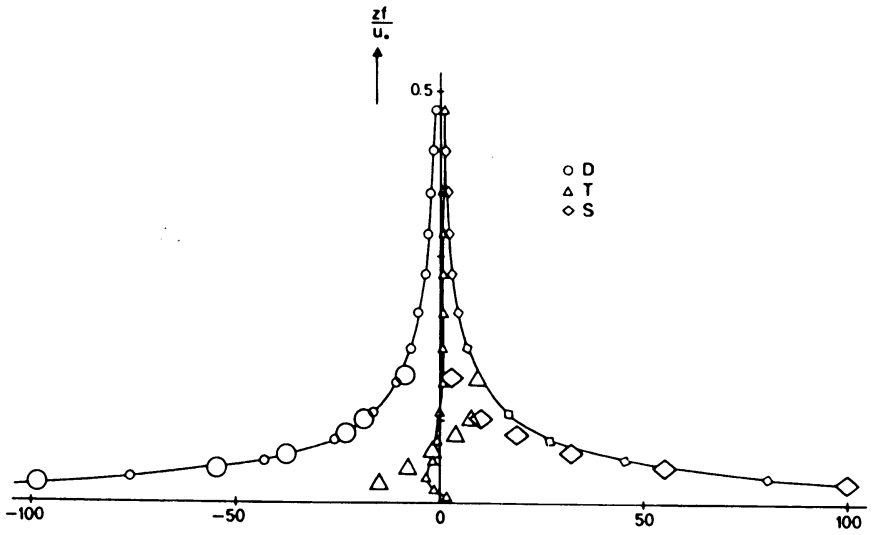

FIG. 15. Vertical profiles of the terms in the turbulent kinetic energy budget; large symbols, observational data of Nicholls (1985); small symbols connected with lines, modified $E - \epsilon$ model.

temperature profiles show a neutral layer up to $0.16u_*/f$ and $0.12u_*/f$, respectively. Above this neutral layer a slightly stable region is being formed. These vertical profiles of potential temperature are very similar to those observed by Nicholls (1982).

In Fig. 18 we have compared the calculated vertical velocity–defect profiles with the "Leipzig Wind Profile" (Lettau, 1950) and the data of Nicholls (1985). The model results give a value for the cross-isobar angle α of 11.4° and 12.7° for a stable lapse rate of 1 and 2 K km^{-1}, respectively. In the "Leipzig Wind Profile" α = 26.1° which is somewhat larger than in our model results. This might be a result of a higher value for z_0, and thus a smaller Rossby number. Although Nicholls (1985) did not quote a mean value of α, this can be obtained from the values A = 1.4 and B = 4.2 in the drag law for neutral Ekman layers. Together with the mean values Ro = 10^9 and u_*/G = 0.026 for the measurements during JASIN we get α = 15°. The data of Nicholls (1985) do not show negative values for $(u_g - u)$ between $z \sim 0.1u_*/f$ and $z \sim 0.2u_*/f$. This might be due to measuring errors because the value of

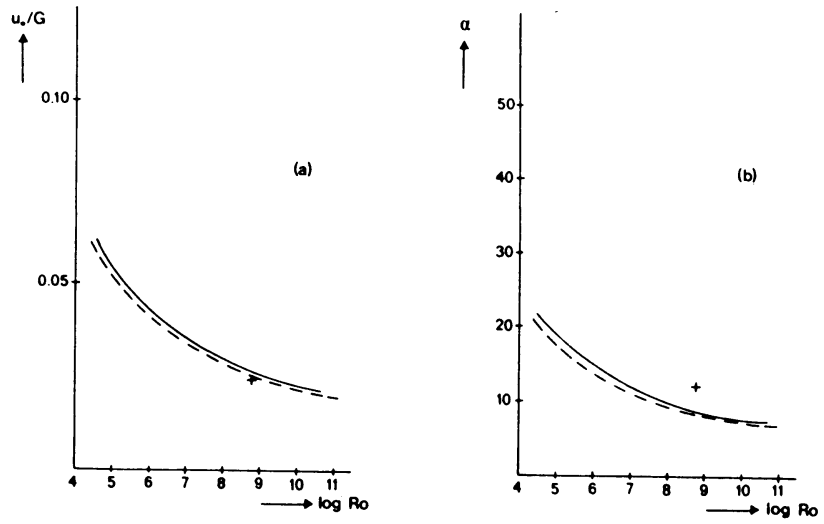

FIG. 16. (a) Geostrophic drag coefficient u_*/G and (b) cross-isobar angle α as a function of surface Rossby number (Ro); modified $E - \epsilon$ (solid); Deardorff (1972) (+); Mason and Thomson (1986) (dashed).

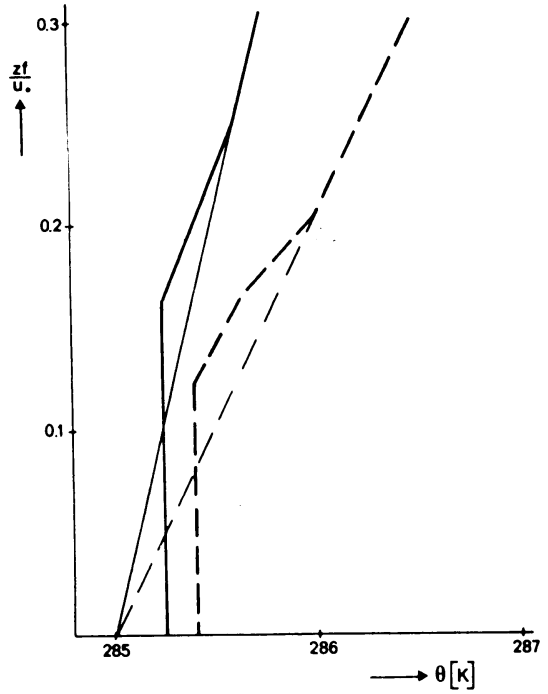

FIG. 17. The initial (thin lines) and final (thick lines) potential temperature profiles for an initial lapse rate of 1 (solid) and 2 K km^{-1} (dashed).

$\int_0^{z_i}(u_g - u)dz$ should be zero by definition (in the experimental data of Nicholls, 1985, the acceleration terms are accounted for in the definition of the geostrophic wind).

In Fig. 19 we have compared the computed stress profiles with the measured profiles of Nicholls (1985), which agree very well. The computed profiles indicate a boundary layer height of $0.2u_*/f$ and $0.16u_*/f$, respectively. Finally, the computed TKE profile is compared with the measurements of Nicholls (1985) in Fig. 20. At the top of the boundary layer, there is an abrupt drop in the calculated turbulent kinetic energy due to the stable stratification.

4. Conclusions

An $E - \epsilon$ closure model has been applied to simulate the neutral and stable atmospheric boundary layer. It is shown that the model results compare well with observations, large-eddy simulations and higher-order closure studies.

In the $E - \epsilon$ model an eddy-exchange coefficient is evaluated from the turbulent kinetic energy E and viscous dissipation ϵ. The exact equations for both E and ϵ need model assumptions. The most rigorous assumptions have to be made for the ϵ-equation. We have used the ϵ-equation in a form proposed by Lumley and Khajeb-Nouri (1974), Eq. (7).

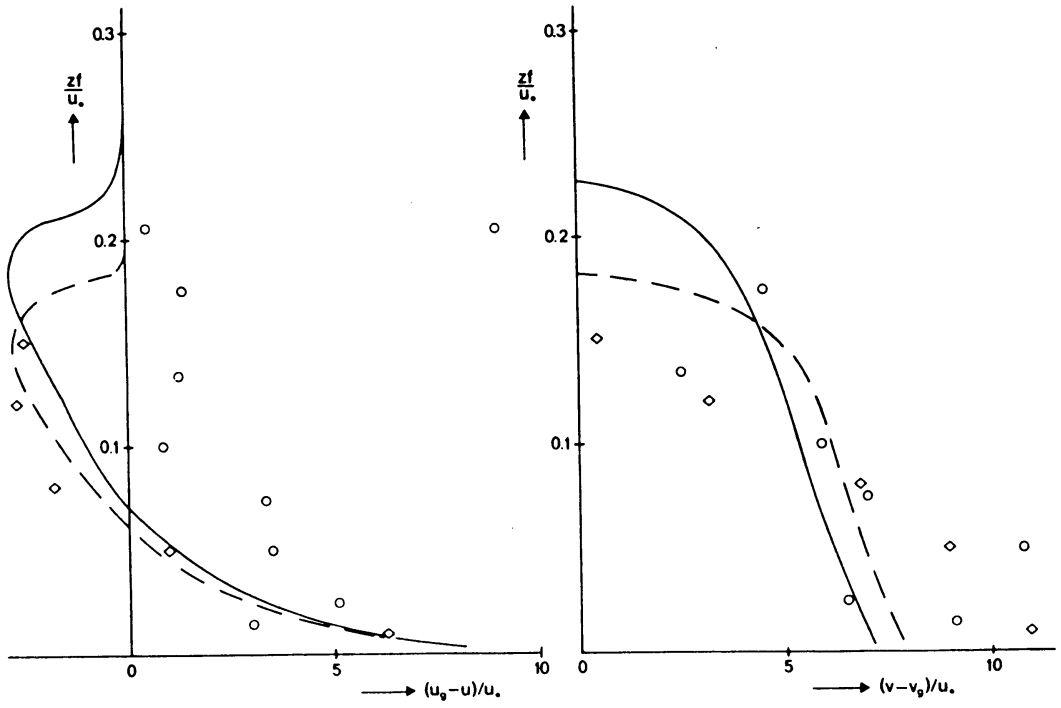

FIG. 18. Nondimensional wind defect profiles for an initial lapse rate of 1 K km^{-1} (solid) and 2 K km^{-1} (dashed) and the observational data of Nicholls (1985) (open circles) and Lettau (1950) (open diamonds).

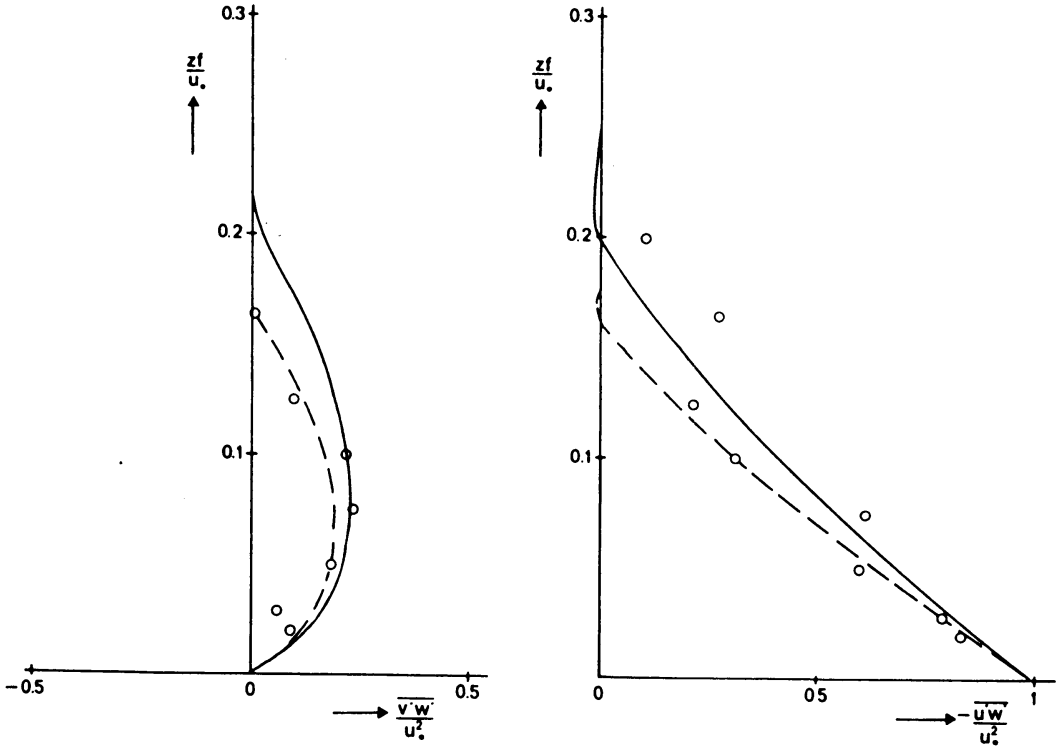

FIG. 19. Nondimensional momentum flux profiles (symbols as in Fig. 18).

Three unknown constants appear in the ϵ-equation: $c_{1\epsilon}$, $c_{2\epsilon}$ and σ_ϵ. The constant $c_{2\epsilon}$ which is connected with the destruction term is determined from the decay of grid turbulence. The value of the constant $c_{1\epsilon}$ is fixed for experiments on homogeneous shear flow (Harris et al., 1977; Tavoularis and Corrsin, 1981). The third constant σ_ϵ is determined in the surface layer in which a balance between viscous dissipation and shear production is assumed.

Besides the constants, the production term P in the ϵ-equation must be specified. Under convective conditions there is a considerable agreement to use the sum of shear production and buoyancy (Wyngaard et al., 1974). However, we showed that under stable conditions only the shear production should be included, which is nearly the same as the formulation proposed by Wyngaard (1975). Results on the neutral atmospheric boundary layer showed that the transport of turbulent kinetic energy is important and should be included in the production term P in the ϵ-equation. We included it analogous to the buoyancy term, only when it was positive (10).

For the stable atmospheric boundary layer we made a comparison with the constant cooling rate results of Wyngaard (1975) and Brost and Wyngaard (1978, 1979) and showed that our $E - \epsilon$ model can reproduce the same results. The critical Richardson behavior of the ϵ-equation is essential, i.e., as in observational data of Nieuwstadt (1983) and Garratt (1982) the model gives a constant Richardson number in the bulk of the boundary layer. We also found that the boundary layer height h obeyed Zilitinkevich's similarity prediction with

$$d = h\Big/\left(\frac{u_* L}{f}\right)^{1/2} = 0.44.$$

Comparison of model results (Deardorff, 1972; Wyngaard et al., 1974; Mason and Thomson, 1986) and observational data (Mildner, 1932; Lettau, 1950; Nicholls, 1985) on the neutral atmospheric boundary layer shows a big discrepancy between both results. For instance the model results give a boundary layer height of $h \sim 0.6u_*/f$ whereas the observations give $h \sim 0.2u_*/f$. We have shown that the observational data on the near-neutral boundary layer are in fact strongly influenced by a stable stratification. In order to do so we initialized the model with a stable lapse rate of 1 K km^{-1} and 2 K km^{-1} and set the surface heat flux to zero. From the results presented in section 3b2 it is clear that the $E - \epsilon$ model can reproduce the observations (Mildner, 1932; Lettau, 1950; Nicholls, 1985) quite well.

The model results for the neutral atmospheric boundary layer are in good agreement with both the large-eddy simulations of Deardorff (1972) and Mason and Thomson (1986) and the second-order closure

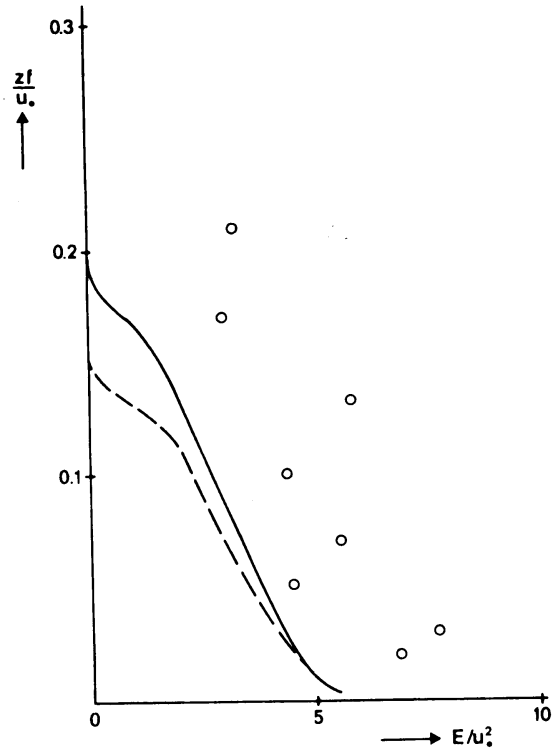

FIG. 20. Turbulent kinetic energy profile (symbols as in Fig. 18).

study of Wyngaard et al. (1974). We have shown that inclusion of the transport of turbulent kinetic energy T in the production term P of the ϵ-equation is essential in obtaining these results.

Acknowledgments. I would like to thank A. Beljaars and F. T. M. Nieuwstadt for their comments on an earlier version of this manuscript.

REFERENCES

André, J. C., G. De Moor, P. Lacarrère, G. Therry and R. du Vachat, 1978: Modeling the 24-hour evolution of the mean and turbulent structures of the planetary boundary layer. *J. Atmos. Sci.*, **35**, 1861–1883.

——, ——, ——, —— and ——, 1979: The clipping approximation and inhomogeneous turbulence simulations. *Turbulent Shear Flow I.* F. Durst, B. E. Launder, F. W. Schmidt and J. H. Whitelaw, Eds., Springer-Verlag, 307–318.

Beljaars, A. G. M., P. Schotanus and F. T. M. Nieuwstadt, 1983: Surface layer similarity under nonuniform fetch conditions. *J. Climate Appl. Meteor.*, **22**, 1800–1810.

Blackadar, A. K., 1962: The vertical distribution of wind and turbulent exchange in a neutral atmosphere. *J. Geophys. Res.*, **67**, 3095–3102.

Brost, R., and J. C. Wyngaard, 1978: A model study of the stably stratified planetary boundary layer. *J Atmos. Sci.*, **35**, 1427–1440; 1979: Reply. *J. Atmos. Sci.*, **36**, 1821–1822.

Businger, J. A., J. C. Wyngaard, Y. Izumi and E. F. Bradley, 1971: Flux-profile relationships in the atmospheric surface layer. *J. Atmos. Sci.*, **28**, 181–189.

Deardorff, J. W., 1972: Numerical investigation of neutral and unstable planetary boundary layers. *J. Atmos. Sci.*, **29**, 91–115.

Detering, H. W., and D. Etling, 1985a: Application of the $E - \epsilon$ turbulence model to the atmospheric boundary layer. *Bound.-Layer Meteor.*, **33**, 113–133.

——, and ——, 1985b: Application of the energy-dissipation turbulence model to mesoscale atmospheric flows. *Seventh Symp. on Turbulence and Diffusion*, Boulder, Amer. Meteor. Soc., 281–284.

Duynkerke, P. G., and A. G. M. Driedonks, 1987: A model for the turbulent structure of the stratocumulus-topped atmospheric boundary layer. *J. Atmos. Sci.*, **253**, 43–64.

——, and F. T. M. Nieuwstadt, 1988: A solution of the $E - \epsilon$ model for nearly homogeneous turbulence with a mean shear. Submitted to *Appl. Sci. Res.*

Dyer, A. J., 1974: A review of flux-profile relationships. *Bound.-Layer Meteor.*, **7**, 363–372.

Fitzjarrald, D. E., 1979: On using a simplified turbulence model to calculate eddy diffusivities. *J. Atmos. Sci.*, **36**, 1817–1820.

Garratt, J. R., 1982: Observations in the nocturnal boundary layer. *Bound.-Layer Meteor.*, **22**, 24–48.

Harlow, F. H., and P. I. Nakayama, 1967: Turbulence transport equations. *Phys. Fluids*, **10**, 2323–2332.

Harris, V. G., J. A. H. Graham and S. Corrsin, 1977: Further experiments in nearly homogeneous turbulent shear flow. *J. Fluid Mech.*, **81**, 657–687.

Hinze, J. Q., 1975: Turbulence. McGraw-Hill, 790.

Lee, H. N., and S. K. Kao, 1979: Finite-element numerical modeling of atmospheric turbulent boundary layer. *J. Appl. Meteor.*, **18**, 1287–1295.

Lettau, H., 1950: A re-examination of the "Leipzig Wind Profile" considering some relations between wind and turbulence in the frictional layer. *Tellus*, **2**, 125–129.

——, 1957: Windprofil, innere Reibung und Energieumsatz in den unteren 500 m über dem Meer. *Beitr. Phys. Atmos.*, **30**, 78–96.

Lumley, J. L., and B. Khajeh-Nouri, 1974: Computational modeling of turbulent transport. *Advances in Geophysics*, Vol. 18A, Academic Press, 169–192.

Mason, P. J., and R. I. Sykes, 1980: A two-dimensional numerical study of horizontal roll vortices in the neutral atmospheric boundary layer. *Quart. J. Roy. Meteor. Soc.*, **106**, 351–366.

——, and D. J. Thomson, 1986: Large-eddy simulations of the neutral-static-stability planetary boundary layer. Submitted to *Quart. J. Roy. Meteor. Soc.*

Mildner, P., 1932: Über die Reibung in einer speziellen Luftmasse in den untersten Schichten der Atmosphäre. *Beitr. Phys. Atmos.*, **19**, 151–158.

Monin, A. S., and A. M. Yaglom, 1975: *Statistical Fluid Mechanics: Mechanics of Turbulence, Vol. 2.* J. L. Lumley, Ed., The MIT Press, 874 pp.

Nicholls, S., 1982: An observational study of the mid-latitude marine atmospheric boundary layer. PhD thesis, University of Southampton. [Available from: Department of Oceanography, Southampton SO9 5NH Hampshire, England.]

——, 1985: Aircraft observations of the Ekman layer during the Joint Air–Sea Interaction Experiment. *Quart. J. Roy. Meteor. Soc.*, **111**, 391–426.

Nieuwstadt, F. T. M., 1983: A model for the stationary, stable boundary layer. *Proc. Conf. on Models of Turbulence and Diffusion in Stably Stratified Regions of the Natural Environment*, Cambridge.

——, 1984: The turbulent structure of the stable, nocturnal boundary layer. *J. Atmos. Sci.*, **41**, 2202–2216.

Panofsky, H. A., and J. A. Dutton, 1984: *Atmospheric Turbulence.* Wiley & Sons, 397 pp.

Rao, K. S., J. C. Wyngaard and O. R. Coté, 1974: The structure of the two-dimensional internal boundary layer over a sudden change of surface roughness. *J. Atmos. Sci.*, **31**, 738–746.

Reynolds, W. C., 1974: Computation of turbulent flows. *AIAA Paper No. 74-556, AIAA Seventh Fluid and Plasma Dynamics Conf.*, Palo Alto. [Available from: AIAA Library, 750 3rd Avenue, New York, New York 10017.]

Rodi, W., 1980: Turbulence models and their application in hydraulics. IAHR, P.O. Box 177, 2600 MH Delft, The Netherlands.

Tavoularis, S., 1985: Asymptotic laws for transversely homogeneous turbulent shear flows. *Phys. Fluids*, **28**, 999–1001.

——, and S. Corrsin, 1981: Experiments in nearly homogeneous turbulent shear flow with a uniform mean temperature gradient. Part 1. *J. Fluid Mech.*, **104**, 311–347.

Tennekes, H., 1973: Similarity laws and scale relations in planetary boundary layers. *Workshop on Micrometeorology*. D. A. Haugen, Ed., Amer. Meteor. Soc., 177–216.

——, 1985: A comparative pathology of atmospheric turbulence in two and three dimensions. *Proc. Int. School of Physics "Enrico Fermi", Turbulence and Predictability in Geophysical Fluid Dynamics and Climate Dynamics*, North-Holland, 45–70.

——, and J. L. Lumley, 1972: *A First Course in Turbulence*. MIT Press, 300 pp.

Wyngaard, J. C., 1975: Modeling the planetary boundary layer-extension to the stable case. *Bound.-Layer Meteor.*, **9**, 441–460.

——, O. R. Coté and K. S. Rao, 1974: Modeling the atmospheric boundary layer. *Advances in Geophysics*, Vol. 18A, Academic Press, 193–211.

Zeman, O., and J. L. Lumley, 1979: Buoyancy effects in entraining turbulent boundary layers: A second-order closure study. *Turbulent Shear Flows I*. F. Durst, B. E. Launder, F. W. Schmidt and J. H. Whitelaw, Eds., Springer-Verlag, 295–306.